An Experimental Study of Compressor Stability in a 450 kW Helicopter Gas Turbine Engine

by

Fouzi Khalid Sultan Al-Essa

B.S., Mechanical Engineering
Purdue University, 1992

Submitted to the Department of Mechanical Engineering in
Partial Fulfillment of the Requirements for the Degree of

Master of Science in Mechanical Engineering

at the

Massachusetts Institute of Technology
September 1997

Signature of Author _____
Department of Mechanical Engineering
July 10, 1997

Certified by _____
Professor Alan H. Epstein
Professor of Aeronautics and Astronautics
Thesis Supervisors

Certified by _____
Professor Kamal Youcef-Toumi
Associate Professor of Mechanical Engineering
Thesis Reader

Accepted by _____
Ain A. Sonin
Chairman, Department Committee on Graduate Students

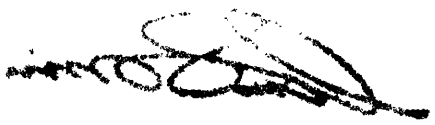

An Experimental Study of Compressor Stability in a 450 kW Helicopter Gas Turbine Engine

by

Fouzi Khalid Sultan Al-Essa

Submitted to the Department of Mechanical Engineering on July 10, 1997
in Partial Fulfillment of the Requirements for the Degree of
Master of Science in Mechanical Engineering

Abstract

Unsteady pressure perturbations and presurge behavior were investigated on an Allison 250-C30 gas turbine engine. The engine was throttled towards the surge line with inserts that produced losses between the compressor and combustor, and water injection down stream of the compressor.

Spectral content growth was observed at 24-26, 110-140, and 330 Hz as the engine speed was varied over the operating range. The 24-26 Hz oscillation was identified as the Helmholtz mode and was seen to increase near the 85% $N1cor$ speed. This oscillation was axisymmetric at the inlet and impeller-diffuser vaneless space. The 110-140 Hz oscillation was observed to increase as the compressor was throttled towards the surge line at the 95% speed. The 330 Hz oscillation, seen at 71% N_{1cor} speed, was found to be a rotating disturbance. The first and second harmonics were observed to rotate at 58-61% of the N_1 shaft speed.

Surge behavior due to both acceleration transients at part power, and to steady throttling towards the surge line at high power, were investigated. Transition from the 84/85% speed to higher power was done with the inducer bleed open to atmospheric pressure as well as blocked off. 150 ms of oscillations at 27 Hz preceded surge when the inducer bleed was open to atmospheric pressure. These oscillations were axisymmetric at the inlet, but had an asymmetric pattern in the vaneless space. Static pressure perturbations in half the annulus was observed to oscillate 90 degrees out of phase compared to the other half. Oscillations at 27 Hz were also observed with the inducer bleed blocked, but surge may have been preceded by a rotating disturbance.

Bursts of high amplitude 100 Hz oscillations preceded surge at the 95% speed. These bursts were characterized by axisymmetric flow at the inlet, but the vaneless space had the same asymmetric pattern seen prior to surge near the 85% speed. Prior to these bursts lower amplitude oscillations at 120 Hz were seen.

Forced response testing was done at 3 points along the 95% speed line. Actuation was achieved by modulating flow injected into the engine through the inducer bleed about a mean injection level. Transfer functions between actuator command and compressor exit pressure showed that the 110-140 Hz mode became less damped near surge.

Thesis Supervisor: Alan H. Epstein
Title: Professor of Aeronautics and Astronautics

Acknowledgment

I would like to start by thanking my Lord, Allah, for the blessings and bounties He bestowed upon me. He is The Merciful, The Compassionate, The Lord of Muslims, Jews and Christians, The one God who had not a son nor is any being equal to him.

When I first arrived at the Gas Turbine Laboratory, and read the acknowledgments of previous students I thought that this page was included to thank individuals who had minor contributions to their work. During my stay at GTL, however, I realized that my work, and the work of students before me, could not have been completed without the support and help of many outstanding people. I would like to thank the following individuals:

Professor Epstein for his continuous support and guidance during my stay at the GTL. Professor Paduano, Professor Greitzer, and Professor Youcef-Toumi for their interest and support.

Dr. Gerald Guenette for his help with data acquisition computers and instrumentation, and Dr. Sabri Deniz for many interesting discussions about centrifugal compressors. Dr. Herald Weigl for data analysis codes and many discussions about system identification.

James Letendre, Mariano Hellwig, Victor Dubrowski and Bill Ames for their friendship, and help in keeping the engine up and running. Without their help this work would not have been completed.

Holly Anderson for taking care of all the financial details, and Lori Martinez for making sure students and staff at the laboratory got their daily requirement of the fifth food group; candy.

Many friends at the Gas Turbine Laboratory have made my stay enjoyable. Brian Corn, Jinwoo Bae, and Eric Nelson have been good friends and excellent people to work with. Ammar Al-Nahwi, Asif Khalak, and Dr. David Tew have provided continuous support and encouragement during my research program.

I would like to especially acknowledge the support of my father, my mother, and my family. Without their love and support, I would have never made it to MIT, or completed my degree.

I would like to acknowledge the support of Dr. James McMichael, Technical Manager at AFOSR, and the Allison Engine Company.

Contents

List of Figures

List of Tables

Nomenclature

p	Pressure
T	Total Temperature
N_1	Compressor shaft speed
N_2	Power turbine shaft speed
A	Area
L	Length
L/A	Length to area ratio
V	Volume
s	Laplace transform variable
$\dot{m}$	Mass flow rate
π	Pressure ratio
θ	Temperature non-dimensionalized by reference temperature
δ	Pressure non-dimensionalized by reference pressure
f	Chapter 2: Ratio of fuel mass flow rate to compressor mass flow rate Chapter 3: Frequency (Hz)
ω	Frequency (Radians/Sec)
a	Speed of sound
ρ	Density

General Subscripts

t	Total pressure or temperature
corr	Corrected mass flow rate or speed

Subscripts used with p, T, θ, δ, A to represent stations in the engine

2	Compressor inlet
3	Compressor exit
$3'$	Downstream of orifice inserts
4	Turbine inlet
45	Power turbine inlet

Subscripts used with $\dot{m}$

inlet	Compressor inlet mass flow rate
exit	Compressor exit mass flow rate
water	Water injection mass flow rate
air	Air injected mass flow rate

Subscripts used with a, ρ, A

d	Duct
p	Plenum

Chapter 1

Introduction

1.1 Background

The operating range of gas turbine engines is limited by many types of instabilities ranging from mechanical vibration of the compressor and turbine blades to aerodynamic instability of mass flow through the engine.

Two aerodynamic instabilities that have been investigated for over 40 years are surge and rotating stall. Surge is a self excited global instability characterized by large fluctuation in massflow and pressure, with periods of reverse flow through the compression system. Rotating stall is a localized flow instability characterized by regions of low massflow that travels around the annulus at a fraction of the rotor speed. A typical compressor map along with the flow instability region is shown in figure (1.1). The surge line is the boundary between the stable flow region and the unstable region. The peak compressor efficiency lies near this line.

Design practice has been to match engine components so that the compressor operates on a stable operating line near the surge line while allowing sufficient " surge margin " to account for manufacturing tolerances and engine aging and wear. This surge margin results in operation away from the peak compressor efficiency and therefore sacrifices the overall engine efficiency. In a high bypass ratio civil transport gas turbine engine, where the surge margin varies from 10-20%, it is estimated that a 10% reduction in surge margin results in a 4% improvement in overall engine efficiency [1].

Feedback control was proposed by Epstein et al. [2] in 1989 to suppress linear growing oscillations that develop into surge and rotating stall. Preliminary experiments on turbocharger test rigs have shown that surge is initiated by small disturbances that increase in amplitude until they destabilize the compression system, and suppressing these disturbances has expanded the stable compressor operating range and allowed operation closer to the peak compressor efficiency.

Many reasons have delayed extension of the above work to gas turbine engines. A few of these reasons include complication of data analysis due to combustion noise, large

variation in observed presurge behavior of different engines, slow development of engine models, and difficulty of implementing well controlled experiments on engines.

The focus of this work is to document the prestall behavior of a gas turbine engine having a high performance centrifugal compressor. Experiments have been performed on an Allison 250-C30 600 HP helicopter engine with a single stage centrifugal compressor.

1.2 Previous Work

Emmons et al. [3] and Nordenson et al. [4] investigated oscillatory behavior in centrifugal compressors. They identified regions of mild classic surge, stable rotating stall and deep surge. Emmons furthermore proposed the analogy between mild surge oscillation in compression systems and the acoustic oscillation in a Helmholtz resonator.

Greitzer [5] developed a nonlinear model that captured post stall limit cycle behavior observed in compression systems. He determined a non-dimensional B parameter that accurately predicted whether surge or rotating stall would occur at the surge line. His model was complimented with experimental results on a low speed 3 stage compressor.

Toyama [6] investigated presurge behavior in a high pressure ratio (10:1) centrifugal compressor with a vaned diffuser. He observed mild surge oscillations at a normally stable operating point, as well as prior to surge. The mild surge oscillations were 1-D and occurred at the Helmholtz frequency. He did not observe rotating stall.

Fink [7] investigated surge in a small centrifugal turbocharger test rig with a vaneless diffuser. He observed mild surge oscillations during the precursor period that slowly developed into surge without the occurrence of rotating stall. He found that the basic surge model, developed by Greitzer and modified to include shaft speed fluctuations, agreed with experimental data.

Huang, Pinsley, Gysling, and Simon [8,9,10,11] demonstrated active surge control on centrifugal turbochargers. Various actuation schemes including a movable plenum wall, a plenum exit bleed valve and a valve close coupled to the compressor achieved flow range extensions of 25-35%.

The above experiments were implemented on compressor test rigs and did not address issues related to the extension of active surge control to gas turbine engines. Several research projects have begun to address such issues. Ffowcs Williams et al. [12,13] demonstrated a 2.6% flow range extension on a 60 HP auxiliary power unit having a compressor pressure ratio of 3. They reported that non axisymmetric actuation was required to affect a 2-D rotating disturbance believed to trigger deep surge.

The MIT Gas Turbine Laboratory has two 600 HP engines with compressor pressure ratios in the range of 7-9. Work is currently underway to demonstrate active surge control on these high pressure ratio compressors where surge behavior has been observed to be different than that observed in low pressure ratio compressors.

Borror [14] and Corn [15] reported abrupt surge behavior with no precursor or rotating stall in an LTS-101 engine. Corn further investigated using diffuser throat injection as a means for actuation. He found that mean air injection into the diffuser changed the compressor characteristic resulting in mild surge oscillations.

This thesis reports results of testing done on an Allison 250-C30. It presents presurge behavior and the preliminary results of forced response testing.

1.3 Objectives of Current Research

The following objectives have been identified as a step towards demonstrating active surge control on the Allison 250-C30 engine:

(1) Measurement of the engine's unsteady pressure fluctuations and determination of their relationship to the Helmholtz resonator mode and other measured acoustic resonances.

(2) Characterization of the engines presurge behavior and investigation of the relationship between system wide oscillations, such as the Helmholtz resonance, and compressor stability. This includes addressing the following issues:

a. Are presurge oscillations observed to increase in amplitude, indicating a decrease in stability of system modes, as the compressor is throttled towards the surge line?

b. What is the nature of presurge oscillations, are they 1-D or non axisymmetric?

c. Does rotating stall occur prior to surge on the engine?

(3) Evaluation of the effectiveness of inducer bleed port injection (actuation scheme chosen for Allison) in forcing the engine, and its suitability for active surge control.

(4) Measurement of the engine's forced response behavior at several operating points along a speed line.

1.4 Organization of Document

This thesis has been organized into six chapters. Chapter two describes the experimental setup. It includes the engine loading procedure and compressor throttling scheme. This chapter also describes the actuation scheme used for forced response testing and the data acquisition systems.

Chapter three covers the engine's unsteady pressure fluctuations and investigates their relationship to acoustic resonances measured while the engine was off. Two models are used to estimate the shift in frequency that occurs due to temperatures that occur during engine operation.

Chapter 4 presents the engine's presurge behavior at the 85% and 95% speed lines. It describes oscillations observed to grow prior to surge, and investigates the nature of these oscillation (1-D or asymmetric). It also discusses the occurrence of rotating disturbances prior to surge.

Chapter 5 discusses the effect of steady, and unsteady, air injection into the inducer bleed port on engine performance. It presents forced response measurements made at several operating points along a speed line and discusses the effectiveness of inducer bleed port actuation in forcing the engine. Chapter 6 provides some concluding remarks and recommendations for future work.

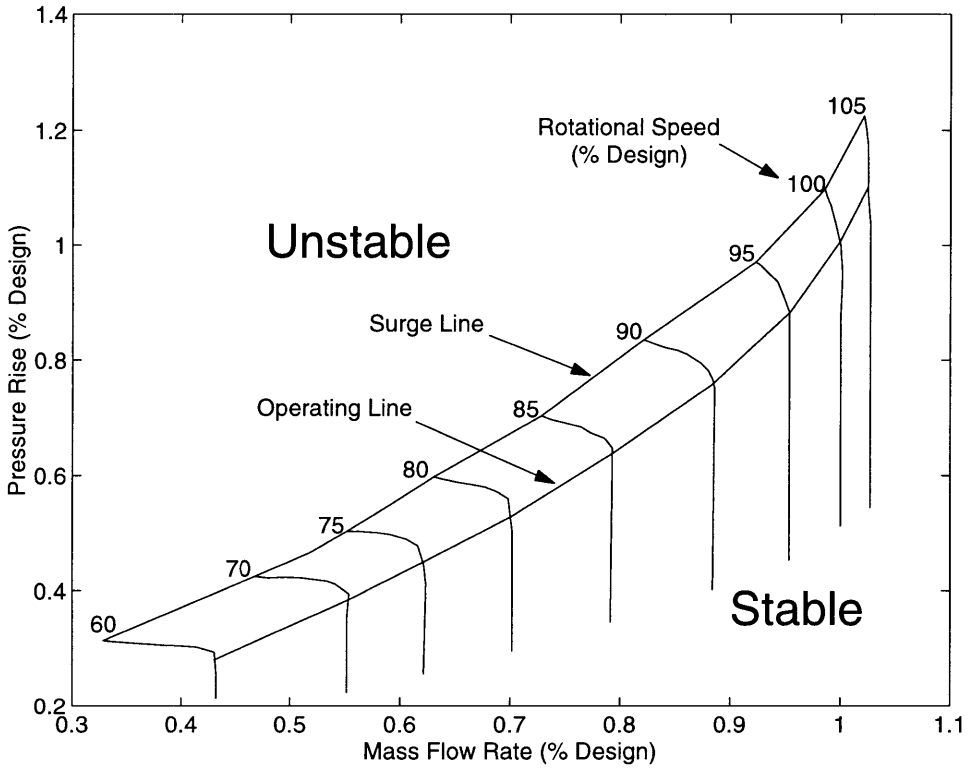

Figure (1.1) Compressor Map

Chapter 2

Experimental Setup

2.1 Introduction

Testing was done on an Allison 250-C30P, a 600 HP gas turbine engine. This engine has a compressor with a pressure ratio of about 9 and corrected mass flowrate of about 6 lbm/s. The engine power output shaft was attached to a waterbrake to load the engine and dissipate the power.

The engine was equipped with high frequency response pressure transducers at 4 axial locations throughout the engine. These were the inlet, vaneless space, scroll and combustor. The inlet and vaneless space axial stations had a circumferential array of 5 transducers each.

The engine was throttled to the surge line using an approach suggested by Allison. Orifice plates, inserted between the compressor and combustor, were used to shift the operating line upward towards the surge line. This modification could not be adjusted while the engine was running and therefore a second throttling scheme was required to further approach the surge line while running. Water injection downstream of the compressor and orifice plates, and upstream of the combustor was used to achieve this and to reduce the turbine inlet temperature so that it did not exceed the maximum allowable limit as the operating point moved towards the surge line.

Actuation, used for forced response testing, was implemented using the standard inducer bleed (IB) port. A valve with a bandwidth of 300 Hz (later referred to as the high speed valve) was attached to the inducer bleed port to allow air injection into the inducer through slots distributed circumferentially around the shroud.

This chapter discusses the following issues related to the experimental setup for the Allison 250-C30 :-

1. Engine setup and operation.
2. Data acquisition :
    a) Steady state performance monitoring.
    b) High speed data acquisition for unsteady phenomena.

3. Engine throttling procedure :
    a) Orifice plate inserts.
    b) Water injection.
4. High speed actuation for forced response testing :
    a) High speed valve.
    b) Inducer bleed port injector.
    c) Actuator performance requirements and testing.

2.2 Engine Setup and Operation

The Allison 250-C30 engine schematic is shown in Figure (2.1) and Figure (2.2). The engine has a single stage centrifugal compressor with a design pressure ratio of about 9, and corrected mass flow of about 6 lbm/s. The impeller flow goes through a vaned diffuser, a scroll, and two discharge tubes connecting the scroll to the combustor. Work is extracted with a two stage gas producer turbine driving the compressor, and a two stage power turbine. The power turbine drives the power output shaft through a set of gears used to reduce the output shaft speed to about 6000 RPM. Table (2.1) summarizes specifications for the engine.

Table (2.1) Engine Design Specifications

Pressure Ratio	about 9:1
Corrected Flow	about 6 lbm/s
N_1 Design Speed	51,000 RPM
N_2 Design Speed	30,650 RPM
Design Power Output	600 HP

The engine power output shaft was connected to a KAHN (model 101-130) waterbrake to dissipate the power. The water level in the waterbrake was regulated to achieve the desired level of power dissipation. This was done using two valves, one upstream of the waterbrake (USV) regulating the feed flow rate and one downstream (DSV) of the waterbrake setting the back pressure and drainage flow rate. Figure (2.3) shows a schematic of the engine test setup.

Engine Loading: The engine had two main control inputs that were used to load the engine and regulate the N_2 shaft speed (power turbine), these were (1) the upstream valve, mentioned above, and (2) the power turbine speed governor lever. The downstream valve remained at 50-60% open during testing and was not changed during an experiment.

The Allison 250-C30P fuel controller, similar to other helicopter engines, regulates fuel flow to maintain the power output shaft speed (N_2) constant. The speed setpoint may be set from 90-100% of design using the power turbine speed governor lever. To demand more power out of a helicopter engine the pilot varies the collective, the N_2 output shaft speed droops momentarily, and the fuel controller compensates by injecting more fuel into the engine. This returns the N_2 output shaft speed to its setpoint and brings the engine to a higher power output level and higher N_1 shaft speed.

The test stand engine was brought to the 95% N_{1cor} speed line (most tests done at this speed) by opening the upstream valve (USV). This increased the water level in the waterbrake, resulted in higher power dissipation, and brought the engine to a new operating point in a manner similar to a change in collective. The upstream valve did not allow loading in fine increments, therefore fine setting of the N_{1cor} speed was done using the N_2 speed governor lever. Increasing the N_2 speed setpoint caused the controller to inject more fuel into the engine bringing it to a higher N_1 and N_2 shaft speed.

2.3 Data Acquisition

Data used in this research was acquired using two data acquisition computers; the first logged steady state performance data, while the second was used for high speed data acquisition. The following subsections describe the data acquisition equipment in more detail.

2.3.1 Steady State Performance Monitoring

Genesis, real time process control software developed by Iconics, was used to monitor the engine's steady state performance. Table (2.2), on the following page, summarizes the measured quantities and the transducers used to make these measurements. All the data was logged at a rate of 2 Hz unless otherwise stated.

Error estimates were done using the RSS method based on the 95 % confidence level. Table (2.3) summarizes the derived quantities and the error analysis results for these quantities.

2.3.2 High Speed Data Acquisition; Sensors and System

The Allison 250-C30 engine was modified to include 15 static pressure taps located at 4 axial locations in the engine. These position were, at the face of the impeller (inlet), between the impeller and vaned diffuser (vaneless space, VS), in the scroll (down stream of the diffuser), and in the combustor. Figure (2.2) shows the pressure tap axial locations. The inlet and vaneless space axial positions each had a circumferential array of 6 pressure taps that were used to monitor rotating waves. Only five of the inlet and vaneless space taps were used. This was sufficient to analyze the first two spatial harmonics of a rotating wave and their direction of rotation.

Figure (2.4) shows the circumferential location of the inlet and vaneless space taps, and Table (2.4) summarizes the pressure tap naming convention and their circumferential location.

Solid state pressure transducers with bandwidths above 100 Khz, were attached to the pressure taps and used to monitor unsteady phenomena in the engine. The complete high speed data acquisition system consisted of pressure transducers with amplifiers, anti-aliasing filters and a computer setup for data acquisition. Table (2.5) summarizes the equipment specifications and settings.

Table (2.2) Engine Steady State Measurements

Reading	Used to Calculate	Transducer	Measurement Location	Estimated uncertainty at 95% N_{1corr}
p_1	$\dot{m}_{corr}$	Setra, model 239	Bellmouth	± 0.59%R (% of reading)
p_3	π	Setra, model 204D	Upstream of fuel controller air filter, taped into scroll	± 0.37%R
$p_{ambient}$	$\dot{m}_{corr}$, π	Setra, model 370	In Upstream Duct	± 0.1%R
Tinlet	N_{1corr}, N_{2corr}	Type K TC	X inches from face of compressor	± 2.1 degrees C
Poil	Diagnostic	Omega PX 603	-	± 0.52%R
Toil	Diagnostic	Type K TC	-	-
Fuel Flow Rate		Signet 3-2507-3S	-	± 0.57%R
N_1	N_{1corr}	Engine tachometer	N_1 tachometer, updated every 2 seconds.	± 0.15%R
N_2	N_{2corr}	Engine tachometer	N_1 tachometer, updated every 2 seconds	± 0.15%R
T45	Diagnostic	Type K TC	Engine T45 harness	-
Texhaust	Diagnostic	Type K TC	Exit of power turbine	-
Torque (Oil)	HP	Omega PX 603	Engine torquemeter	-
Torque (Load Cell)	HP	Sensotec, 41-275-01	On the waterbrake	± 2.1%R
Air Flow Rate	Air Injection	Ficher & Porter 10A3555 Float: 2 GSVGT, 97 T50	Upstream of high speed valve	± 3.3%R

Table (2.3) Uncertainty Estimates for Derived Quantities

Derived Quantity	Uncertainty Estimate at 95% N_{1corr}
$\dot{m}_{corr}$	±0.28%R (%R used to mean "percent of reading")
π	±0.38%R
N_{1corr}, N_{2corr}	±0.39%R : 2.1 degrees C inlet temperature error ±0.87%R : 3 degree C temperature distortion and 2.1 degree C error
Power (Load Cell)	±2.1%R

Table (2.4) Pressure Tap Location and Naming Convention

Axial Station	Tap ID	Used In This Work	Angle (deg) CCW from TDC (front view)	Transducer Used (Kulite Model)
Inlet	I01	Y	15	XCS-062-5D
	I02	Y	75	XCS-062-15G
	I03	Y	135	XCS-062-5D
	I04	N	180	None
	I05	Y	255	XCS-062-5D
	I06	Y	295	XCS-062-5D
Vaneless Space	S07	Y	0	XCQ-062-50G
	S08	Y	60	XCQ-062-50G
	S09	Y	120	XCQ-062-50G
	S10	N	180	None
	S11	Y	240	XCQ-062-50G
	S12	Y	300	XCQ-062-50G
Scroll	SCR	Y	90 (left side)	XCQ-062-250G
Combustor	COM	Y	180 (bottom)	XCQ-062-250G
Inducer Bleed	IBP	Y	-	XCQ-062-50G

Table (2.5) Data Acquisition System

Computer	Dell 425E
DAQ Cards	2 X 8 Channel 12 bit Adtek AD830 A/D card 4 kHz sampling
Anti-aliasing Filters	Onsite Instruments, TF-16-04 Cauer, 16 Channel, 8 Pole Roll off : 75 db/octave Cuttoff : 1020 Hz.
Amplifiers	Pacific Model 8650
Pressure Transducers	See Table (2.4)

2.4 Engine Throttling Procedure

One problem that adds complexity to surge testing in an engine, compared to compressor test rigs, is throttling the compressor toward the surge line.

In most test rig compressors there is a variable area throttle (valve down stream of the compressor) that reduces the mass flow through the compressor and moves the operating point towards the surge line along a constant speed line. In an engine there are many constraints that need to be considered when designing a scheme to throttle the compressor, two such constraints are geometry and the turbine inlet temperature (T_{t4}). Engines are designed to minimize weight and space requirements in the helicopter, therefore it is often true that the engine geometry allows little or no space to design a variable area nozzle capable of withstanding a temperature of 600 degrees C and 700 lbf of thrust.

Turbine inlet temperature is another constraint that often restricts the design of a throttling scheme; as the compressor is throttled, and the mass flow rate through the engine is reduced, the turbine inlet temperature increases and often reaches the maximum recommended temperature limit. This limits the allowable throttling and may prove certain schemes unacceptable.

A number of throttling schemes were considered for the Allison 250-C30. Two such schemes were a variable area nozzle downstream of the power turbine, and high pressure air (or steam) injection into the engine.

The variable area nozzle was predicted to raise the turbine inlet temperature (T_{t4}) by more than 250 degrees C in moving from the op-line to the surge line at the 98 % N_{1cor} speed line. This would lead to a turbine inlet temperature near the maximum recommended limit and was therefore deemed unacceptable.

High pressure air/steam injection downstream of the compressor and upstream of the turbine was found to be an attractive solution. It would throttle the compressor, but would not affect the mass flowrate through the combustor and therefore would not raise the turbine inlet temperature. The supply pressure required for this approach (150 Psig) was not readily available and therefore a third alternative requiring two modifications to the engine was implemented.

The first modification was to include orifice plates between the compressor and combustor which shifted the op-line toward the surge line. The second modification was made to allow water injection into the engine downstream of the orifice plates and upstream of the combustor. This has an effect similar to air/steam injection with the advantage of reducing the turbine inlet temperature. Water injection could not be used alone because the flow rate required to reach the surge line would extinguish the combustor. The following sections discuss the modifications made to throttle the compressor in greater detail.

2.4.1 Orifice Plate Inserts

Figure (2.5) Shows a schematic of the engine with the orifice plate and water injectors shown. Conservation of mass, cast into the corrected flow form, provides insight about the first order effects of the orifice plate inserts and water injection.

$$\frac{\dot{m}_4\sqrt{\theta_4}}{\delta_4 A_4} = (1+f)\frac{\dot{m}_2\sqrt{\theta_2}}{\delta_2 A_2}\left(\frac{p_{t2}}{p_{t4}}\right)\sqrt{\frac{T_{t4}}{T_{t2}}}\left(\frac{A_2}{A_4}\right) + \frac{\dot{m}_{water}\sqrt{\theta_2}}{\delta_2 A_2}\left(\frac{p_{t2}}{p_{t4}}\right)\sqrt{\frac{T_{t4}}{T_{t2}}}\left(\frac{A_2}{A_4}\right) \qquad (2.1)$$

Simple reasoning will be used to demonstrate the effect of the orifice plate inserts. The reasoning will first be applied to speed lines that are flat ($\partial\pi/\partial m_{cor} \approx 0$) and then extended to the case of arbitrary speed lines.

The orifice plate inserts result in a pressure drop in p_{t4}, the turbine inlet pressure;

$$p_{t4} \approx p_{t3'} < p_{t3} \qquad (2.2)$$

Equation (2.1), with no water injection, shows that for choked nozzle guide vanes (left hand term is constant) the drop in pt4 must be balanced by a reduction in the compressor corrected mass flow rate, $\dot{m}_{cor}$. Therefore it is seen that the orifice plate inserts' throttling

effect is proportional to the pressure drop occurring across them for relatively flat speed lines. The term "throttling" will be used to refer to the reduction in compressor corrected flow.

The reduction in flow rate has no further effect for the flat speed line case. There is, however, an additional effect that needs to be considered for steep speed lines, and that is the increase in pressure ratio (or p_{t3}) due to the reduction in compressor corrected flow (moving along a speed line). This increase in p_{t3} reduces the overall throttling effect due to the inserts.

The above reasoning neglects the effect of a reduced engine mass flow rate on the turbine inlet temperature; as the compressor is throttled and the engine mass flow rate is reduced the turbine inlet temperature (T_{t4}) increases. This increase in turbine inlet temperature complements the effect of the drop in p_{t4} and increases the throttling effect.

Implementation: The orifice plate inserts were designed to fit into the two discharge tubes on the sides of the engine. Several inserts with varying loss levels were designed by Allison and are shown in Figure (2.6). Most the experiments reported in this thesis were done with the 5 bar insert and any exceptions will be clearly labeled.

Figure (2.7) shows the op-line for the baseline engine with no inserts, and the 5 bar insert case. Table (2.6) summarizes the inserts effect on pressure ratio, corrected mass flowrate, and T_{45}; the power turbine inlet temperature. T_{45} should be kept below 716 degrees C for safe continuous operation of the turbine.

During the initial periods of operation the operating line was observed to shift upwards towards the surge line. The new operating line, which will be labeled the "shifted 5 bar operating line", is compared to the 5 bar operating line in figure (2.8). The reason for this shift is not known. The results presented in this thesis were mostly taken after the op-line had shifted and any exceptions shall be clearly specified.

2.4.2 Water Injection

Water injection was used to throttle the compressor during operation to approach the surge line. Equation (2.1) provides insight about the effect of water injection on the compressor; As the water injection flow rate is increased, the compressor corrected mass flow rate decreases moving the operating point towards the surge line. Because water is injected as a liquid, and evaporates in the discharge tubes and combustor, the compressor throttling effect is accompanied by a reduction in turbine inlet temperature (T_{t4}). This reduction in turbine inlet temperature reduces the compressor throttling effect as shown

by equation (2.1). Therefore injecting 5 % of the compressor mass flowrate results in less than 5 % reduction in compressor corrected mass flow.

During the initial design stages of the experiment steam injection was considered. The reduction in T_{t4} due to steam injection would be less than that due to water injection and therefore would have a greater throttling effect. The use of steam was found to be expensive in this installation and generated many safety concerns, and was therefore not implemented.

Two water injectors were used, one in each discharge tube, resulting in a combined maximum injection flow rate of about 6.4% of the design point flow rate . Figure (2.9) shows a picture of the discharge tubes with the orifice plates and water injectors. The supply pressure to the injectors was regulated in the range of 0-1500 Psia and was used to vary the injection flow rate. Table (2.7) summarizes information about the water injection system.

Water injected into the engine was de-ionized to prevent salt buildup on the discharge tubes, combustor liner, and nozzle guide vanes.

Table (2.6) Effect of Insert on Engine Operation

	No Insert	5 Bar Insert	Shifted 5 Bar Insert
Pressure Ratio, π	83.2%	85.7%	85.5%
m_{corr} (% design)	94.6%	91.6%	89.5%
N_{1cor} (% design)	95.2	95.1	95.2
N_{2cor} (% design)	90.7	95.1	94.6
T_{45} (degrees C)	647	698	674
Power (HP)	491	478	463

Table (2.7) Information about the Water Injection System

Supply Pressure	0-1500 Psia, Used to regulate flow rate.
Injectors	Spraying Systems, Hollow Cone ¼-NN14
Maximum Flow Rate	6.4% design
Injector Location	12" downstream of orifice plates
Water Flow Meter	Micromotion, CMF 050M

2.5 Actuator for Forced Response Testing

2.5.1 Introduction

Actuation is an integral part of any feedback control system. Several actuation methods have been evaluated to determine their effectiveness for surge control. These included compressor inlet injection, diffuser throat injection, close-coupled valve, compressor exit bleed, and an aerodynamic damper (see figure (2.10)). McNulty [16] compared these methods of actuation using a lumped parameter model of a Lycoming LTS-101 engine and concluded that actuation methods close coupled to the compressor were most effective because they modulate momentum in the duct. These included compressor inlet injection, diffuser throat injection and a close-coupled valve.

Diffuser throat injection was used for surge control actuation on a Lycoming LTS-101 engine at the Gas Turbine Laboratory as part of an ongoing active control effort, refer to Borror and Corn [14,15].

The actuator for the Allison 250-C30 consisted of a high speed (H/S) valve, used to modulate the flow, attached to the standard inducer bleed port which was used as an injector. This injector allowed unsteady mass perturbation to be injected radially into the inducer of the centrifugal compressor. The term "injector" will be used to refer to volumes and ducts that move fluid from the valve to the inducer. Sections 2.5.2 and 2.5.3 describe the H/S valve and inducer bleed port injector in greater detail.

The actuator was required to provide circumferentially uniform actuation well above the engine's Helmholtz resonator frequency. It was expected that surge instability occurred following growing oscillation with a frequency equal to the Helmholtz resonator

frequency, and damping these oscillations may extend the compressor's stable operating range [7,9]. The actuator bandwidth was determined experimentally while the engine was off and the results of these experiments are covered in section 2.5.4.

2.5.2 High Speed Valve

The H/S valve was composed of two components; a linear servo motor supplied by Moog Inc., which transforms electrical signals into motion, and a valve, which transforms mechanical displacement into mass flow modulation. Figure (2.11) shows a schematic of the motor and valve.

High pressure air enters the body of the valve, travels through choked slots in the cylinder, and then enters the injector. A sleeve attached to the motor regulates the area of the choked slots and modulates the mass flow into the injector. Figure (2.12) shows the steady mass flow characteristic for the valve. The mass flow rate is seen to be linear with position in the range from -5 to 5 volts and therefore all testing was limited to this range. The minimum flow rate is set by leakage through the valve and is seen to be about 2% of the nominal engine flow rate at the 95% speed line.

Figure (2.13) shows the valve transfer function (valve command to valve position). The valve has a bandwidth of about 310 Hz and a phase delay at this frequency of 165 degrees. Table (2.7) summarizes important information about the H/S valve.

Development of the H/S valve was done by Berndt [17] and readers interested in design details should refer to his work.

2.5.3 Inducer Bleed Port

During the Allison 250-C30 development program a localized dip in the surge line was encountered. Detailed analysis of the impeller inlet static pressures revealed that the surge line around the 80-85% speed line was influenced by inducer stall. The problem was resolved by adding an inducer bleed (see figure (2.14)) and a bleed valve at the compressor discharge that would operate at low speeds. The inducer bleed would bleed air out at low speeds, increasing the airflow into the inducer, reducing blade incidence angles and possibly reducing the boundary layer thickness on the shroud. At high speeds, air flows in through the bleed, reducing inducer choking. The inducer bleed was found to increase the compressor efficiency by 1.5 - 3.2 % between the 85 % and 100% speed lines [18].

Actuation was implemented by attaching the H/S valve to the inducer bleed port. The flow leaving the H/S valve traveled through a circumferential plenum to slots distributed around the circumference of the compressor shroud and into the flow path.

There were several reasons for using the inducer bleed for actuation. The first is that inducer injection was expected to be similar to inlet injection, which was shown to be a favorable means of actuation by McNulty. Another reason was that steady inducer inbleed at low speed and outbleed at high speeds was found to have a profound affect on compressor stability leading to the expectation that unsteady blowing result in further improvement. Finally, inducer bleed injection was easy to implement and did not require any permanent modifications, or disassembly of the engine.

2.5.4 Actuator Testing

As mentioned previously, it was expected that axisymmetric actuation was required well above the Helmholtz resonator frequency to stabilize the surge instability. The engine's Helmholtz resonator frequency was estimated to be at most 35 Hz (details presented in chapter 3) and a bandwidth of twice this frequency would be the minimum requirement for actuation. Note that bandwidth in the following discussion is used to refer to the point where the amplitude ratio changes by +/- 3db. The actuator bandwidth, therefore, may be limited due to amplitude roll off (-3db), or a resonance (+3db).

Work by Berndt had shown that actuator bandwidth may be limited by acoustic delays for long injectors, or by amplitude roll off for injectors with a "large" injector *volume to nozzle area ratio*. Figure (2.15) shows the model used by Berndt to predict amplitude roll off. The injector volume represents all the volume from the high speed valve to the inducer shroud slots. The nozzle area represents the area of the slots.

There were several concerns about the inducer bleed port actuation scheme that lead to its testing. The Allison injector had larger internal volume and longer flow paths than the injectors designed by Berdt and was expected to be bandwidth limited. Furthermore, the high speed valve injected air into the distribution plenum from one circumferential location, which could lead to non-axis-symmetric actuation.

Figure (2.16) shows the experimental setup for actuator testing and forced response experiments described in later chapters. Three hotwires were located at the exit of the inducer shroud slots 90 degrees apart. Figures (2.17) show the transfer function from valve position to the 3 hotwires. Figures (2.18) show the transfer functions from the velocity at 0 degrees to the velocity at 90 degrees and 180 degrees respectively.

Figure (2.17) shows that the bandwidth is about 230 Hz and is limited by an acoustic resonance occurring at 320 Hz. The fact that the bandwidth is limited by an acoustic resonance instead of amplitude roll off implies that the injector internal length (not *volume to injector area ratio*) is limiting the actuator bandwidth [17].

Figure (2.18) show that the velocity at 90 and 180 degrees from the injection location has a maximum velocity 60% and 70% of that seen at 0 degrees, respectively. The amplitude ratio is seen to be flat up to 350 Hz. This amplitude flatness, however, does not guarantee axis-symmetric actuation; one must also consider the phase difference as well. The actuation is seen to be clearly axisymmetric up to 100-120 Hz.

The above testing was done while the engine was off and the effect of flow through the compressor, and elevated temperatures observed during operation on the actuator bandwidth need to be considered. Flow through the compressor is expected to increase the back pressure observed at the inducer bleed slots (up to about the 95% speed). This increase may be assumed to have an effect similar to increasing the size of the inducer shroud slots (less resistance to flow) and as shown by Berndt, for an actuator limited in bandwidth by amplitude roll off, this would increase the bandwidth. The Allison injector was not limited in this manner (it was limited by a resonance at 320 Hz) and this is not expected to affect the observed bandwidth. The elevated air temperature in the plenum would raise the acoustic resonant frequency, increasing the injector bandwidth, and improving axisymmetric actuation.

2.6 Conclusions

Experiments reported in this thesis were done on an Allison 250-C30P; a 600 HP gas turbine engine with a single stage centrifugal compressor. This compressor had a pressure ratio of about 9 and corrected mass flow of about 6 lbm/s.

The engine was equipped with high frequency response pressure transducers at 4 axial locations throughout the engine. These were the inlet, vaneless space, scroll and combustor. The inlet and vaneless space axial stations had a circumferential array of 5 transducers each.

The engine was throttled towards the surge line using orifice plate inserts and water injection. The orifice plate inserts shifted the operating line towards the surge line and increased the turbine inlet temperature. Water injection was shown to throttle the engine towards the surge line by displacing flow coming through the compressor. Water injection was also seen to reduce the turbine inlet temperature, alleviating concerns about exceeding the maximum temperature limit.

Actuation for forced response testing was implemented by attaching a valve with a bandwidth of about 300 Hz to the inducer bleed port. Testing this actuator, while the engine was off, showed that actuation was axisymmetric up to 120 Hz. Above this frequency phase delays resulted in asymmetry even though the amplitude of velocity perturbations was constant up to almost 350 Hz.

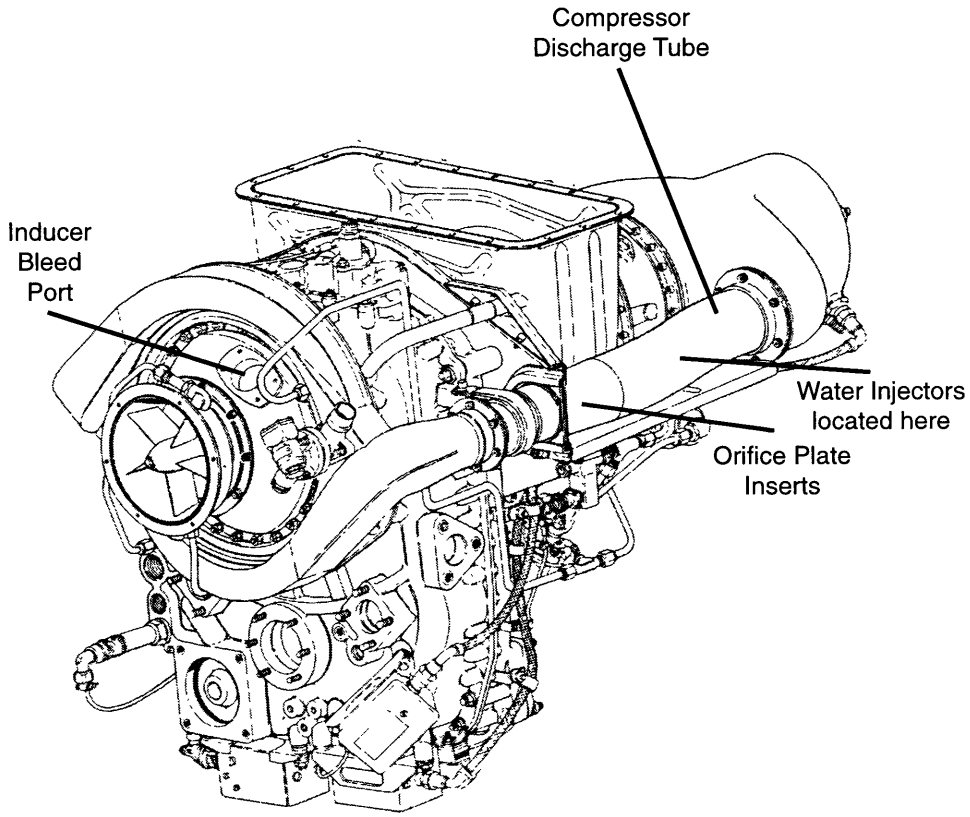

Figure (2.1) Allison 250-C30 gas turbine engine

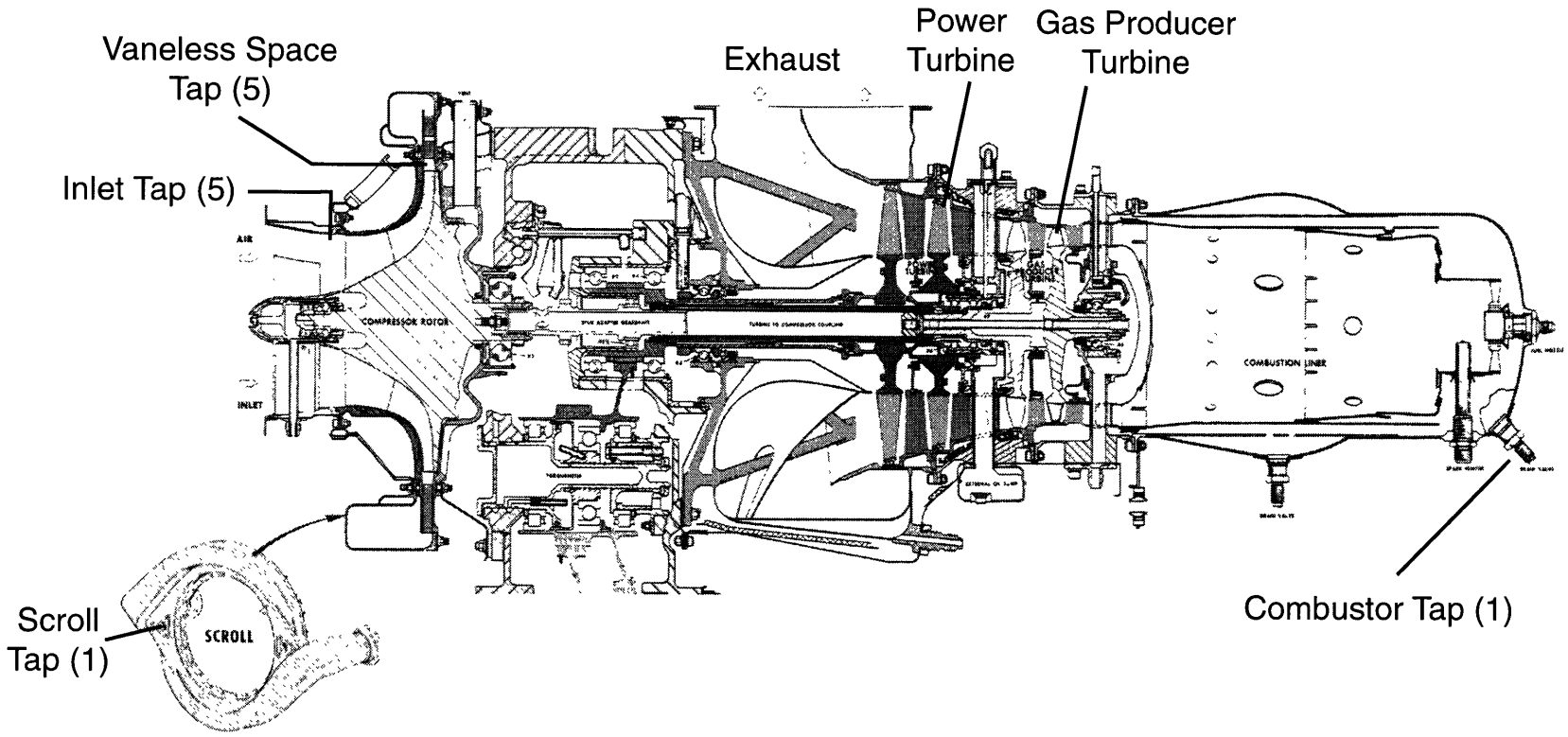

Figure (2.2) Pressure tap axial location (number of circumferential taps).

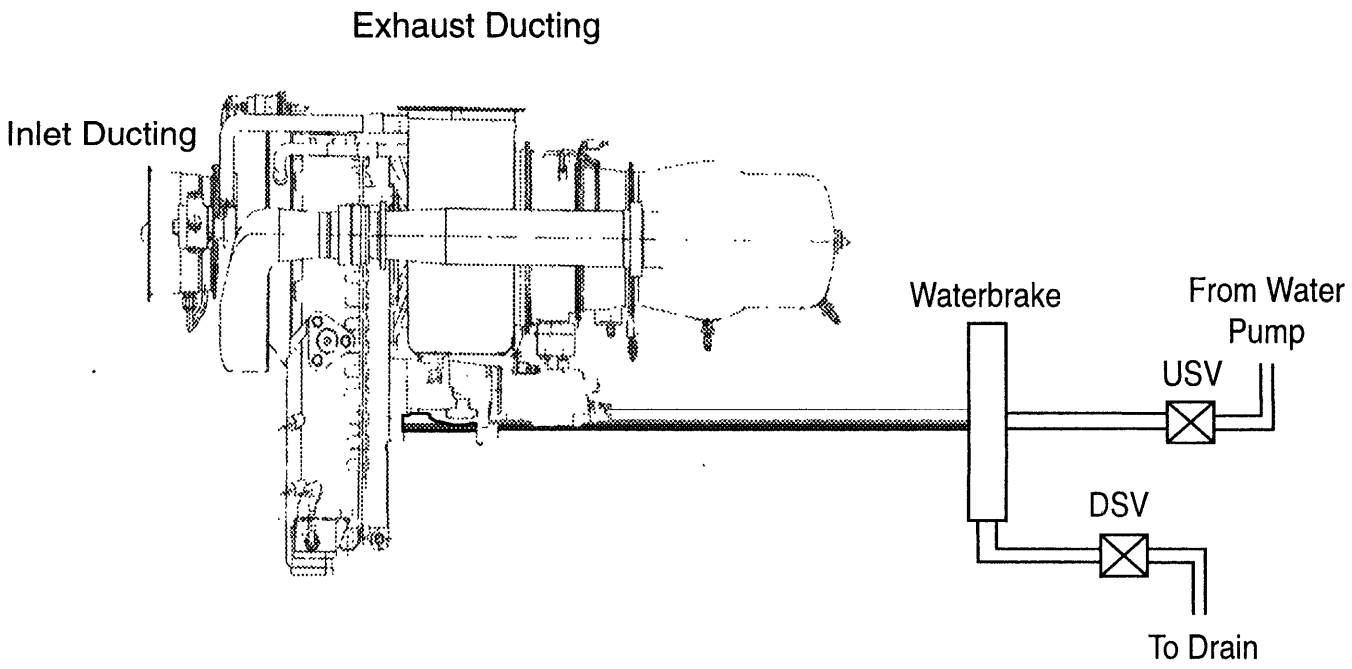

Figure (2.3) Engine and waterbrake setup.

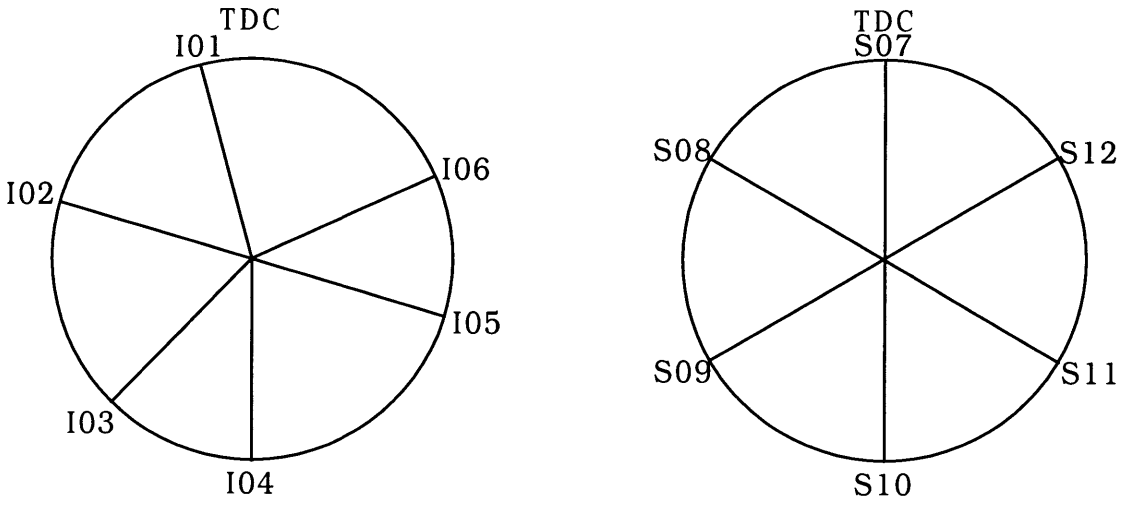

Figure (2.4) Circumferential location of the inlet & vaneless space pressure taps

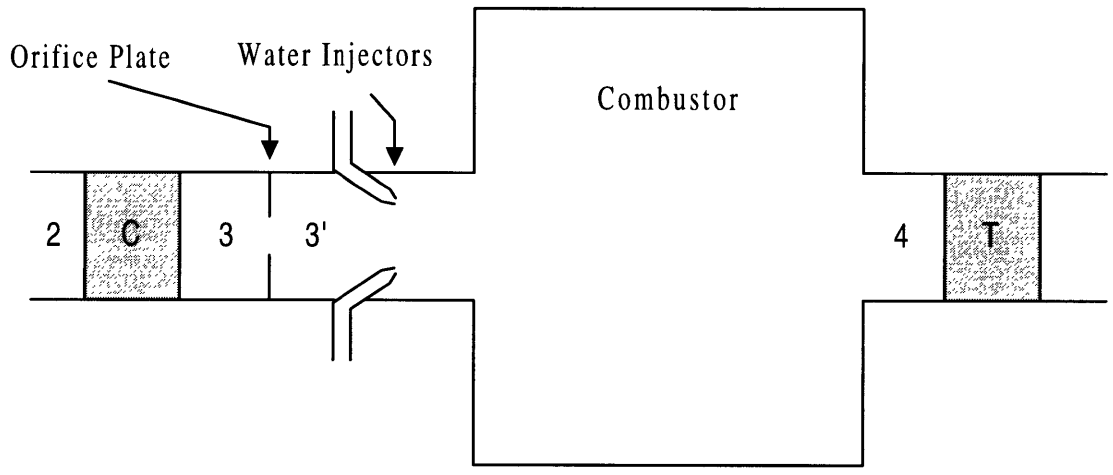

Figure (2.5) Schematic of Engine with Orifice Plates & Water Injection

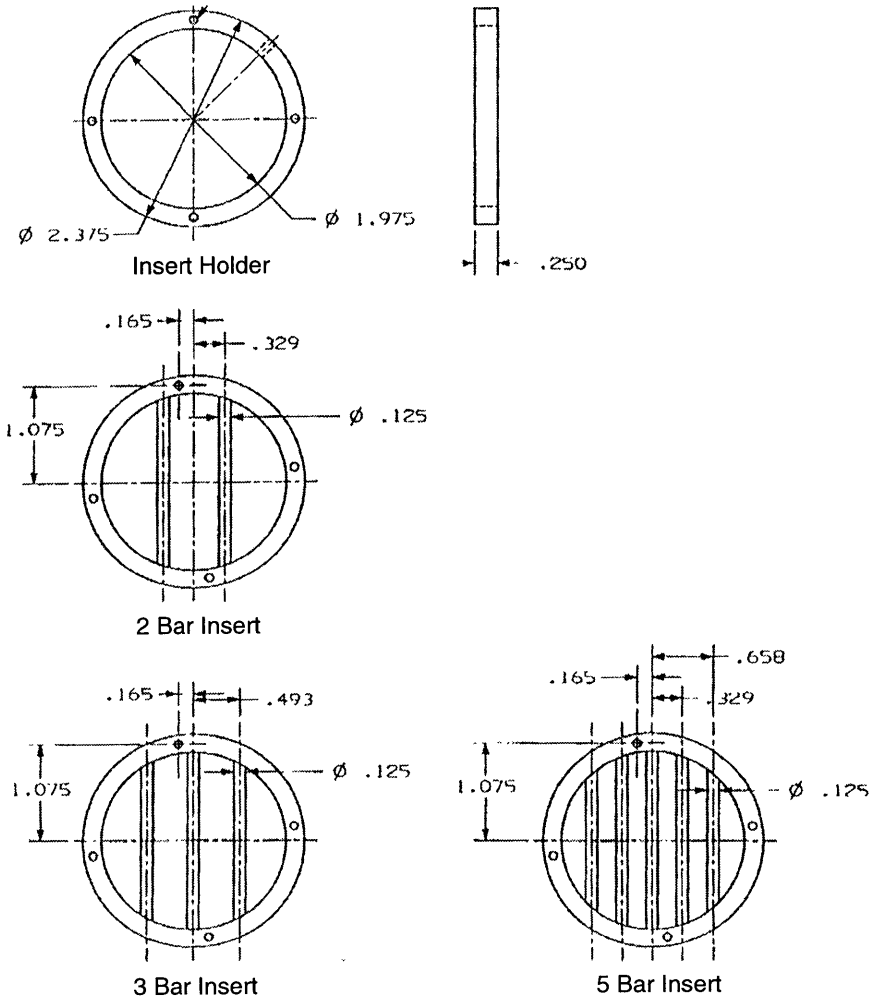

Figure (2.6) Inserts used in discharge tubes.

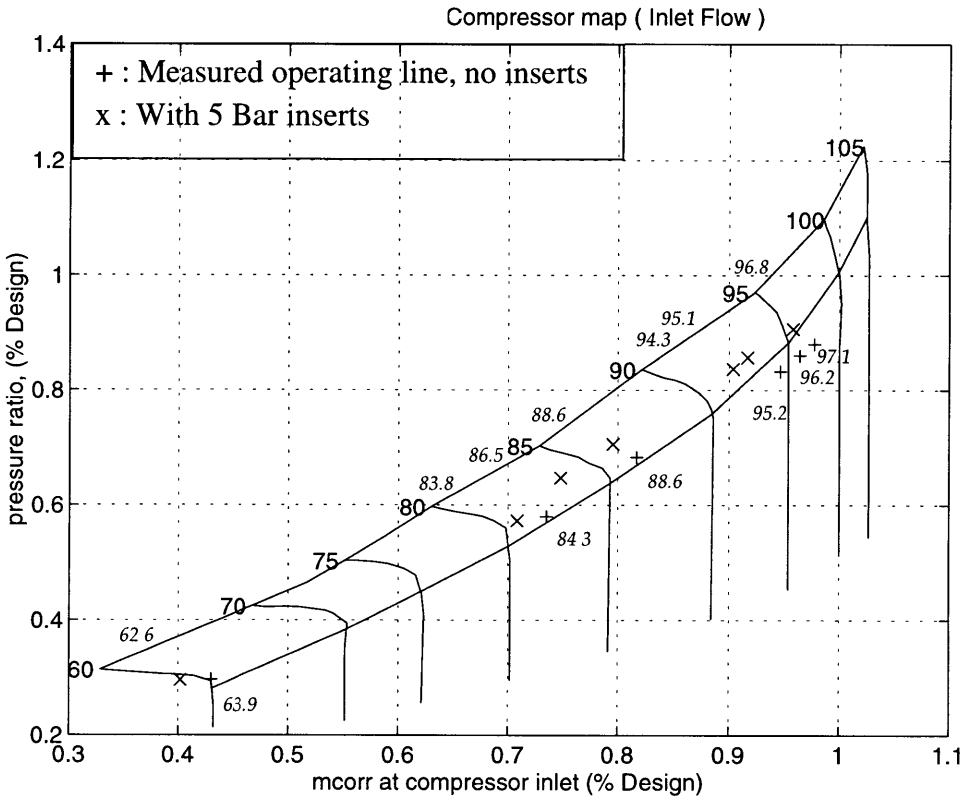

Figure (2.7) Nominal engine op-line compared to 5 bar insert.

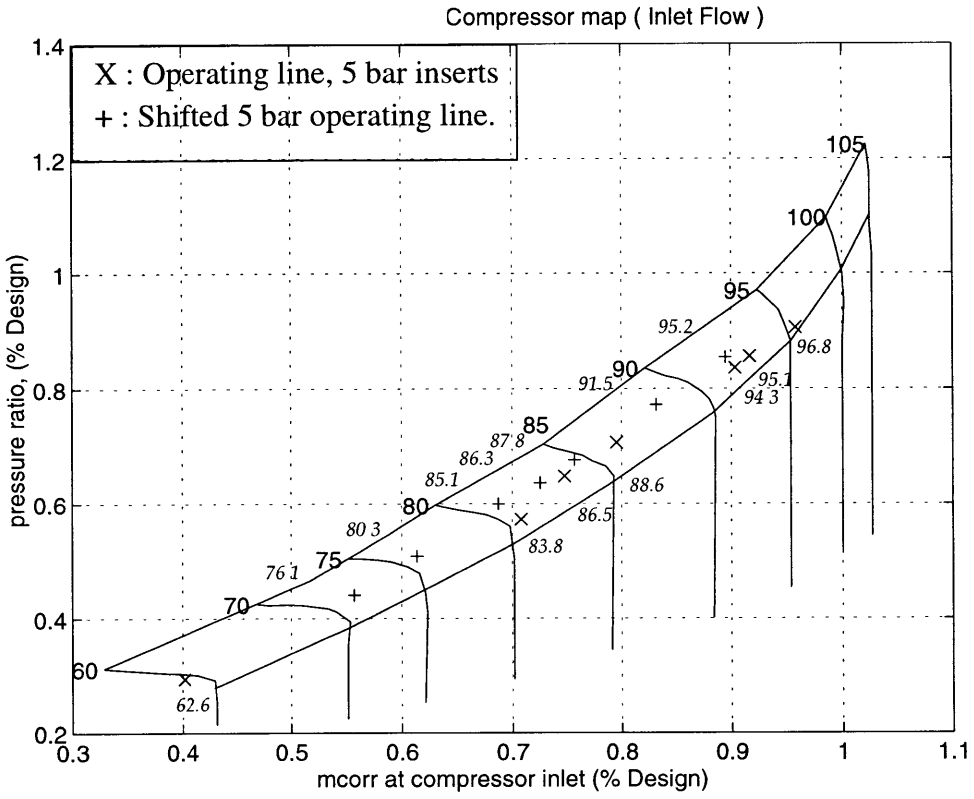

Figure (2.8) 5 bar insert initial operating line compared to the final shifted operating line.

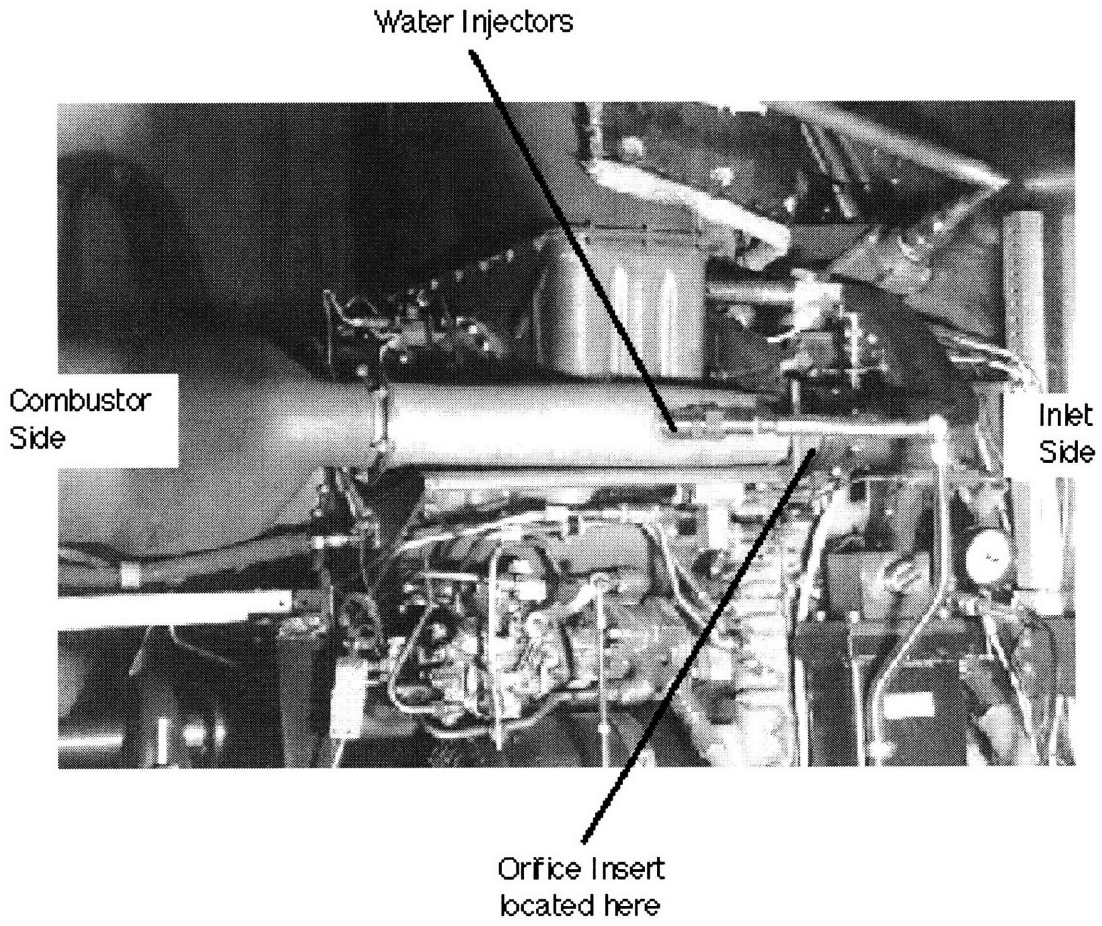

Figure (2.9) Discharge tubes modified to include orifice plates and water injectors.

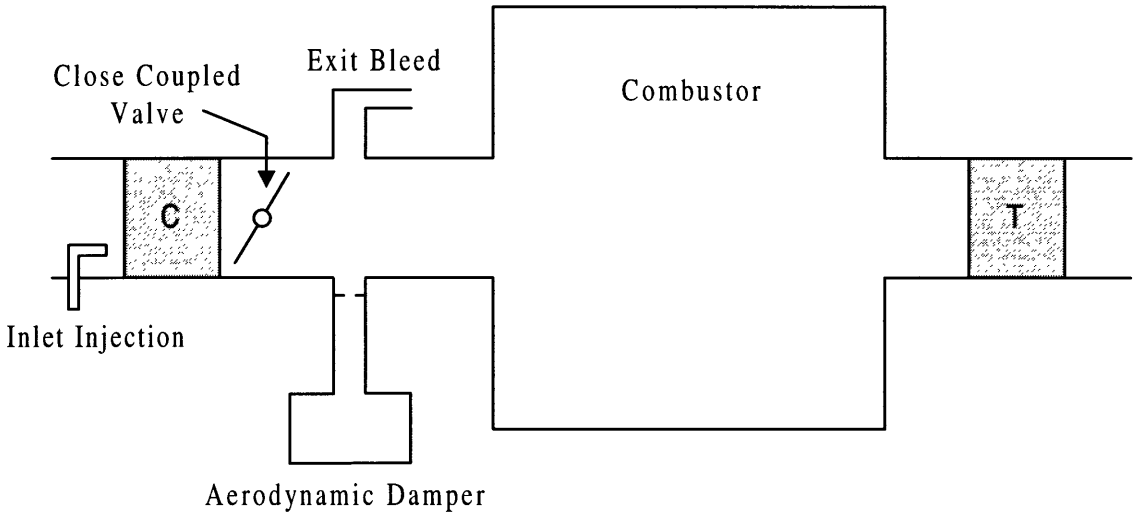

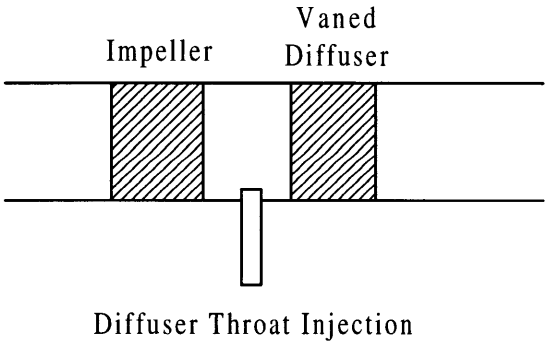

Figure (2.10) Actuation Methods considered by McNulty for the LTS-101.

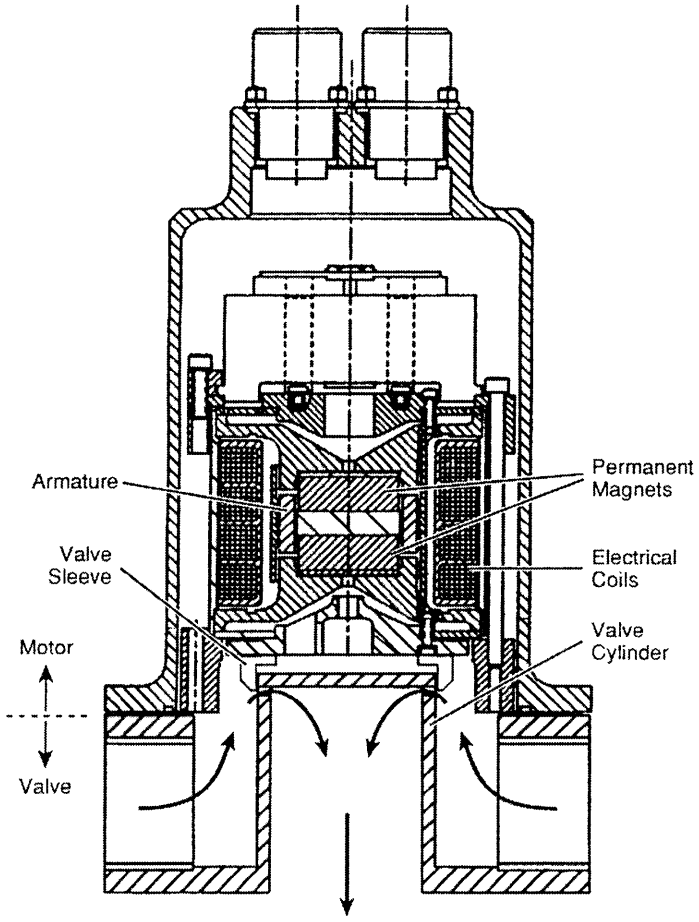

Figure (2.11) Schematic of motor & valve.

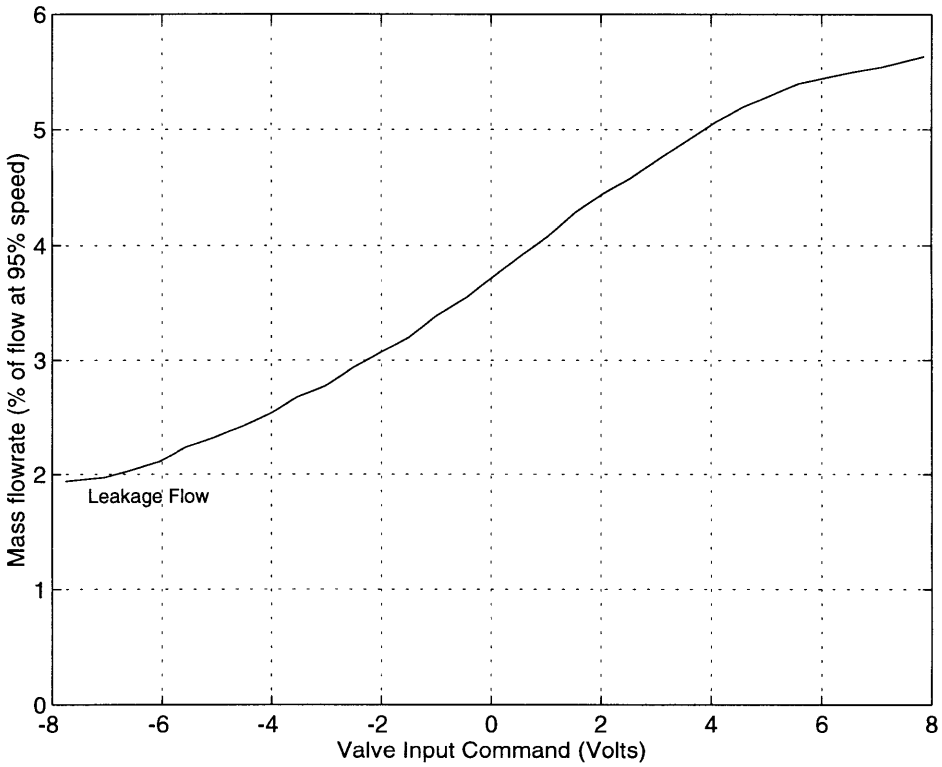

Figure (2.12) Steady massflow characteristic for high speed valve.

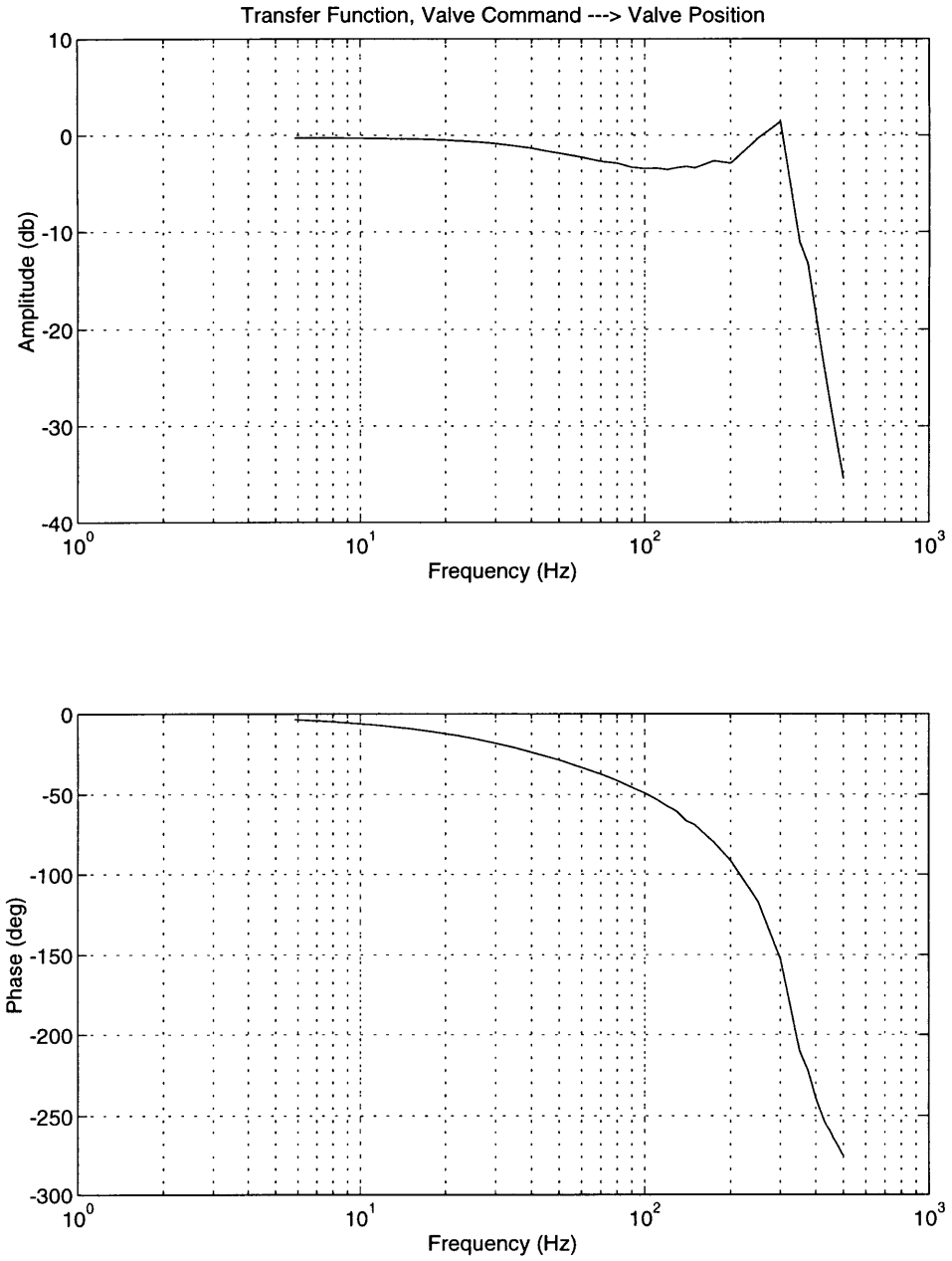

Figure (2.13) Transfer function; valve command to valve position.

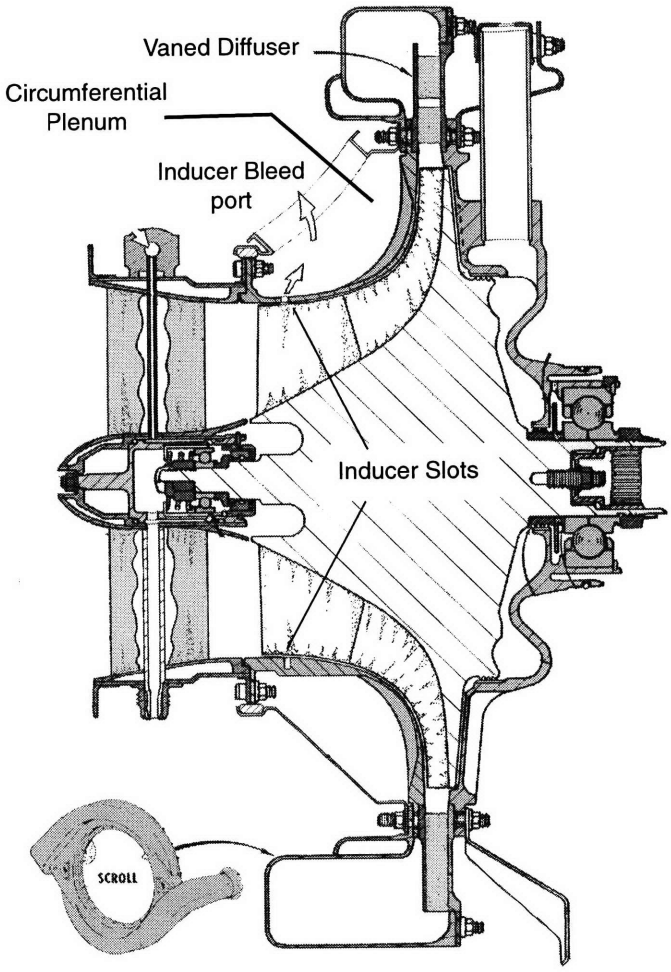

Figure (2.14) Inducer Bleed on Allison 250-C30.

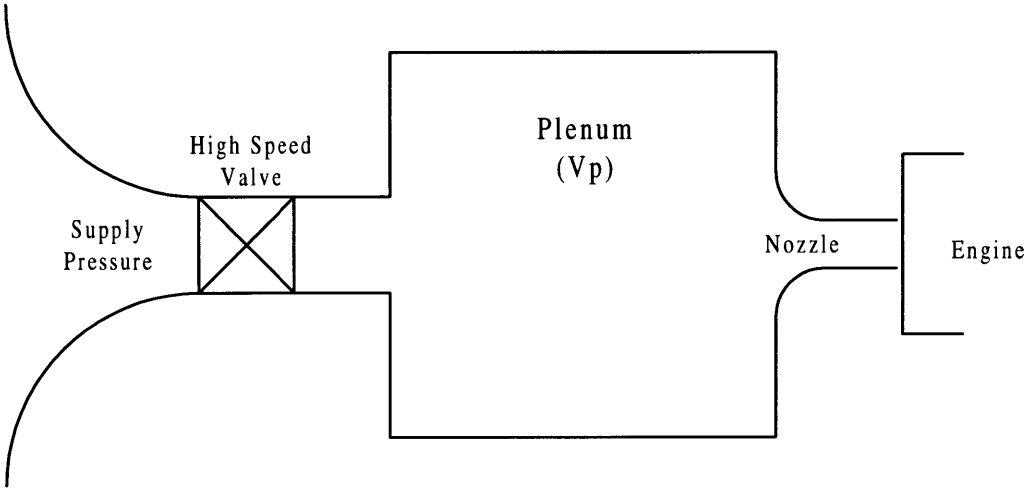

Figure (2.15) Model for the actuation system (from Berndt)

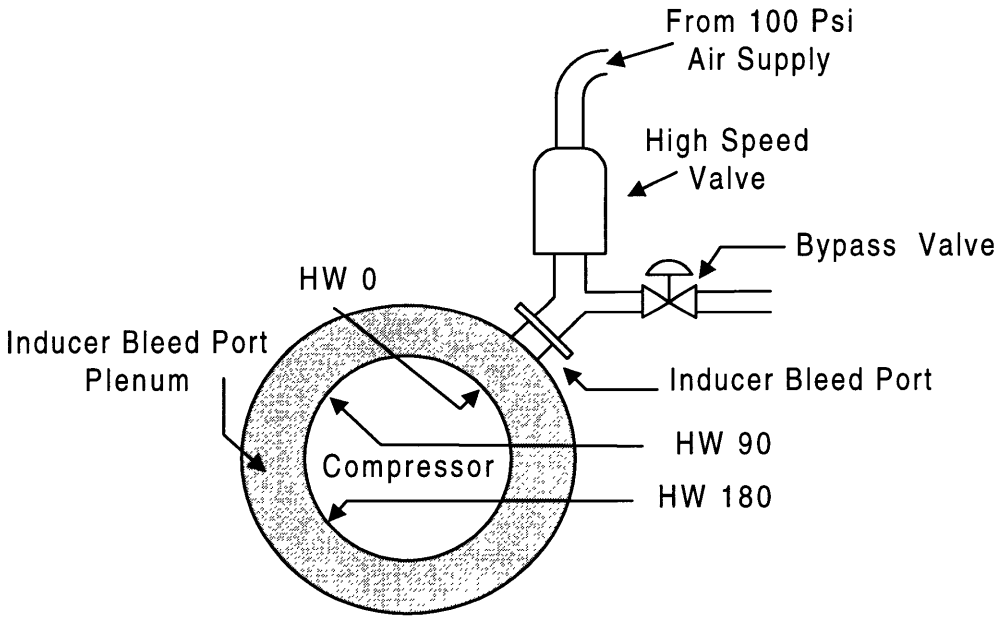

Figure (2.16) Inducer bleed port actuation setup. Hotwires were set up at 3 locations 90 degrees apart.

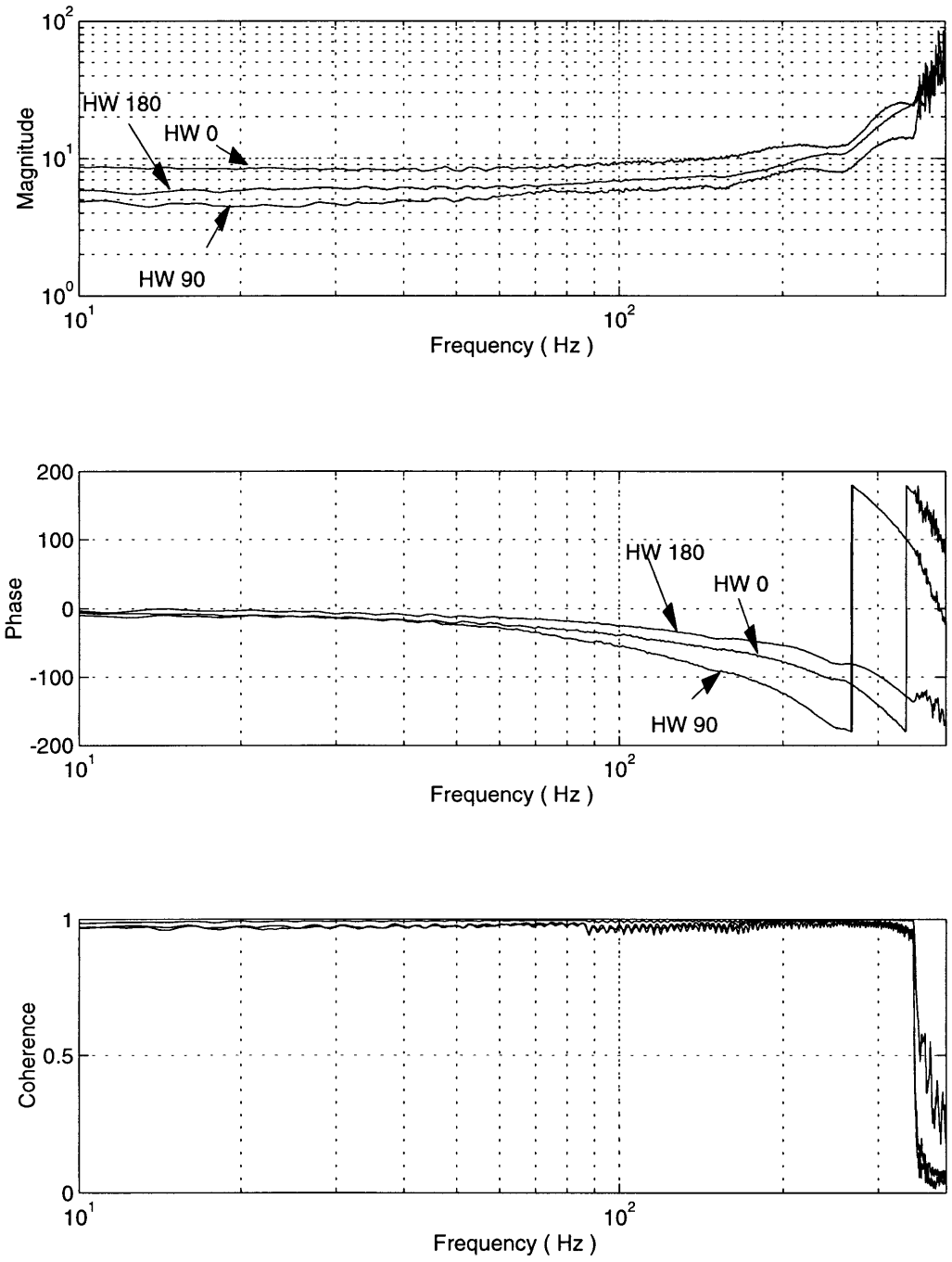

Figure (2.17) Transfer function; valve position to velocity at 0, 90 and 180 degrees from the actuation port.

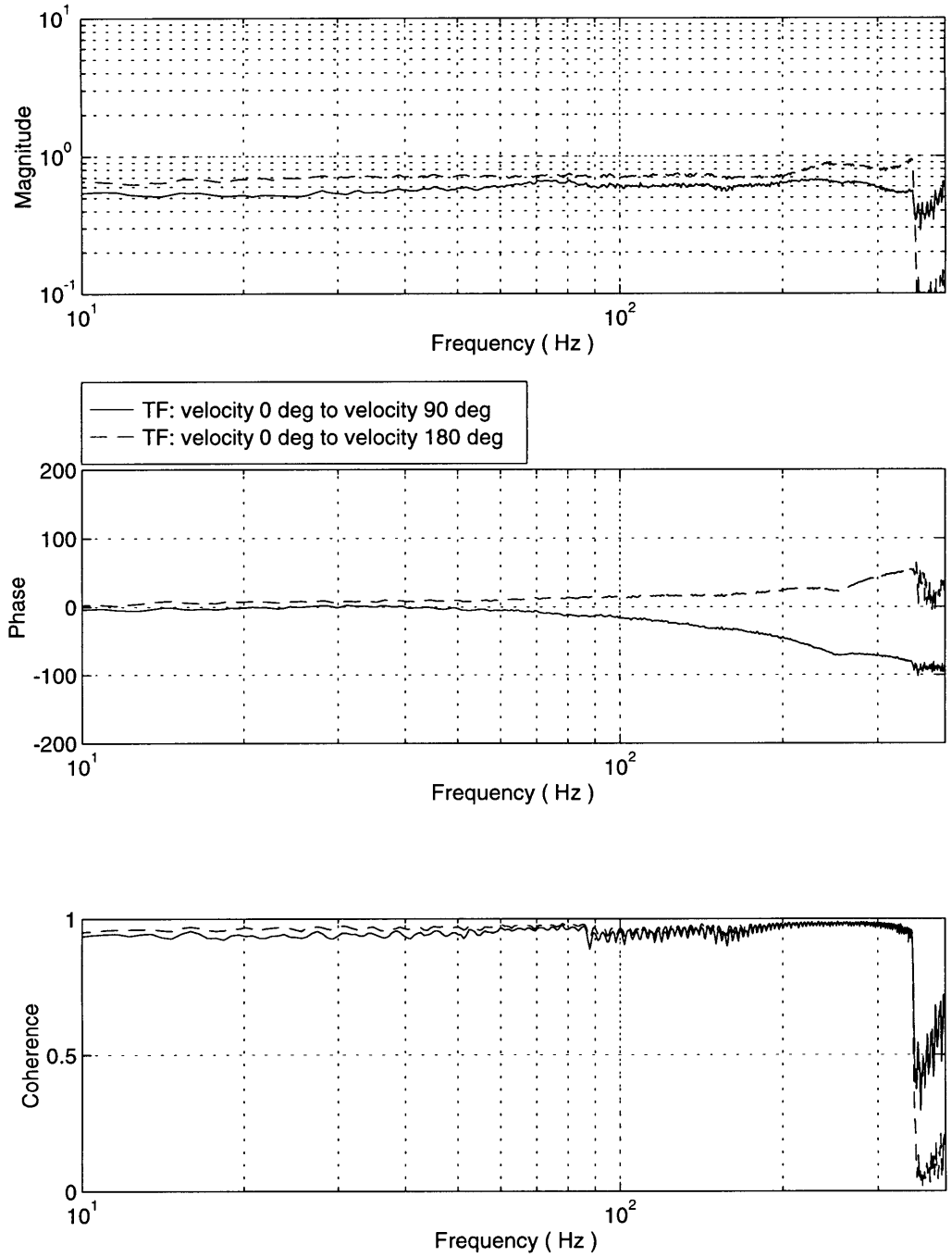

Figure (2.18) Transfer function; velocity at 0 degrees to velocities at 90 degrees and 180 degrees from the actuation port.

Chapter 3

Helmholtz Testing and The Engine's Spectral Content

3.1 Introduction

Compressor stability has long been known to be effected by the geometry of the engine, and not only the compressor design. In 1955 Emmons proposed that Helmholtz resonances may be used to explain mild surge oscillation observed in compression systems. Since then researches investigating low pressure ratio compressors have shown that the Helmholtz resonator mode may destabilize the compressor due to growing oscillations and that damping these oscillations may extend the stable compressor operating range [7,9].

The objective of this chapter is to present the unsteady pressure perturbations observed in the engine at various operating points, and to investigate the relationship between these perturbations and the engine's acoustic resonances (these include the Helmholtz mode). Section 3.2 covers the acoustic resonances measured while the engine was off. It uses the Helmholtz model and an acoustic duct model to predict the frequency shift that may occur during operation due to elevated temperatures.

Section 3.3 covers the unsteady pressure perturbations observed in the engine during operation. Engine data at various speeds along an operating line with the 5 bar inserts are investigated and the main peaks are determined. The effect of the 5 bar inserts, mean air injection and water injection are also investigated in this section. Section 3.4 compares the predicted resonances to those observed during engine operation.

3.2 Helmholtz & Acoustic Resonances

The Helmholtz resonance is estimated in section 3.3.1. Section 3.3.2 presents data illustrating the measured acoustic resonances in the cold engine. Section 3.3.3 discusses the differences between a cold and running engine, and estimates the running engine acoustic resonances.

3.2.1 Estimating the Helmholtz Resonance

The engine Helmholtz resonance was estimated using the dimensions of the engine. A reasonable bracket for this frequency was determined by reducing the engine to the model in various ways that are listed below (refer to figure (2.1) for an engine schematic).

Method 1 : Inertia : From the inlet duct to the end of the discharge tubes.

Volume : Combustor side tubes (discharge tubes connect to these on the combustor side) and the combustor.

Method 2 : Inertia : Same as Method 1.

Volume : Scroll, discharge tubes, combustor side tubes, and combustor.

Method 3 : Inertia : From the inlet to the combustor side tubes.

Volume : Diffuser, Scroll, discharge tubes, combustor side tubes, and combustor.

Table (3.1) lists the estimated dimensions of various engine components. All dimensions were estimated from the exterior and are expected to have an error band in the range of 20%. The term "sides of combustor" is used to refer to the volume from the end of the discharge tube to the combustor pressure vessel.

Table (3.1) Dimensions of engine components

Component	L/A (1/in)	Volume (in^3)	L (in)
Inlet Duct	0.227	158.3	6
Impeller + Vaneless space	0.371	81.9	5.1
Diffuser	0.455	26.1	5.1
Scroll	1.707	170.1	10.8
Discharge Tubes (2)	2.03	289.7	23.8
Sides of Combustor	0.142	283.0	5.5
Combustor	-	541.0	-

The Helmholtz resonator frequency was estimated using equation (3.1). The range was calculated to be from 27-34 Hz. Details of this calculation are provided in Table (3.2).

$$f_{Helm} = \frac{a_p}{2\pi}\sqrt{\frac{1}{V}\left(\frac{A}{L}\right)} \tag{3.1}$$

Table (3.2) Helmholtz resonator calculation

Case	L/A (1/in)	V (in^3)	Helmholtz frequency
I	4.79	824.0	34.3
II	4.79	1283.8	27.5
III	4.93	1310.0	26.8

Upon measuring the engines cold acoustic resonances it was realized that the Helmholtz model may not be sufficient in explaining oscillations observed in the running engine and other acoustic resonances may be important. Two issues of particular interest were determining the level of modelling required to predict the observed acoustic resonances, and determining the effect temperature changes may have on shifting these resonances.

A model composed of an acoustic duct and a lumped parameter plenum was developed to address the above issues (see appendix A). This model overestimated the resonant frequencies when the estimated engine dimensions were used. For a duct length 35% longer than previously estimated, however, it predicted a few of the frequencies within 10%. These frequencies will be presented in the following section along with the measured acoustic resonances.

3.2.2 Experimental Determination of Acoustic Resonances

Two methods were used to measure the cold engines resonant frequencies. The first used the inducer bleed port actuation to excite the system and monitored pressures in the scroll and combustor. The second method, " The Boombox Test ", used broad band noise to power a speaker placed at the face of the compressor.

Inducer Bleed Port Forcing: The setup used for this experiment was similar to that shown in figure (2.16). The high speed valve was used to modulate flow through the inducer bleed port to excite the engine. Figure (3.1) shows the transfer functions from valve position to the scroll and combustor pressures. Peaks are clearly seen at 20, 52, 75-78, 98, 151, and 250 Hz. Small peaks are also visible at about 135, 176 and 207 Hz.

During the above testing the high speed valve was not functioning properly and two mechanical resonances at 151 and 245Hz were observed. Figure (3.2) shows the transfer function from valve command to valve position. It was expected that these resonances resulted in the two large peaks seen at 151 and 250 Hz seen in figure (3.1) and it was, therefore, decided to test for acoustic resonances using a speaker.

Boombox Test: Power spectral densities (PSD) of noise generated by the speaker (measured using a solid state pressure transducer) and the corresponding combustor pressure tap response are shown in figure (3.3). The peaks at 20, 52, and 78 Hz are all clearly seen. Two additional peaks that were not previously observed occur at 11 and 400 Hz, and the ambiguous peaks at 151 and 244 Hz are now confirmed as acoustic resonances, and are not solely due to actuator effects.

Figure (3.4) shows PSDs of noise generated by the speaker and the response of a pressure transducer inserted into the discharge tubes through the water injection ports. This PSD shows the same peaks observed previously with the exception of one peak that is clearly seen at 100 Hz. The clear appearance of this oscillation in the discharge tubes may imply that it is a discharge tube duct resonance. Table (3.3) summarizes the observed resonant behavior and compares them to frequencies predicted using the acoustic duct model.

Table (3.3) Cold engine resonant frequencies. The Helmholtz resonator predicted 27-34.

Acoustic Duct Prediction	Observed Frequency	Observed in following figures
-	11	(3.3), (3.4)
22.2	20	(3.1), (3.3), (3.4)
-	52	(3.1), (3.3), (3.4)
81	75-78	(3.1), (3.3), (3.4)
-	100	(3.1, scroll), (3.4)
150	151	(3.1), (3.3), (3.4)
-	small peak at 176	(3.1, scroll)
220	small peak at 207	(3.1, scroll)
-	244	(3.1), (3.3), (3.4)

3.2.3 Estimating the Running Engines Resonant Frequencies

A running engine differs from a cold engine in many ways that may cause the above measured frequencies to shift. The simplest and easiest to model is the temperature change that occurs due to the compression and combustion processes. Other more complicated issues, that have not been addressed here, include boundary condition changes in the compressor and turbine, and the thermo-acoustic interaction known to be important in combustion instabilities.

In this section the simple Helmholtz model is used to predict the frequency shift that may occur when the duct and a fraction of the combustor volume are at the compressor exit temperature and the remaining fraction of the combustor is at an elevated combustion temperature. The process of assuming that all volume with significant compliance is at the turbine inlet temperature is shown to overestimate the frequency shift by 30%.

During engine operation at the 95% speed line, the compressor exit temperature is estimated to be 550 degrees K and the hot section of the combustor is about 1200 degrees K. For these temperatures the Helmholtz resonator, assuming all volume with substantial

compliance to be at 1200 degrees K, would predict the frequency to shift by a factor of 1.95. Observing engine data it was realized that the peaks shifted by less than this factor and more detailed modeling was pursued. Figure (3.5) shows a plenum with two regions having different temperatures. Two assumptions may be made at the boundary between the two regions, each providing a different expression for the Helmholtz frequency:

1. The volumes V_1 and V_2 may be assumed to be constant. This implies that the air traveling across the boundary into a new region immediately attains the temperature of that region.
2. The Mass in the hot region may be assumed to be constant, implying that the heat transfer time scales are slower than the oscillation time scales and negligable heat transfer occurs during the oscillations.

Assumptions made in both cases include isentropic compression and uniform pressure in the plenum, as well as slug flow in the duct (fluid traveling in unison).

Conservation of mass along with the momentum equation in the duct yield that the Helmholtz resonator frequency, for the first case mentioned above;

$$f_{Helm} = \frac{a_2}{2\pi}\sqrt{\frac{1}{V_{eq}}\left(\frac{A}{L}\right)} \tag{3.2}$$

Where

$$V_{eq} = V_1\left(\frac{a_2}{a_1}\right)^2 + V_2 \tag{3.3}$$

Figure (3.6) plots the frequency shift ratio (hot to cold) for the Allison engine using two estimated bounds on V_1 and V_2. The frequency shift factor is seen to be about 1.46 at 1200 degrees Kelvin and is seen to only vary from about 1.4 to 1.55 over a temperature range of 1000 degrees K.

The Helmholtz resonator frequency for the second case is given by:

$$f_{Helm} = \frac{a_2}{2\pi}\sqrt{\frac{1}{V_{eq}}\left(\frac{A}{L}\right)} \tag{3.4}$$

Where

$$V_{eq} = V_1\left(\frac{a_2}{a_1}\right)^2 + \frac{\rho_1}{\rho_2}V_2 \tag{3.5}$$

Equation (3.5), for $\gamma_1 = \gamma_2$, reduces to

$$V_{eq} = \frac{T_2}{T_1}(V_1 + V_2) \tag{3.6}$$

and the Helmholtz frequency may be written as

$$f_{Helm} = \frac{a_1}{2\pi}\sqrt{\frac{1}{(V_1 + V_2)}\left(\frac{A}{L}\right)} \tag{3.7}$$

The frequency shift ratio predicted using this model is 1.35. The frequency shift ratios, determined using the above two models, were applied to the experimentally determined resonances to estimate the hot engines resonant frequencies. Table (3.4) summarizes the predicted frequencies.

The acoustic duct model was also used to predict the frequency shift ratio. This ratio was similar to those predicted by the two previous models. It ranged between 1.36-1.43 for the first four acoustic resonances (see appendix A).

Table (3.4) Frequency shift due to temperatures at the 95% speed.

Observed Peaks (Cold Test)	First model shift ratio applied to observed peaks	Second model shift ratio applied to observed peaks
11	16	14.7
20	29.2	26.8
52	76	70
75-78	111	102
100	146	134
151	220	202
(176)	257	235
(207)	302	277
244	356	327
400	584	536

3.3 Spectral Analaysis

Spectral analysis of pressure perturbation during engine operation are presented in this section. It is organized into four subsections; section 3.4.1 covers the engine's spectral content along the operating line with the 5 bar inserts. Section 3.4.2 and 3.4.3 deal with the effects of the 5 bar inserts, mean air injection, and water injection on the engine's spectral content. Section 3.4.4 investigates the nature of peaks observed to effect compressor stability.

Data presented in the following sections for the inlet and vaneless space axial locations are averages of multiple transducers and represent the zeroth mode.

3.3.1 Spectral Analysis Along the Operating Line with 5 Bar Inserts

PSD plots of engine pressures at the inlet, vaneless space, scroll, and combustor are presented in Figures (3.7-3.10). They are organized according to corrected speed and vary from 71.3% - 95% N_{1cor}. Trends for engine data were determined for the speeds shown as well as other speeds (63.5, 75.7, 79.8, 88.8, 91.4, 92.6) that were not included because no significant change was observed. The major trends observed over the engine's operating range are summarized below and a detailed discussion about the nature of these peaks will be covered in section 3.4.4. To simplify referring to the corrected speeds they will be rounded down to the nearest integer.

Inlet Tap:

1) A clear peak at 24-30 Hz is visible at speeds ranging from 84% to 86% with the highest peak occurring at the 85% speed line. Its frequency at the 85% speed is 24-26 Hz. This peak was observed throughout the engine and will not be repeated in the following sections.

2) A peak at 110-140 Hz is seen at speeds ranging from 71% to 82%. The amplitude of this peak is seen to decrease until it is no longer visible after the 82% speed.

3) A small peak at about 330 Hz is seen at the 71% speed but does not occur at any other speed.

Vaneless Space Tap:

1) The 110-140 Hz peak is seen at speeds ranging from 71% to 82.8% with its maximum amplitude occurring at the 71% speed.

2) The 330 Hz peak, observed at the inlet, is also seen at the vaneless space while at the 71% speed.

Scroll Tap:

1) A peak occurring at 100 Hz at idle and 110-140 Hz at higher speeds is clearly observed at the scroll tap over the complete speed range.

2) A peak at 330-340 Hz appears at the 71% speed line.

3) A high frequency peak ranging from 480 Hz at idle to 500 Hz at the 95% speed is clearly visible.

Combustor Tap:

1) The 110-140 Hz peak is observed at the combustor in the idle[1] to 84% speed range. This peak is always smaller than the peak observed in the scroll.

2) A peak at 300-320 Hz appears over most the speed range. It is most visible at the 71.3% to 75.7% speed range and at the 95% speed.

3) A high frequency peak ranging from 430 Hz at idle to 500 Hz at the 95% speed is observed.

4) A small peak that does not increase in amplitude is seen to shift from 820 Hz at idle to 870 Hz at the 95% speed.

Table (3.5) summarizes the main peaks observed over the speed range. Five main peaks were identified and the nature of these peaks will be discussed following presentation of spectral data at the 95% speed.

---

[1] Idle is the operating point the engine goes to at start up, prior to loading the engine. The N_{1cor} speed at idle is 65%.

Table (3.5) PSD peaks observed in engine at various speeds.

Frequency (Hz)	Inlet	Vaneless Space	Scroll	Combustor
24-26 Hz	Large at 85%.	Same	Same	Same
110-140	Seen in the range of 71%-82%	71%-75%, maximum amplitude at 71%	Seen at all speeds. No growth observed	Seen at all speeds. Largest at 71%.
330	Seen at 71% speed.	Seen at 71% speed.	Occurs at 330 Hz, only at 71% speed	Seen at all speeds. Largest amplitude at 71%
High Frequency	-	-	480-500 Hz seen at all speeds.	430-500 Hz. Small peak at 820-870 Hz
Compressor Forcing	Broad peak that does not match N1 exactly.	-	-	-

3.3.2 Effect of 5 Bar Inserts

Figure (3.11) and figure (3.12) present PSDs of engine pressures with and without the orifice inserts at the 95% speed line. The inserts were found to reduce the power spectral density of peaks occurring at 10-16 Hz, 70 Hz and 135 Hz (110-140 Hz peak).

The 10-16 Hz peak was mainly observed in the scroll and combustor pressure taps. It was observed to increase in amplitude as the N_1 shaft speed was increased. The inserts reduced the power spectral density by about 20 db. The peak at 135 Hz was observed throughout the engine when operated without the inserts. The inserts were found to significantly reduce the spectral power of this oscillation also. The reduction in spectral power may be due to increased damping caused by the orifice inserts (unsteady effect) or due to the change in the steady operating point that occurs when the they are included. Namely, the orifice inserts were shown to shift the operating point towards the surge line (chapter 2), and the new operating point may be more damped to such oscillations.

The peak at 70 Hz was only observed at one inlet transducer during operation without the 5 bar inserts. The source of this peak is not known and it does not appear in later runs.

3.3.3 Effect of Closing the Inducer Bleed Valve, Air Injection and Water Injection

Figure (3.13) shows the compressor operating map based on inlet mass flow and indicates the points at which data analyzed in this section was taken. The plot is marked with numbers that correspond to the following cases :

(1) 95% speed operating point with the 5 Bar inserts.
(2) Closing the inducer bleed valve.
(3) Mean air injection, 4% of engine flow rate. All the flow rates will be referenced to the engine corrected flow rate at the 95% speed line with the inserts.
(4) Water injection, 4% of engine flow.
(5) Water injection, 5.4% of engine flow.

Comparing PSD plots for cases 1-3 showed that no significant change occurred due to closing the inducer bleed bypass valve and mean air injection, therefore only one data set will be presented, and it will be used for comparison to the water injection cases. Figures (3.14-3.17) present the PSD plots for cases 3-5.

The 110-140 Hz peak was observed to increase and shift to lower frequencies as the water injection rate was increased. Significant growth of this peak was accompanied by appearance of a large 80 Hz oscillation only observed at the combustor tap. This is seen in the transition from point 4 to point 5, and occurs for water injection levels in the range of 5.4 - 6% of engine flow. Damping of frequencies above 130 Hz was also observed to occur during this transition.

The 110-140 Hz mode was first observed as a broad peak centered around 140 Hz. This peak continued to shift as the water injection flow rate was increased until it reached 120 Hz near the surge point. Immediately prior to surge bursts of high amplitude oscillations, discussed in later sections, were observed at frequencies as low as 100 Hz.

Once the 80 Hz peak appears it is not observed to further increase as the water injection flow rate is increased to 7.2% of engine flow. This oscillation may be due to the water pump's piston cycle which was estimated to occur at 86 Hz.

3.3.4 Nature of Peaks

The main peaks observed during operation are further analyzed in this section. The 24-26 Hz peak was observed to be axisymmetric at the inlet. The vaneless space, for the most part, was observed to be axisymmetric with excursions visible at all times.

The 110-130 Hz oscillation was also observed to be axisymmetric at the inlet, but no clear pattern could be identified at the vaneless space for operating points that were far from the surge point. As the engine approached surge a pattern became visible; half the annulus was observed to oscillate 90 degrees out of phase compared to the other half.

The 330 Hz frequency was found to be a rotating mode. It rotated at 58-61% of the N_1 shaft speed.

24-26 Hz Peak:

Figure (3.18) shows the inlet and vaneless space time traces. These were digitally filtered through a lowpass filter with the cutoff set at 50 Hz. The inlet pressure fluctuations are clearly observed to be axisymmetric. The vaneless space fluctuation are more difficult to characterize. For the most part, they are observed to be axisymmetric, but deviations occur frequently, and there is always a trace that does not align with the other traces.

Comparing the inlet traces to the vaneless space traces shows that they are 180 degrees out of phase. This implies that an increase in inlet flow (low inlet pressure) is accompanied by a pressure increase in the vaneless space.

110-140 Hz Peak:

The 110-140 Hz oscillation was observed to be axisymmetric at the inlet, but no clear pattern could be identified for the vaneless space pressure traces over most the engine's operating range. One exception to this occurred prior to surge at high water injection levels; half the compressor annulus was observed to oscillate 90 degrees out of phase compared to the other half

Figure (3.19) shows the pressure traces for the inlet and vaneless space taps during burst of high amplitude oscillations occurring prior to surge. The bottom 3 traces in the vaneless space are found to be in phase. These traces were taken at pressure taps located 0, 60 and 120 degrees CCW from TDC (refer to figure(2.4)). The top two traces, taken at 240 and 300 degrees, are observed to lag the bottom 3 traces by about 90 degrees. This trend is fairly consistent in regions were burst of high amplitude oscillations are observed. Further analysis of presurge behavior will be covered in chapter 4.

330 Hz Peak:

Centrifugal compressors are prone to inducer stall at low speeds. A rotating mode was observed on the Allison engine at the 71% speed.

Figure (3.20) and figure (3.21) show the PSDs of the 1st and 2nd harmonics. The first inlet and vaneless space harmonic is observed to rotate at 330 Hz, while the second harmonic is observed to rotate at 350 Hz.

Figure (3.22) shows time traces for the inlet and vaneless space. The pressure wave is clearly observed to rotate and its speed is in the range of 58-61% of the N_1 shaft speed.

High Frequency Peaks:

There are two high frequency peaks that will be discussed in this section. The first is the 500 Hz peak observed at the scroll, and in later experiments in the combustor. The second is the inlet peak that usually appears near the N_1 shaft frequency but rarely matches it exactly.

The 500 Hz peak was observed at the scroll over the complete speed range and in all engine runs. It varies from about 480 Hz at idle to 500 Hz at high power, and is expected to be a high frequency resonance.

A peak in the range of 450-500 Hz was observed at the combustor tap after its modification. This tap was modified to prevent water injected into the discharge tubes from reaching the pressure transducer. Immediately following this modification the 450-500 Hz peak was clearly observed (compare figures (3.10) and (3.12)) and a broad peak near the compressor forcing could no longer be seen. Estimating the pressure taps natural frequency from Borror's tap dynamics experiments [14] predicted a resonance at 520 Hz.

In conclusion, there may be a 500 Hz resonance that is observed at the scroll pressure tap. This resonance does not increase as the engine is throttled towards surge and is not observed to influence engine stability.

A broadband peak near the N_1 shaft frequency appears in the inlet tap's spectral content. At low speeds this peak is observed above the N_1 shaft speed, while at high speeds it is observed below it. The reason for this behavior is not clear.

3.4 Comparison of Cold and Hot Resonances

Many cold engine resonances and hot engine PSD peaks have been observed. Table (3.6) summarizes the predicted hot engine resonances and peaks consistently observed during engine operation. The 110-140 Hz peak was found to reasonably correspond to two predicted resonances and is therefore listed twice.

No clear explaination for the 10-16 Hz mode is known. Modeling showed that a duct length at least 3 fold the length estimated for the engine would be required to predict such a frequency and therefore it is probably not the Helmholtz mode. The peak may be due to out of phase oscillations in the two discharge tubes which would resonate at a lower frequency than the Helmholtz mode. The Helmholtz mode is the 24-26 Hz oscillation.

A general comparison between the predicted resonances and observed PSD peaks shows that the hot prediction over estimates resonances in the running engine.

Table (3.6) Comparison between observed and predicted peaks.

Frequency measured (cold)	Frequency predicted (hot)	Peaks observed in the PSDs during engine operation (Hz)	Observed at
11	14.7-16	10-16	All speeds prior to inserting the 5 bar inserts.
20	26.8-29.2	24-26	85% speed line with 5 bar inserts
75-78	102-111	110-140	All speeds prior to inserting 5 bar inserts.
100	134-146		Growth with water injection.
244	327-356	320	This was observed in the scroll and combustor at various speeds with the 5 bar insert. This is not the rotating disturbance seen at the 71% N_{1cor} speed.
400	536-584	500	Only observed at scroll tap

3.5 Conclusions

Chapter 3 has shown that spectral growth occured at 3 frequencies during engine operation; These frequencies were 24-26 Hz, 110-140 Hz and 330 Hz.

The 24-26 Hz oscillation was the Helmholtz resonator mode with flow at the inlet and vaneless space axisymmetric. This mode was found to increase near the 85% speed line.

The 110-140 Hz oscillation was observed to increase as the compressor was throttled towards the surge line at the 95% speed. Although inlet flow was axisymmetric, no clear structure was observed in the vaneless space far from the surge point. Near surge, however, oscillations in half the annulus were 90 degrees out of phase compared to the other half.

The 330 Hz mode was observed to be a rotating mode. The 1^{st} and 2^{nd} harmonics were rotated at a speed of 58-61% of the N_1 shaft speed.

Comparing the 24-26 and 110-140 Hz oscillations to frequencies predicted from the engine's cold resonant behavior showed that the prediction overestimated the frequency shift by 10%. Modeling showed that assuming all volume with significant compliance to be at an elevated combustion temperature overestimates the frequency shift.

Chapter 3 also presented data showing the effect of the orifice insert and water injection on the engines spectral content. The power spectral density of two peaks at 10-16 Hz and 135 Hz was seen to drop upon including the inserts. This drop may be due to damping added by the orifice inserts, or due to increased damping caused by a shift in the steady state operating point. The peak at 10-16 Hz never reappeared while the 135 Hz peak was observed to increase with water injection.

Aside from growth in the 135 Hz peak, that occurred as the compressor was throttled towards surge, water injection above a level of about 5.4 - 6% of engine flow was found to significantly dampen combustor spectral content above 130 Hz and result in a very large peak at 80 Hz. This peak did not increase further with water injection and may be due to the high pressure pump's piston cycle.

Chapter 4 presents the engines surge data and further discusses the role of the above mentioned oscillations on compressor stability.

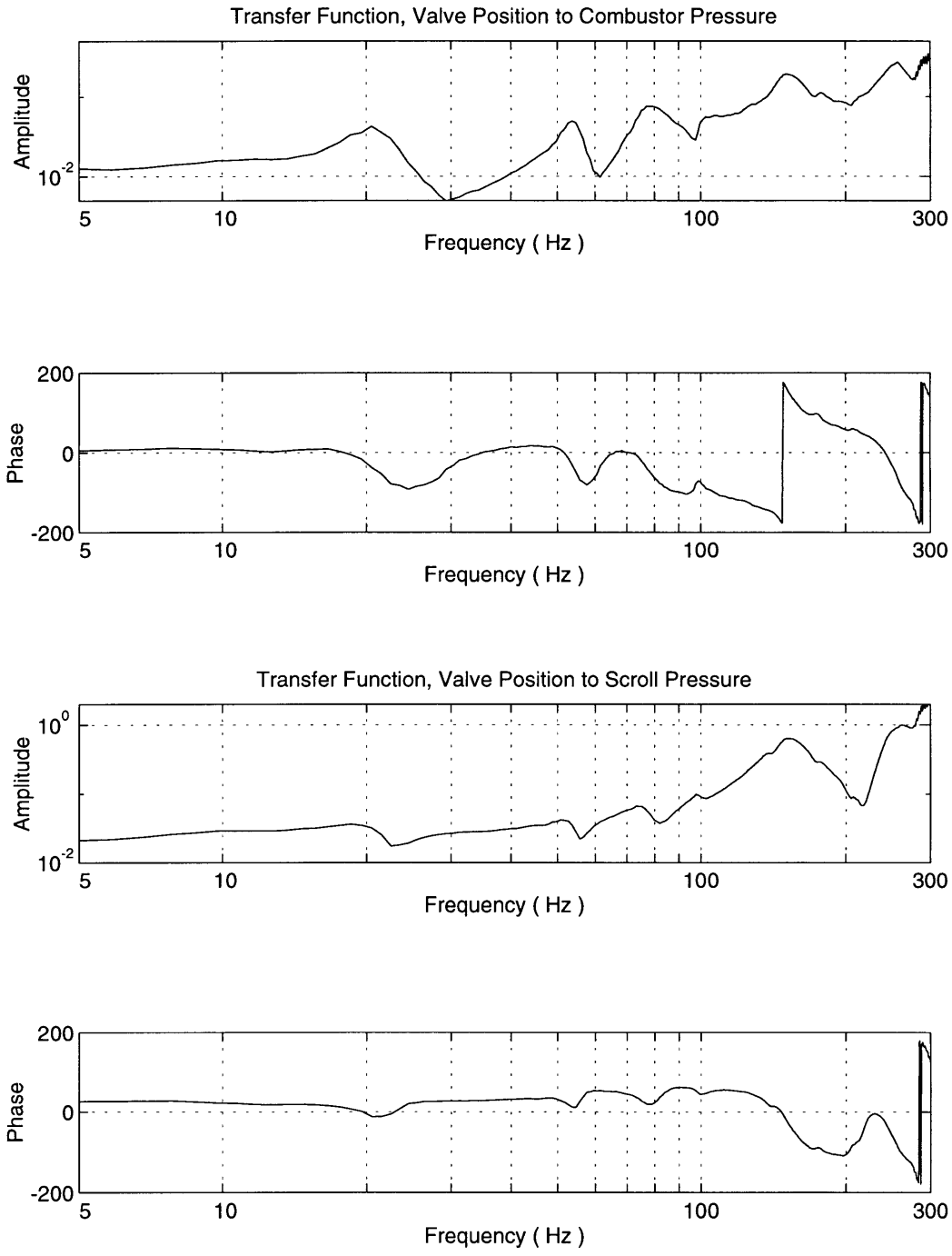

Figure (3.1) Transfer functions: Valve position to scroll and combustor pressure.

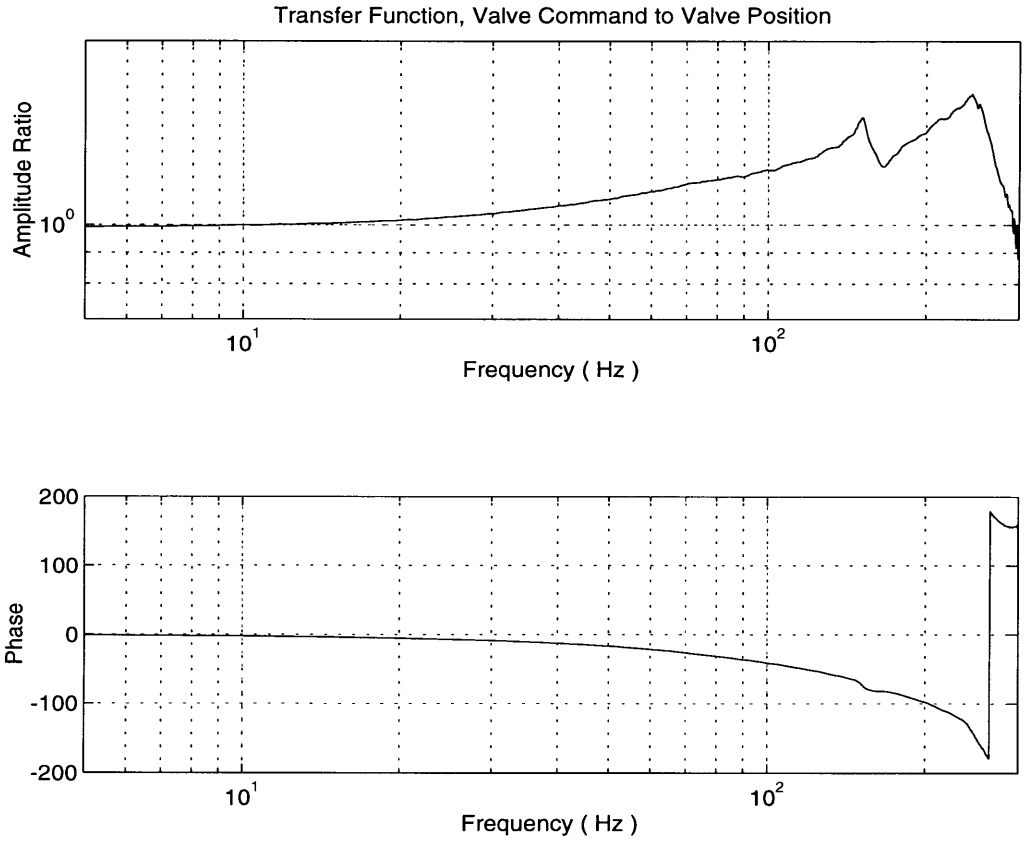

Figure (3.2) Transfer function: Valve command to valve position.

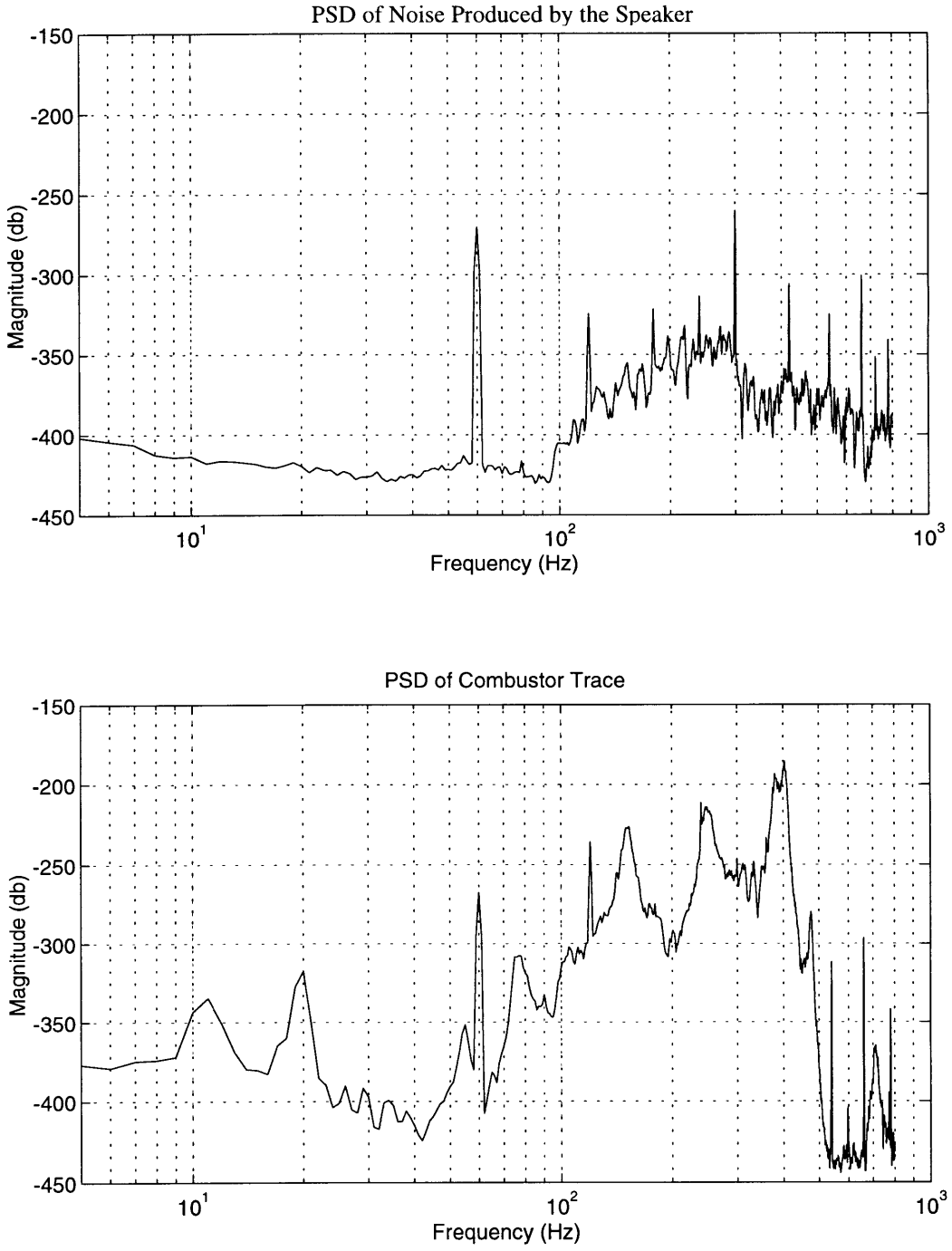

Figure (3.3) PSD of white noise and combustor pressure.

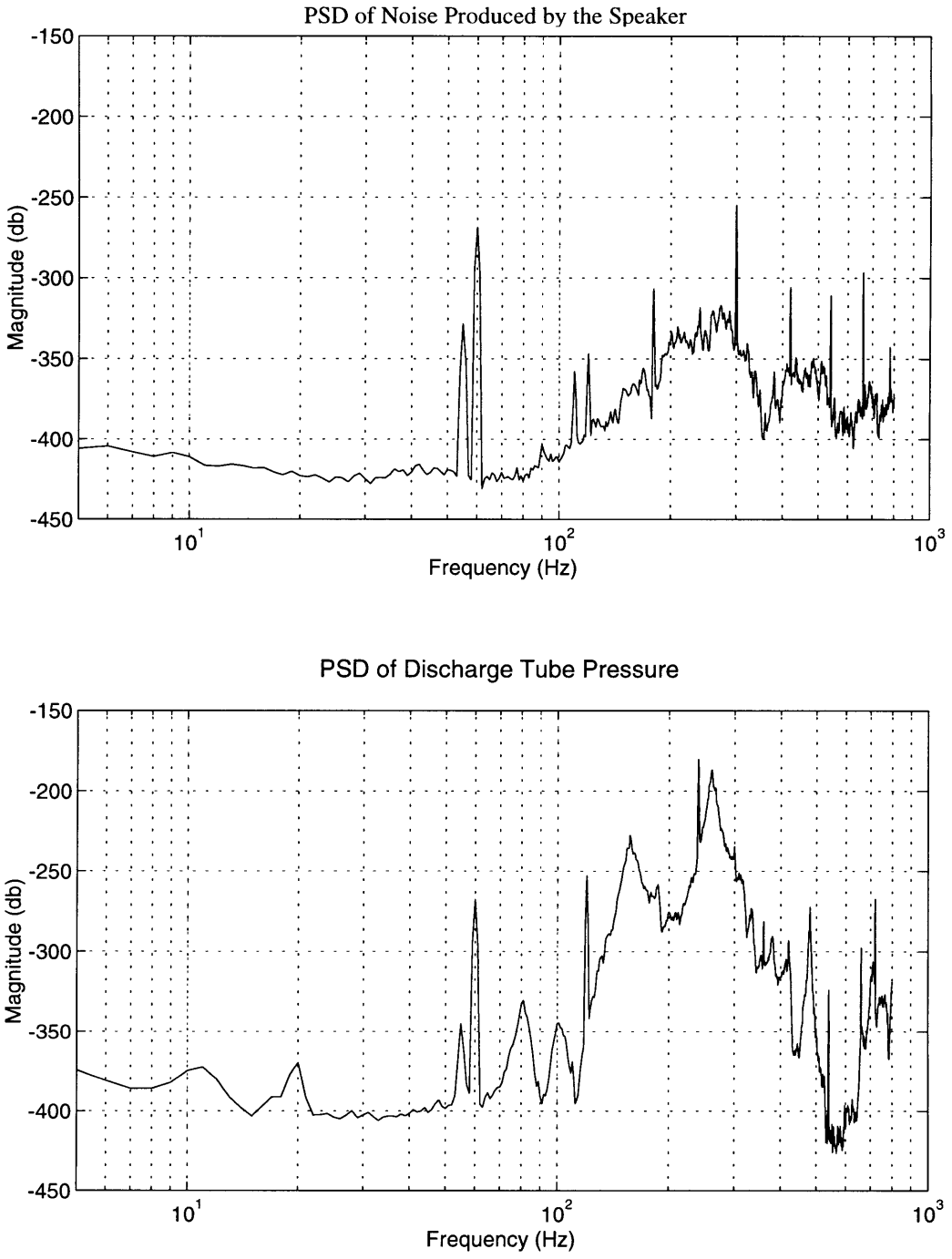

Figure (3.4) PSD of white noise and discharge tube pressure

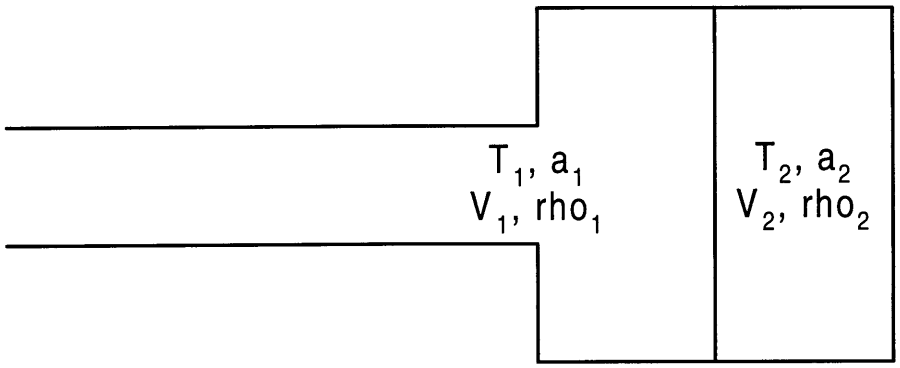

Figure (3.5) Model of plenum with two separate temperatures.

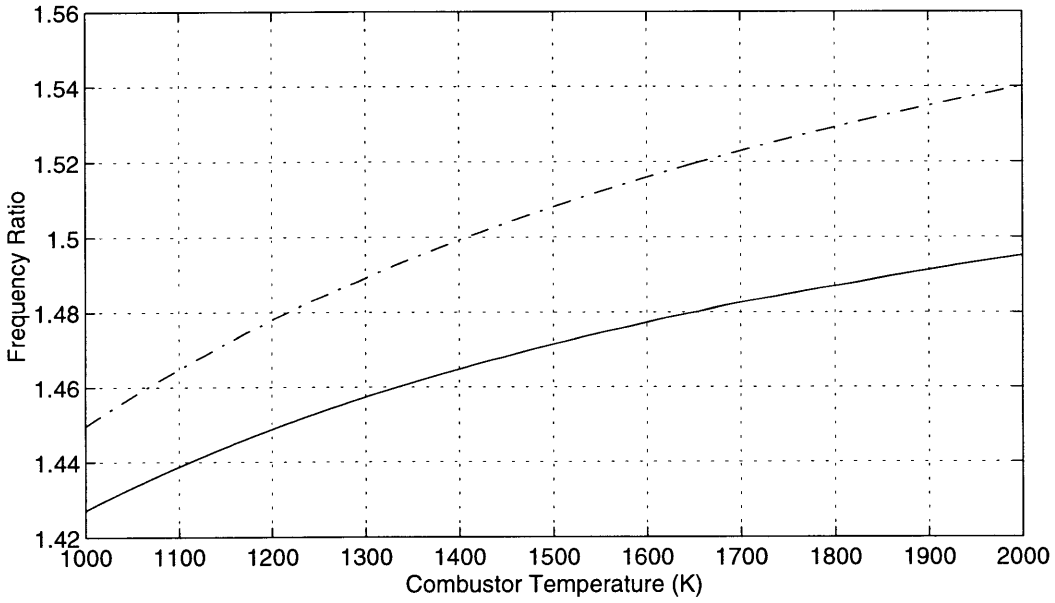

Figure (3.6) Frequency shift ratio due to elevated temperatures for the Allison engine at the 95% speed. (dashed) upper bound on combustion liner volume, (solid) lower bound on liner volume.

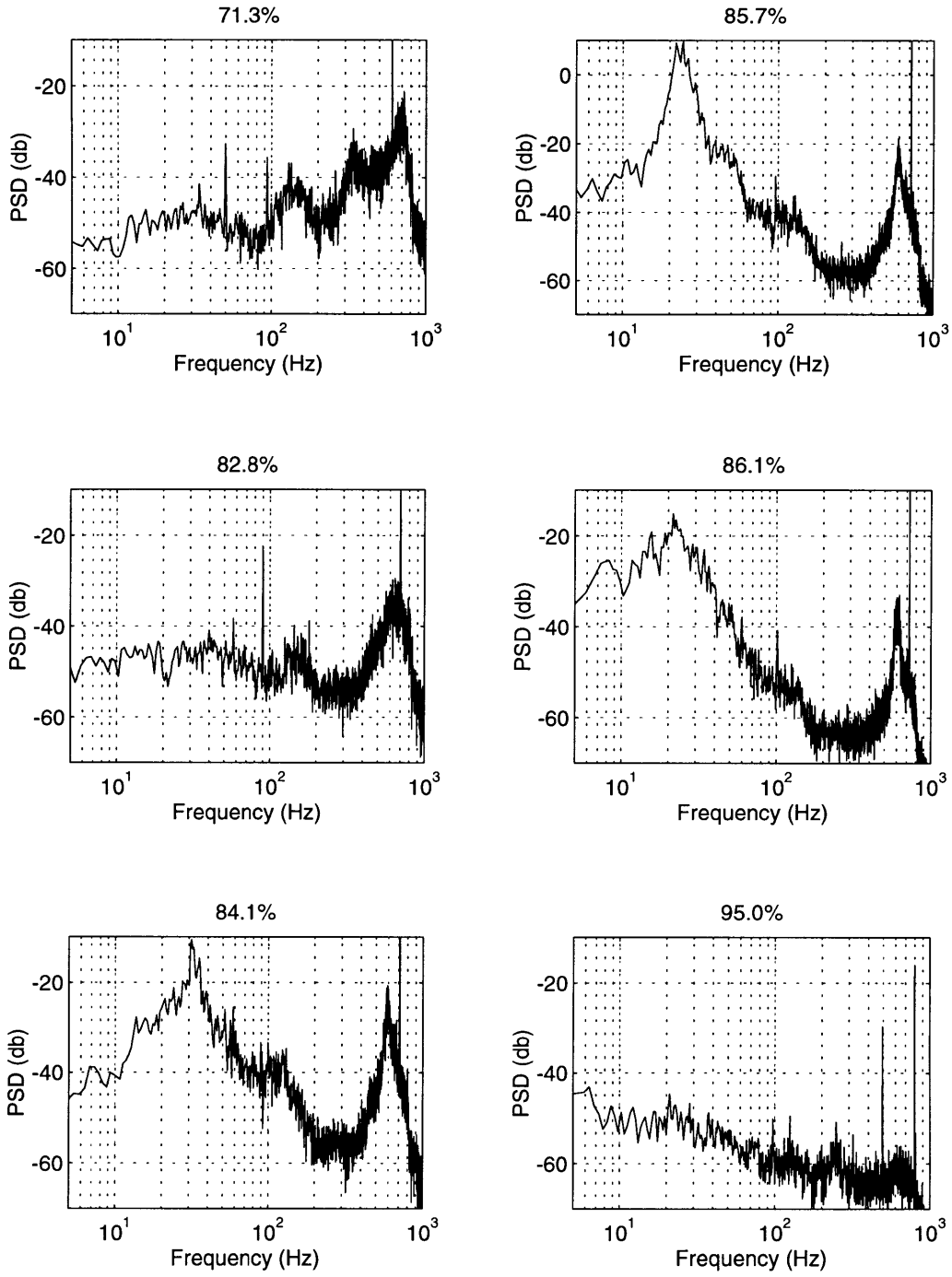

Figure (3.7) Power spectral densities of inlet tap pressure at various speeds along the operating line with the 5 Bar inserts.

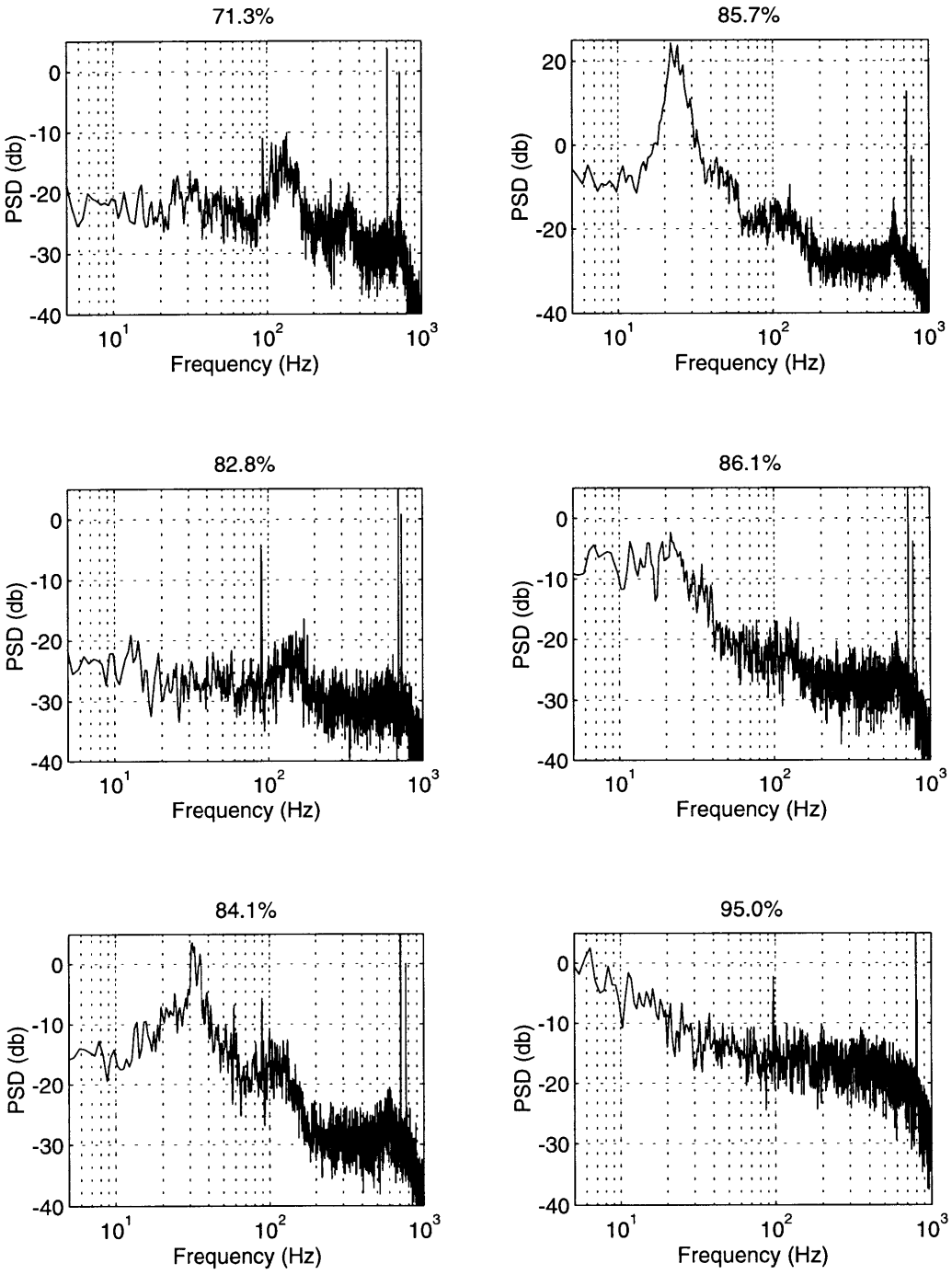

Figure (3.8) PSD's of vaneless space pressure at various speeds.

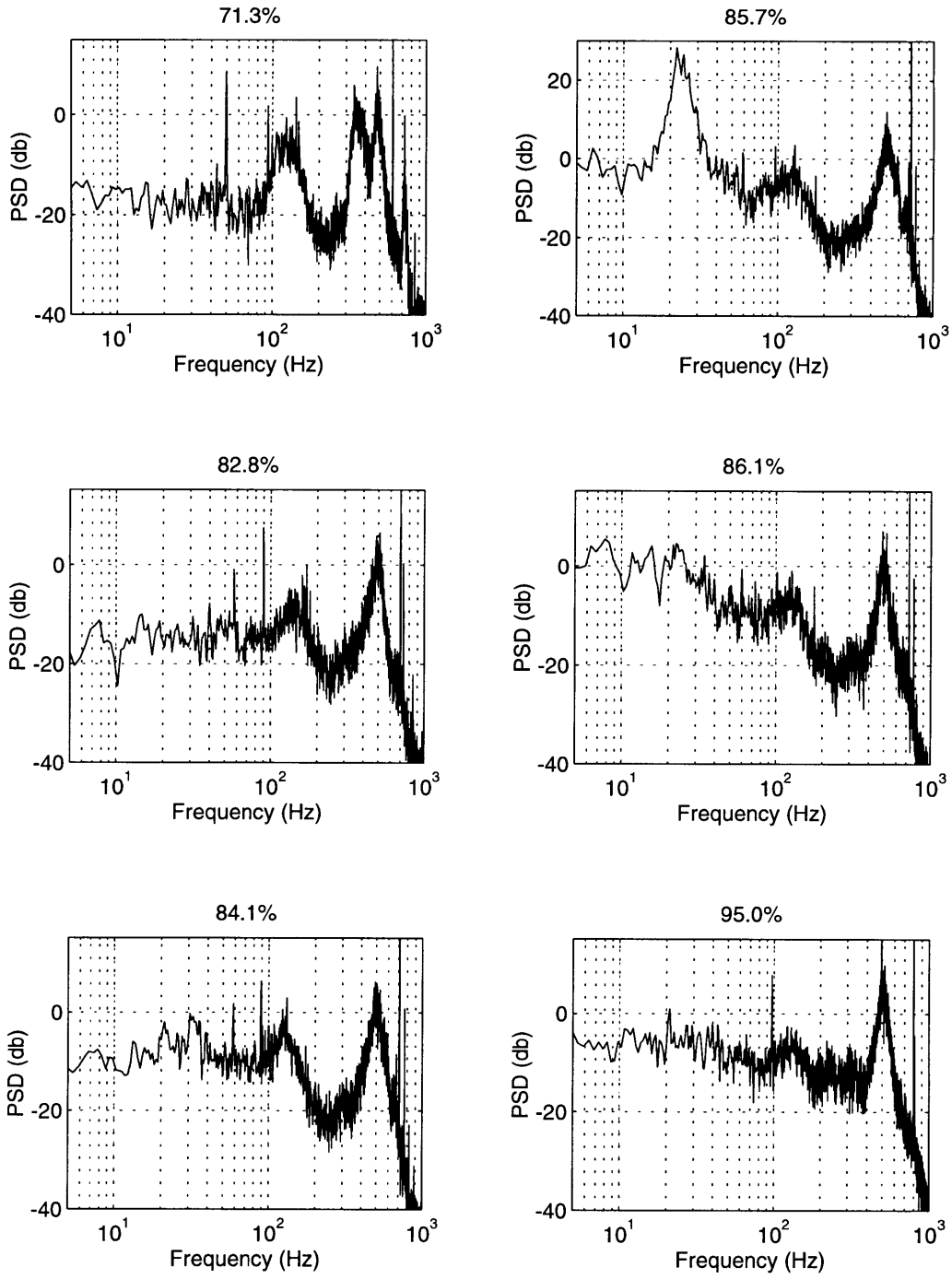

Figure (3.9) PSD's of scroll pressure at various speeds.

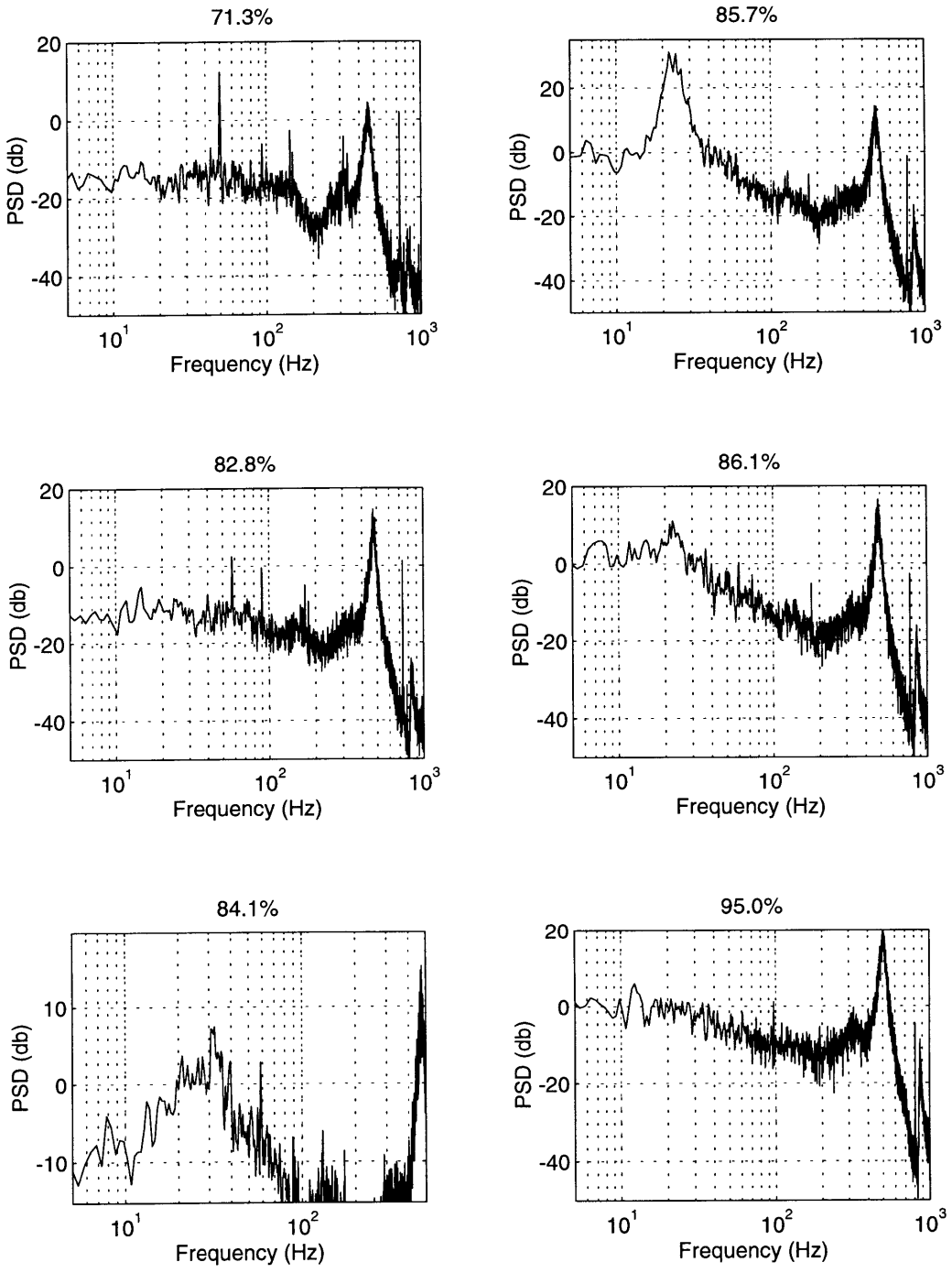

Figure (3.10) PSD's of combustor pressure at various speeds.

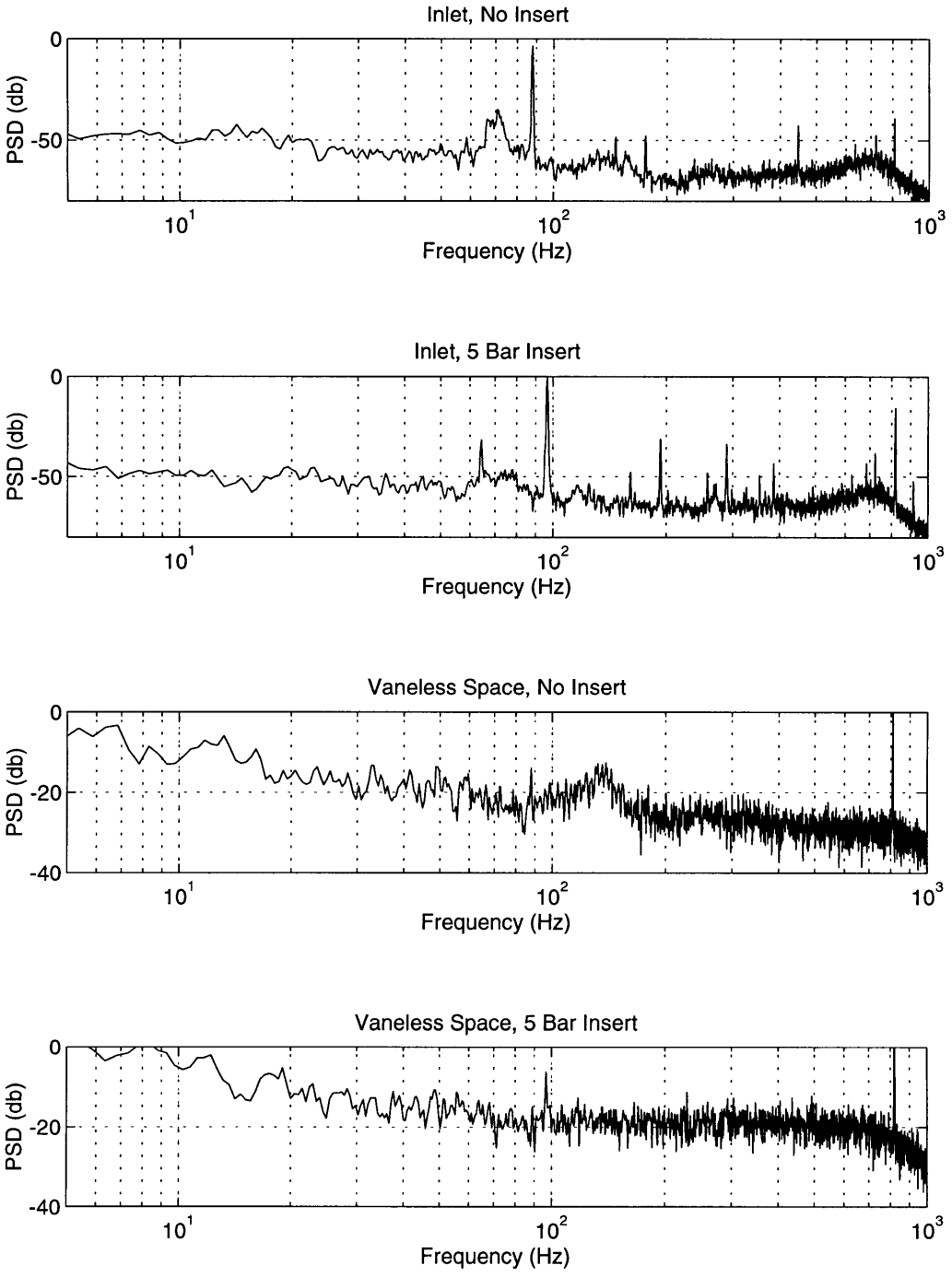

Figure (3.11) Comparison of the engine spectral content with and without the 5 Bar inserts.

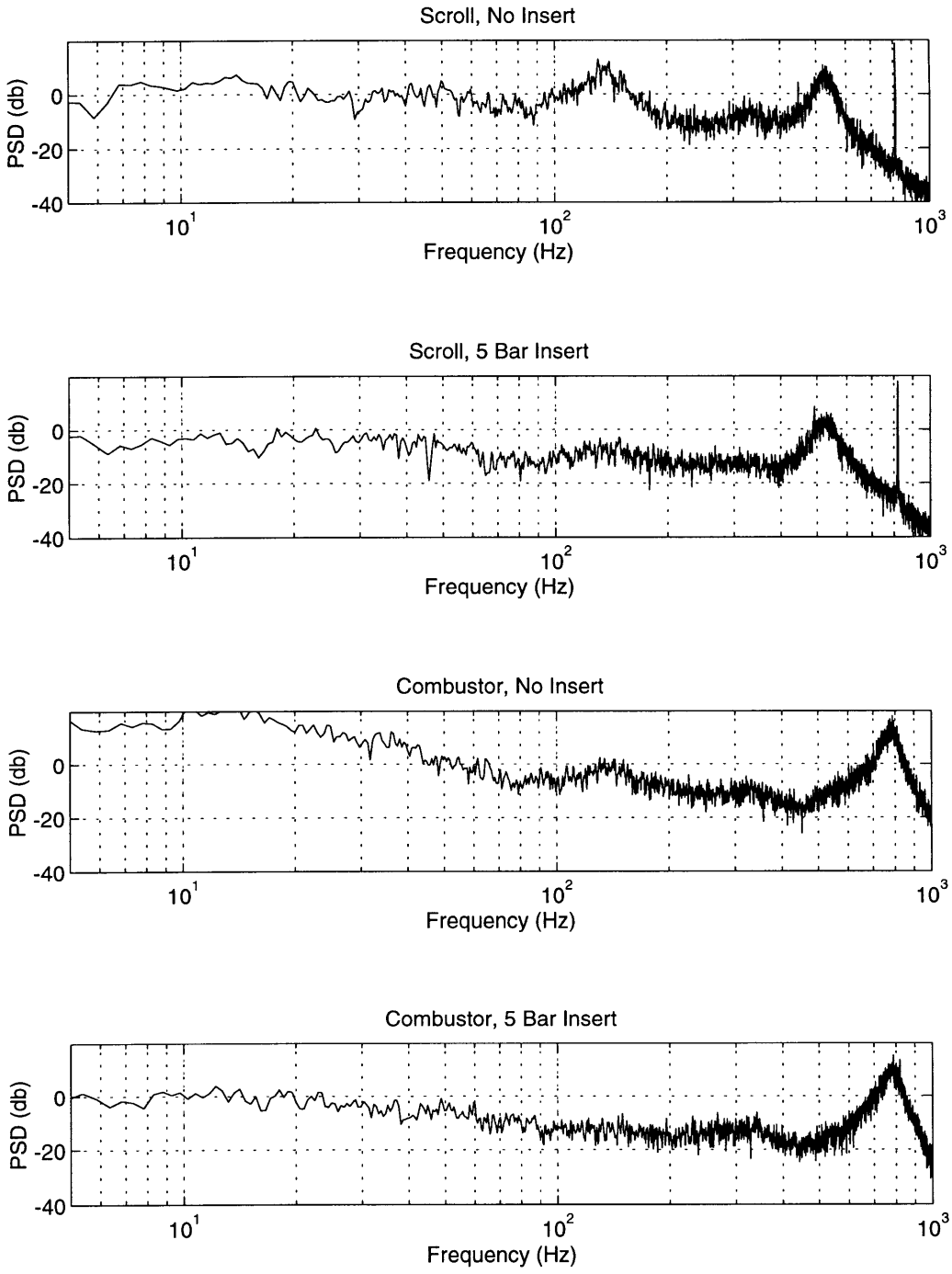

Figure (3.12) Comparison of the engine spectral content with and without the 5 Bar inserts.

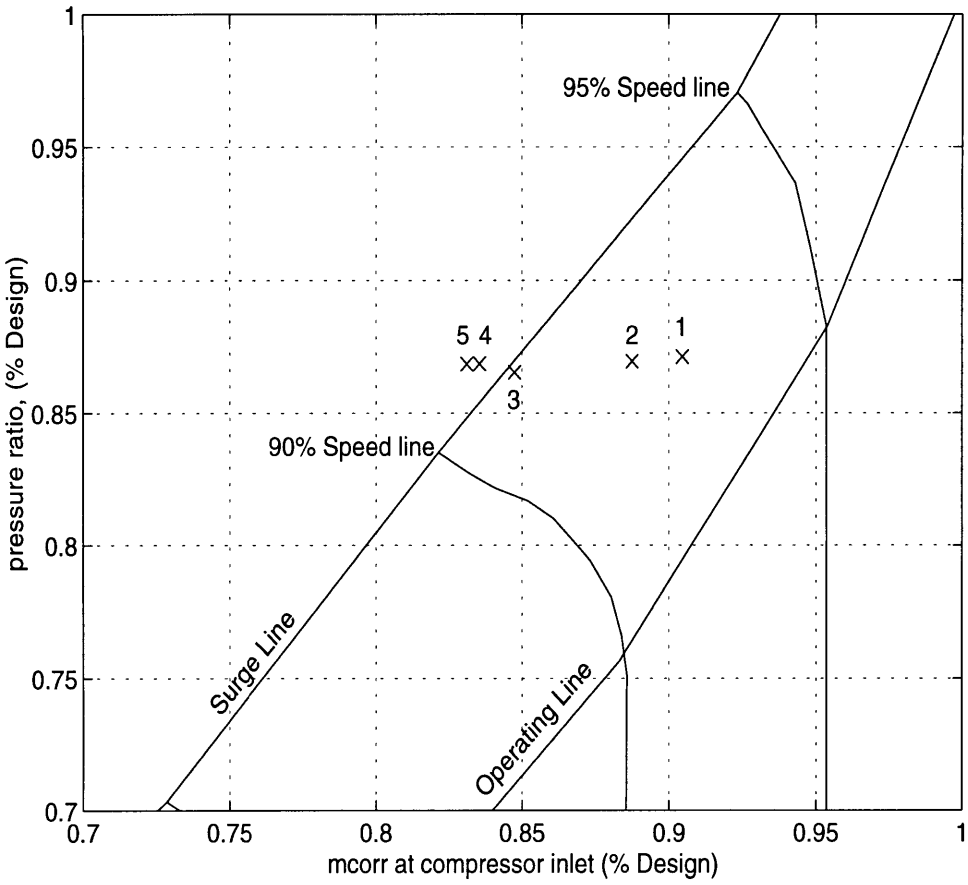

1 : Operating point at 95% speed
2 : Closing the inducer bleed valve
3 : Mean air injection, 4% of engine flow
4 : Water injection, 4% of engine flow
5 : Water injection, 5.4% of engine flow

Figure (3.13) Compressor operating map based on inlet flow.

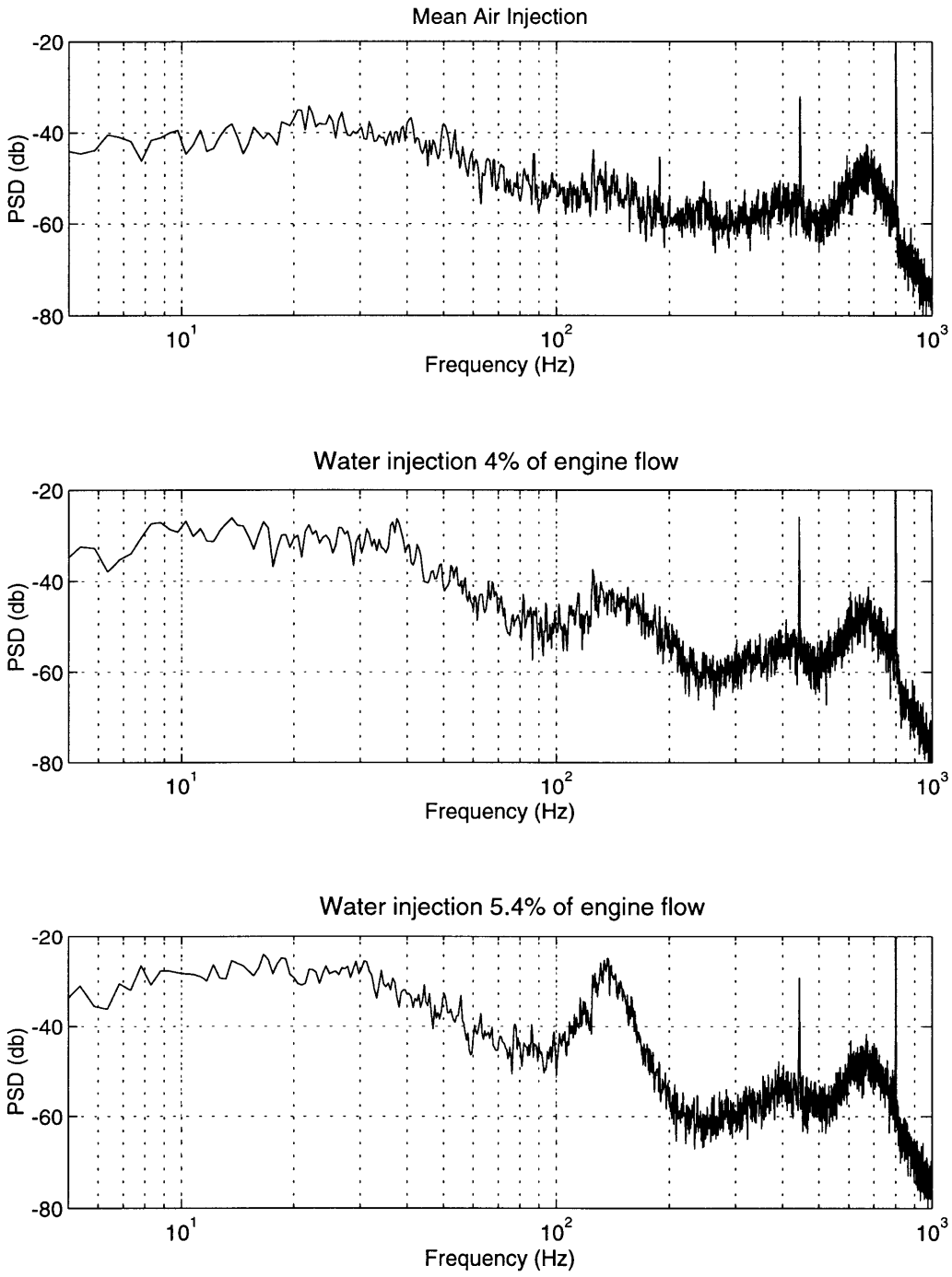

Figure (3.14) Inlet PSD's for mean air injection and two water injection levels.

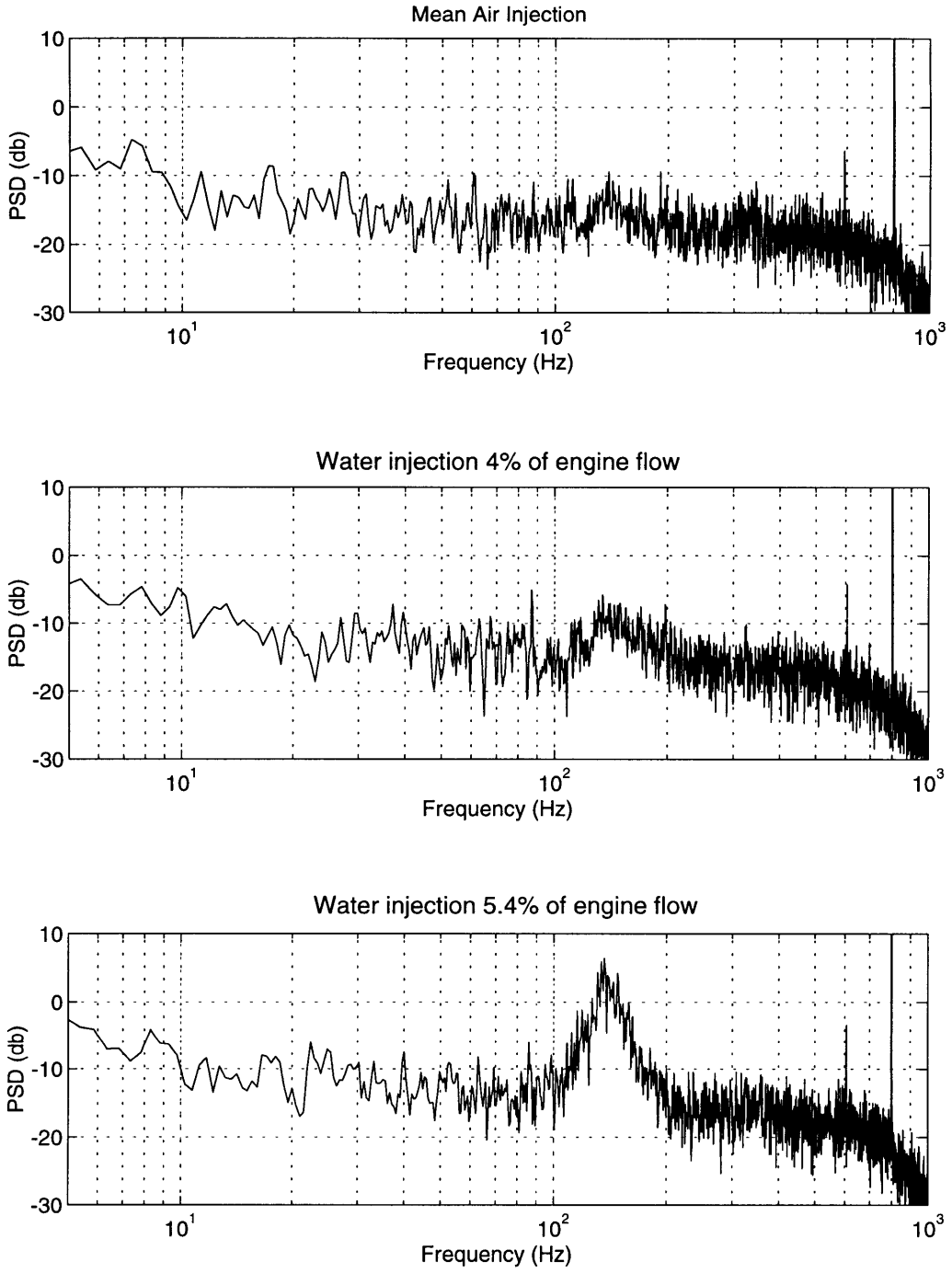

Figure (3.15) Vaneless space PSD's for mean air injection and two water injection levels.

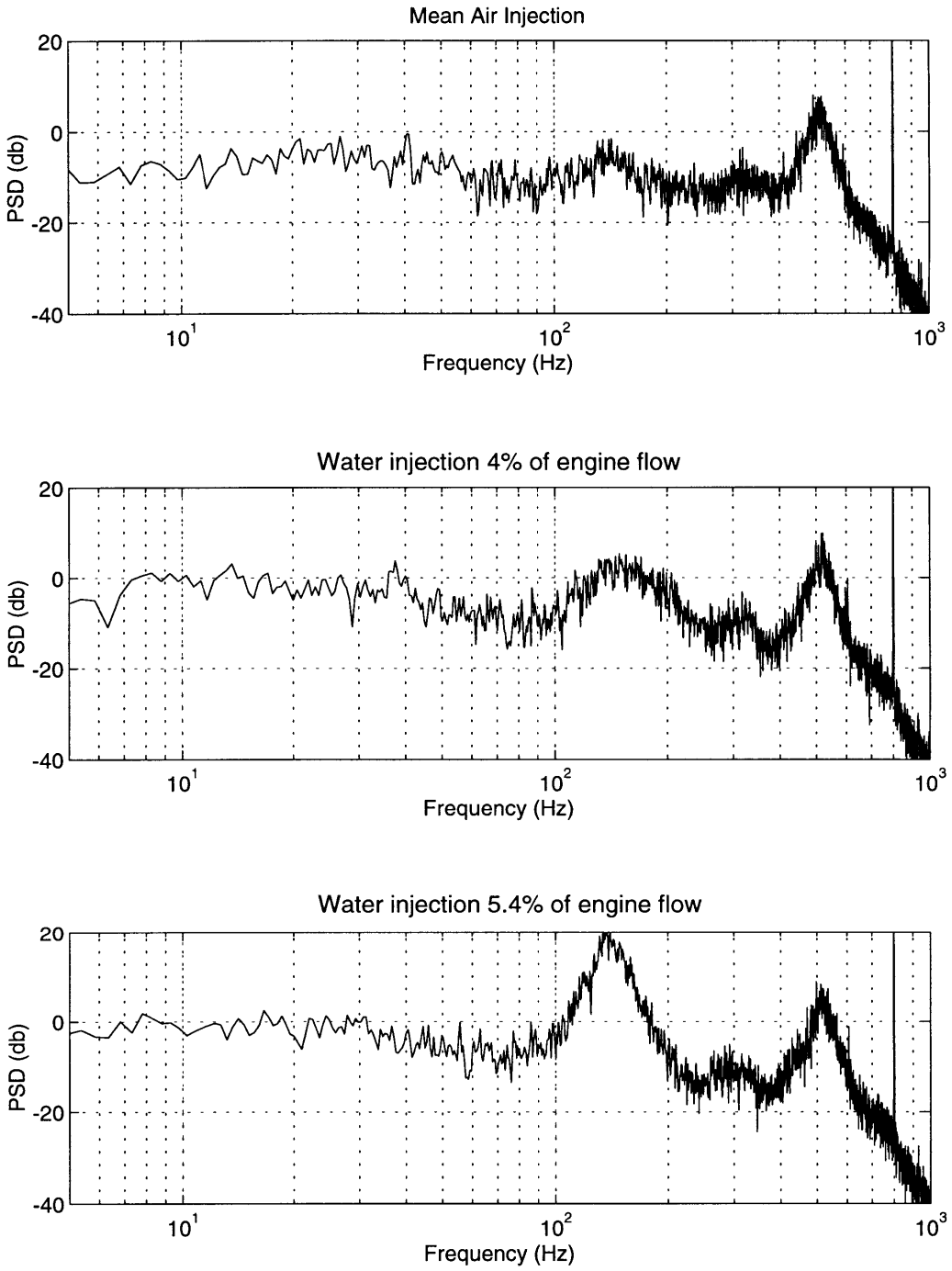

Figure (3.16) Scroll PSD's for mean air injection and two water injection levels.

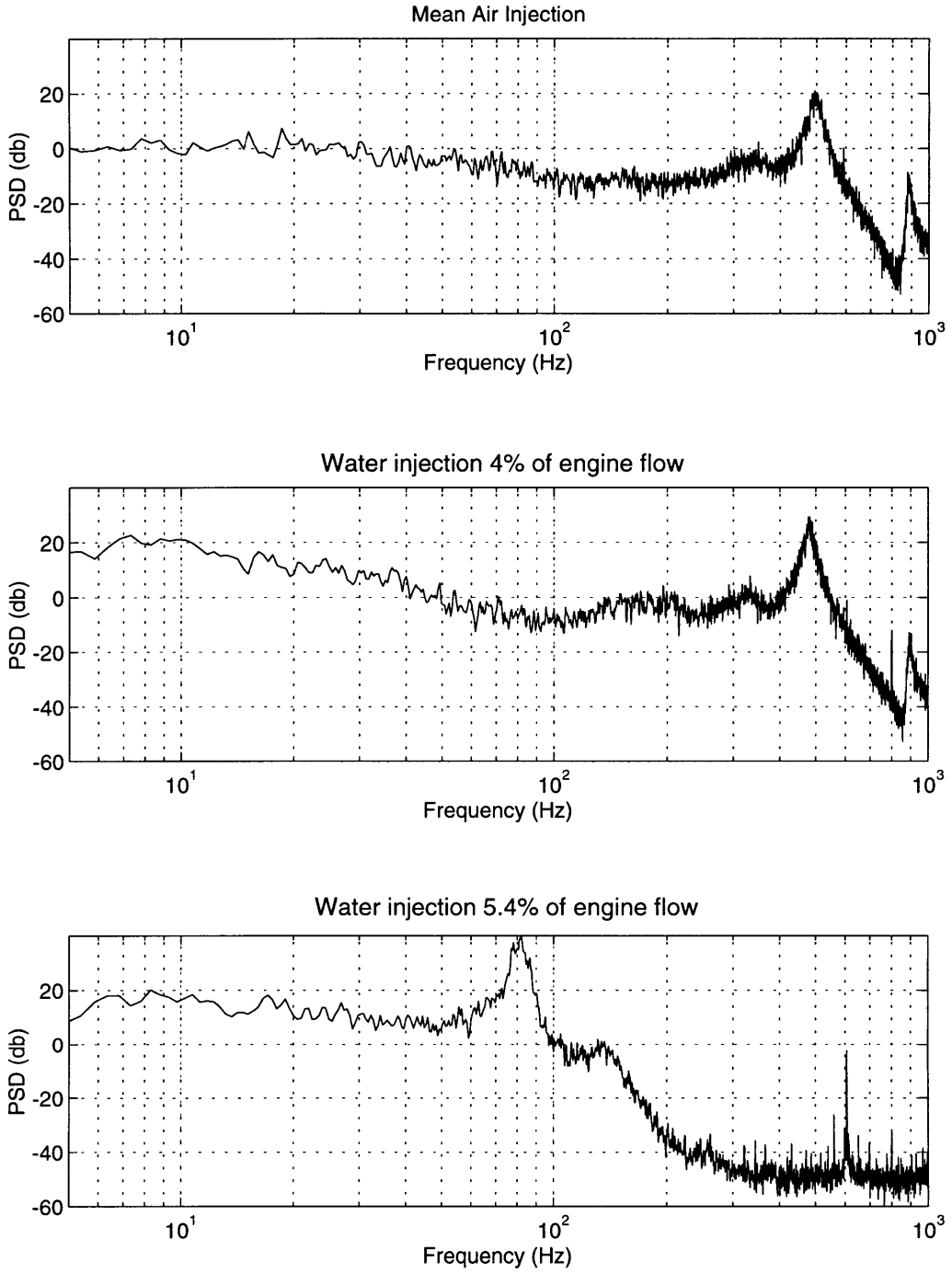

Figure (3.17) Combustor PSD's for mean air injection and two water injection levels.

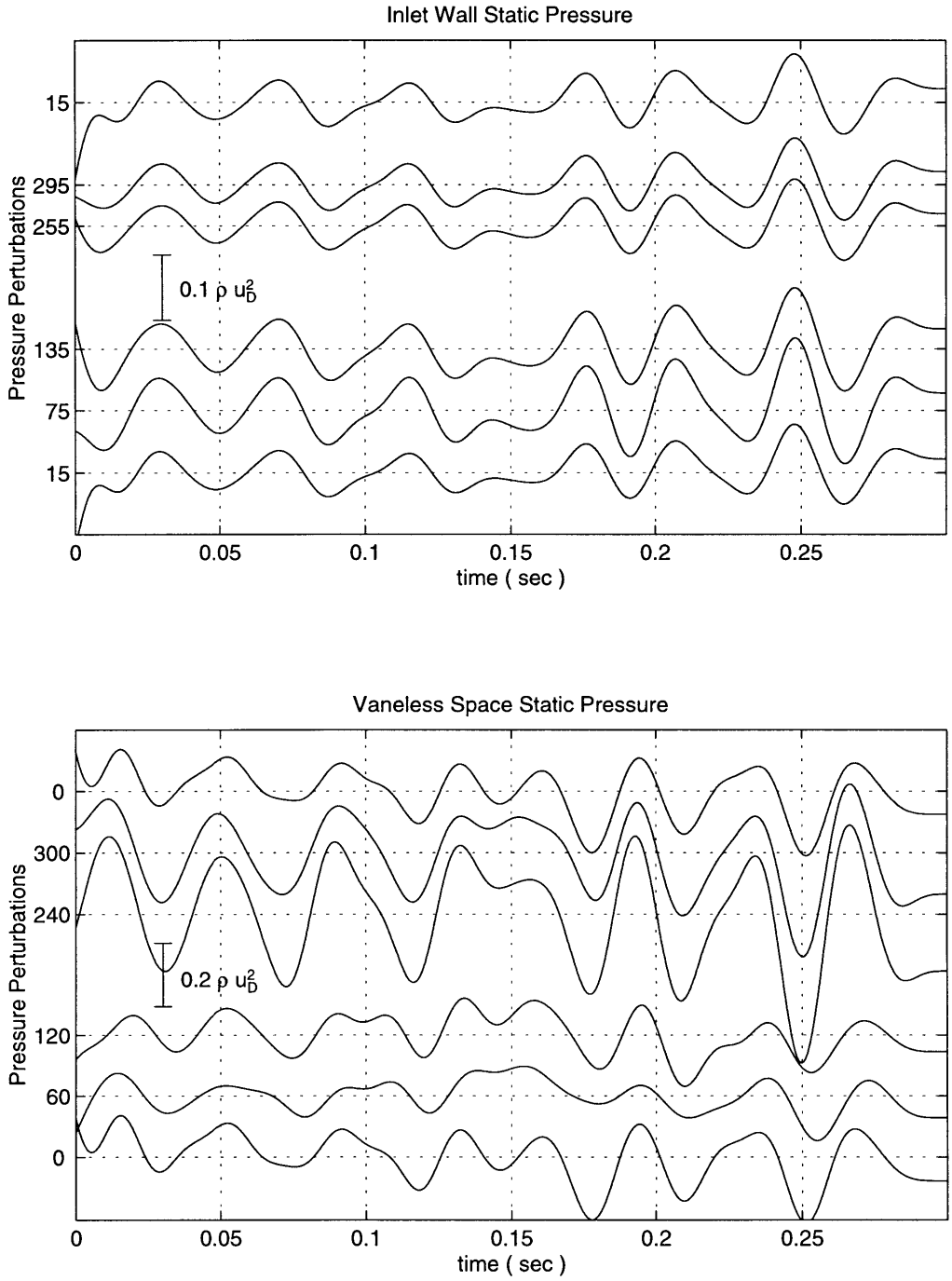

Figure (3.18) 24–26 Hz oscillations at the 85% speed line. Pressure perturbations non dimensionalized by compressor inlet dynamic head at the design point. Pressure tap circumferential position given along y-axis (CCW from TDC). 50 Hz low pass filtering.

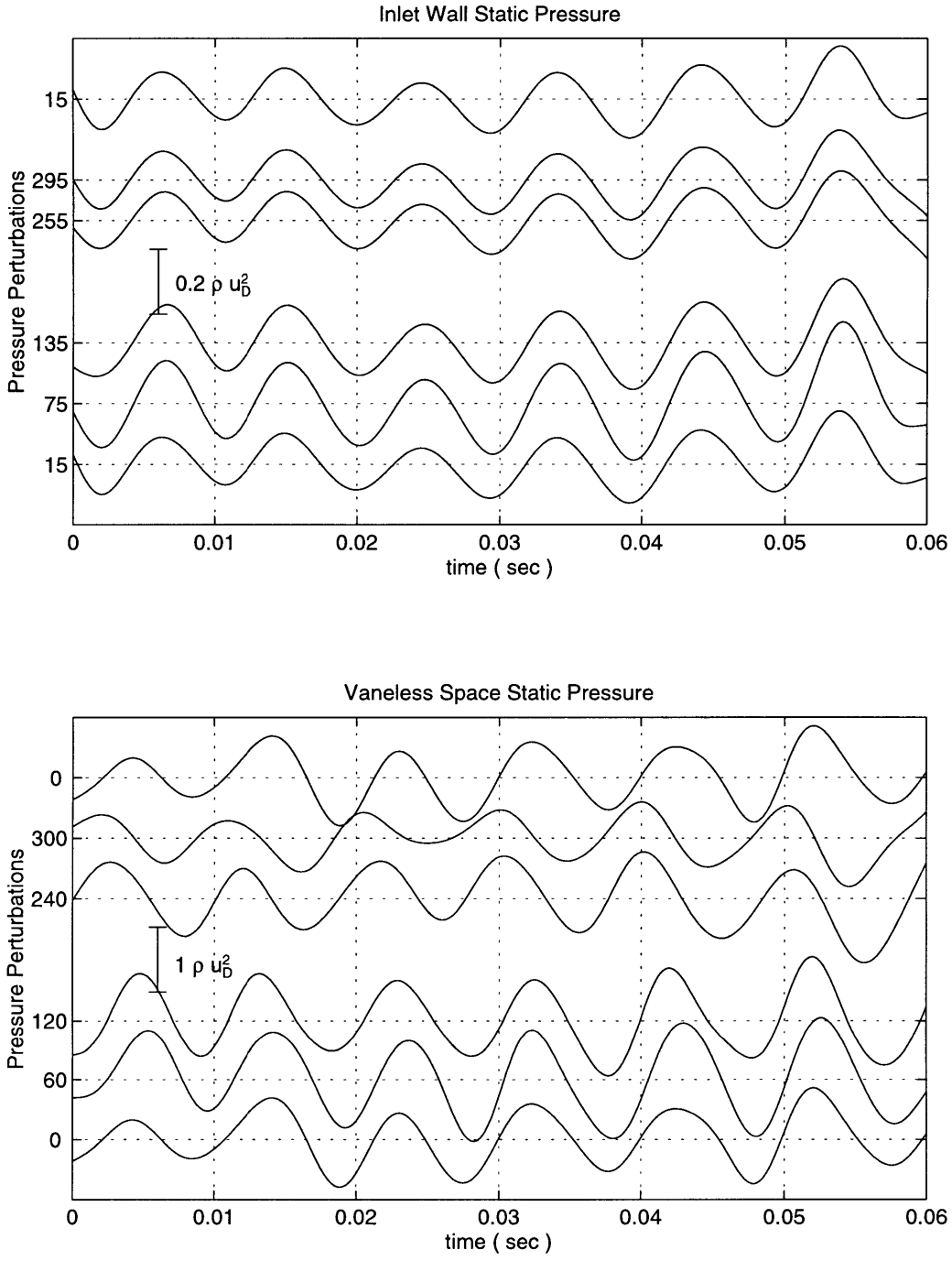

Figure (3.19) Bursts of high amplitude oscillations prior to surge at the 95% speed. Pressure perturbations non dimensionalized by compressor inlet dynamic head at the design point. Pressure tap circumferential position given along y-axis (CCW from TDC). 200 Hz low pass filtering.

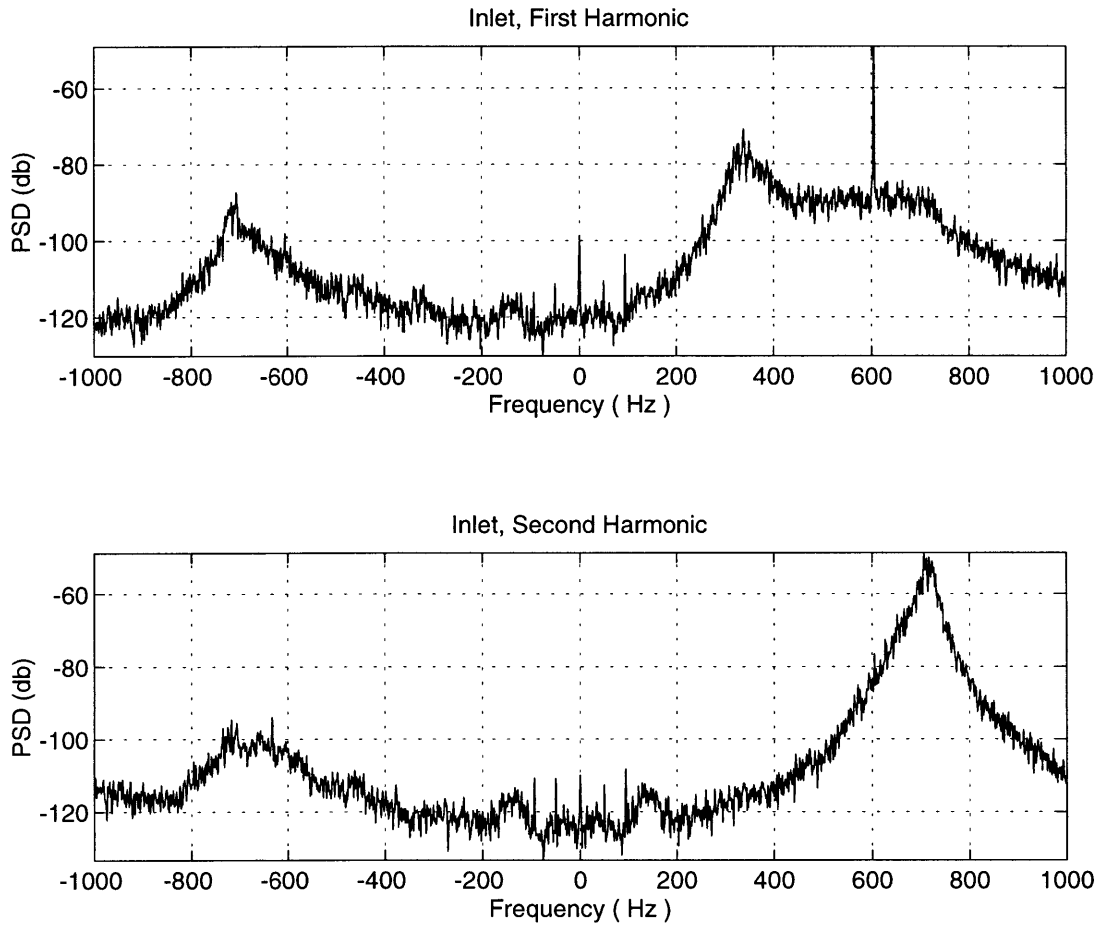

Figure (3.20) First and second harmonics of inlet pressure perturbations at the 71% speed.

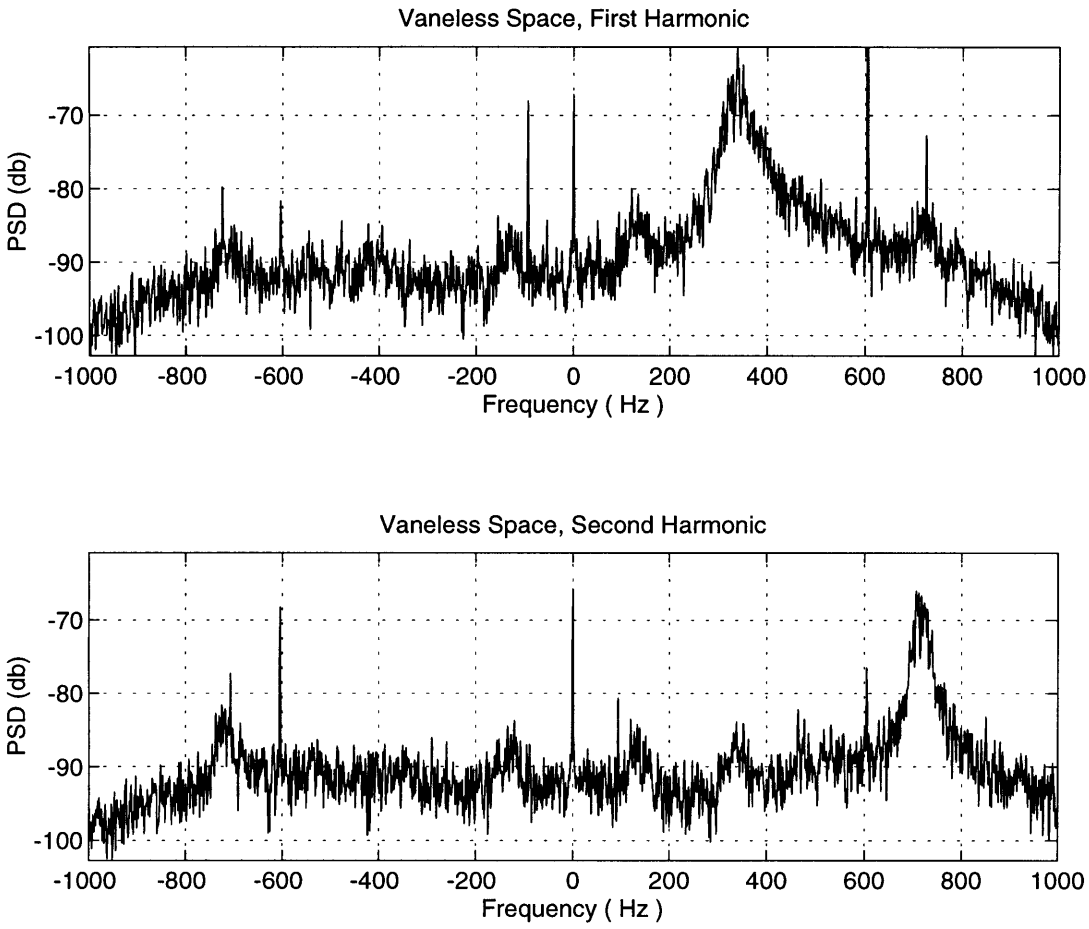

Figure (3.21) First and second harmonics of vaneless space pressure perturbations at the 71% speed.

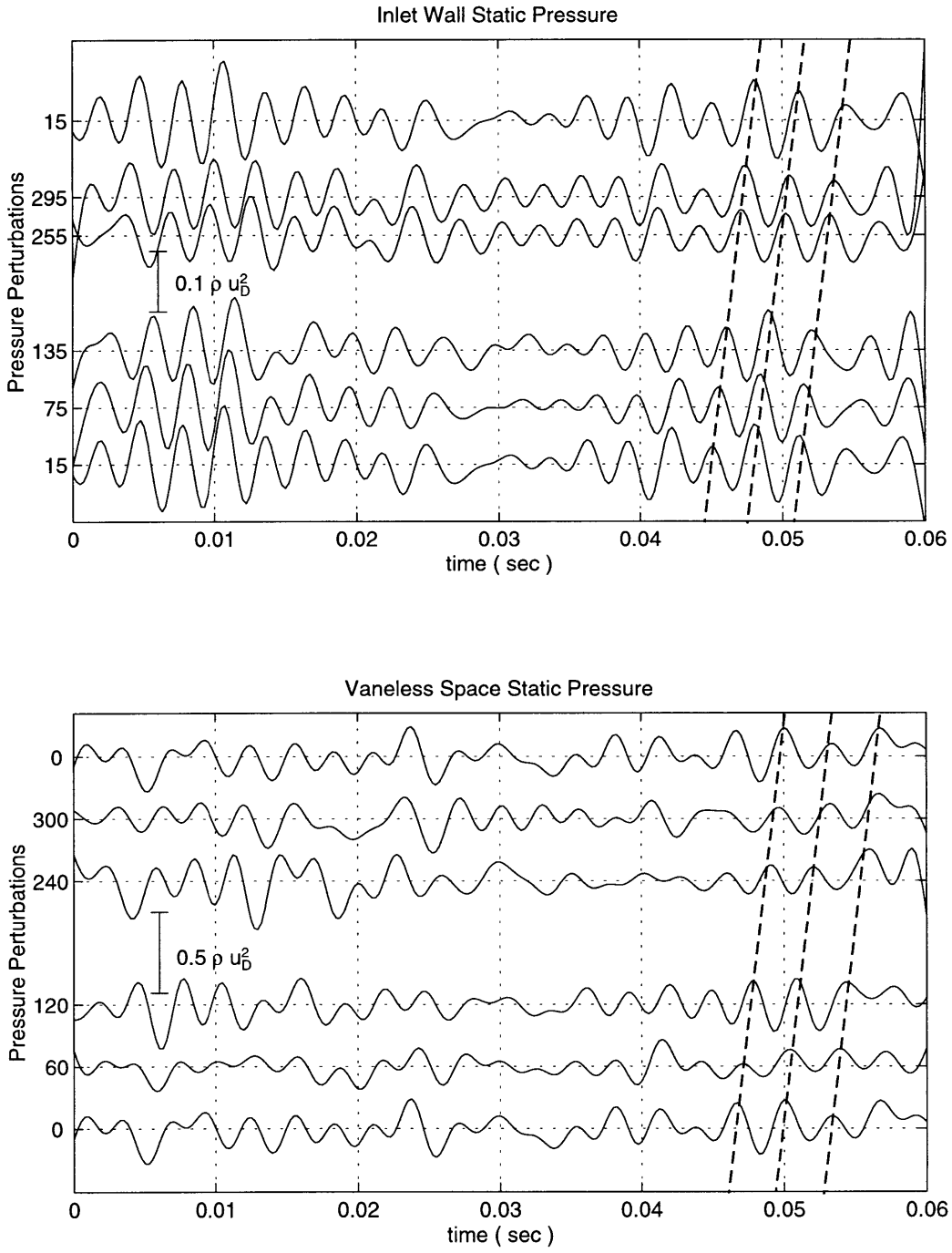

Figure (3.22) Time traces at the 71% speed. Pressure perturbations non dimensionalized by compressor inlet dynamic head at the design point. Pressure tap circumferential position given along y-axis (CCW from TDC). 400 Hz low pass filtering.

Chapter 4

Presurge Behavior

4.1 Introduction

Two benefits of surge control are improved efficiency (SFC) at high power, and improved acceleration performance. Instabilities, amongst other constraints, often limit the acceleration performance in gas turbine engines. Surge behavior during acceleration transients was investigated for the Allison engine near the 85% speed line. It was triggered by a transition from the 84% speed to higher power. Surge inception data was acquired with the inducer bleed bypass valve open and closed.

The benefit of active control at high power is to allow operation closer to the maximum compressor efficiency point. Surge inception data at high power was acquired at the 95% speed where the engine produces 500 HP. Surge at this speed was investigated with steady air injection into the inducer bleed port. Water injection was used to throttle the engine towards the surge line.

Chapter 4 is organized into the following sections :

4.2 Surge inception at the 95% speed.
4.3 Surge inception at the 85% speed with the inducer bleed valve open.
4.4 Surge inception at the 85% speed with the inducer bleed valve closed.
4.5 Conclusions

4.2 Surge at the 95% Speed

As previously mentioned, surge at the 95% speed line was investigated with a mean level of air injection through the inducer bleed port, and water injection into the discharge tubes. The sequence of events to reach the surge point was to :

(1) Accelerate the engine to the 95% speed.
(2) Close the inducer bleed bypass valve.
(3) Increase air injection to the mean level of 4.2%.
(4) Start water injection and successively throttle the compressor towards surge.

Figure (4.1) shows the effect of steps 2-4 on the compressor operating map. Two operating maps are presented, one for the compressor inlet flow (measured) and the other for the compressor exit flow (deduced). Figure (4.2) demonstrates the relationship between compressor inlet and exit flow. Compressor exit flow is defined to be the mass flow rate going through the inlet minus (or plus) the mass flow rate leaving (or injected into the engine) through the inducer bleed valve.

The inlet mass flow rate was measured using a bellmouth upstream of the compressor. It was then used to calculate the compressor exit flow rate during periods where the inducer bleed flow rate was measured. This flow rate was only measured during periods of air injection into the engine, with the inducer bleed bypass valve closed.

Because the turbine nozzle guide vanes (NGV) are choked, and therefore set the compressor exit mass flow rate, any reduction in the mass flow rate leaving the compressor through the inducer bleed should also reduce the compressor inlet flow rate by the same amount. One exception to this may occur if the compressor flow field is disturbed and additional losses cause a reduction in compressor pressure ratio.

Figure (4.1) shows that closing the inducer bleed valve reduces the inlet corrected flow rate and results in a pressure drop due to increased losses. Note that point (1) is not shown on the compressor exit map because the inducer bleed valve was open.

Air injection into the inducer bleed port is observed to reduce the inlet corrected flow and result in a smaller reduction in compressor exit corrected flow. A 0.3% pressure drop is also observed due to air injection.

Water injection is observed to throttle the compressor towards/past the nominal engine surge line. Several levels of water injection are shown and the surge point is labeled. Note that there is a discontinuity that occurs because the compressor speed (power turbine speed governor lever) was adjusted to remain at the 95% speed. During operation variations in corrected speed were observed due to inlet temperature fluctuations. These variations could not be compensated for because they occurred rapidly (1-2 minutes per cycle). One attempt to correct for such variations resulted in the observed discontinuity. A minor drop in pressure ratio occurs as the engine is throttled towards surge and the speed lines are essentially flat up to a few points prior to surge where the pressure ratio drops and the speed line becomes positively sloped. The steady state effects of air injection into the inducer bleed port, and water injection will be discussed further in chapter 5.

A comparison between the mass flow rate at surge and the mass flow rate on the nominal surge line for the same pressure ratio is provided in Table (4.1). The surge point mass flow rate matches the nominal surge mass flow rate on the compresssor inlet and

exit maps to within 2.2% and -7.8% respectively. This implies that compressor inlet flow may be a better measure of compressor stability than compressor exit flow, and mean air injection into the inducer bleed port (observed to shift the operating point on this map) reduces the surge margin. This reduction in surge margin may deem the current actuation scheme impractical, but this conclusion may not be confirmed without verifying that the engine surge point with the inducer bleed valve open matches the nominal surge line.

Table (4.1) Comparison between massflow rate at surge, and mass flow rate of on nominal surge line

Compressor Map	$\frac{\dot{m}_{surge} - \dot{m}_{surgeline}}{\dot{m}_{surgeline}}$
Inlet Map	2.2%
Exit Map	-7.8%

Figure (4.3) shows a scroll pressure trace prior to surge. Burst of high amplitude 100-105 Hz oscillations are observed every few seconds, immediately prior to surge. As shown in chapter 3, these high amplitude bursts are axisymmetric at the inlet and show clear structure in the vaneless space. Namely, oscillations in half the annulus was found to be 90 degrees out of phase compared to the other half. Between these high amplitude bursts, lower amplitude oscillations are observed at 115-120 Hz. These bursts of oscillations are characteristic of a lightly damped system about to go unstable [19].

The nature of the vaneless space oscillations are not understood and investigation of pressure perturbations at various points in the scroll, and in the discharge tubes may provide more insight about the source of these oscillations.

Surge inception data at the inlet and vaneless space are shown in figure (4.4). It is difficult to identify the exact time when surge occurs, but it is within a few milliseconds after t=0. No rotating disturbances are observed in the time traces prior to surge.

Figure (4.5) shows a waterfall plot of the scroll pressure tap prior to surge. 100-120 Hz activity is observed to vary in amplitude until the final growth to surge occurs.

Figure (4.6) shows power spectra of the spacial fourier coefficients for the inlet and vaneless space static pressures. The convention used in this chapter for plotting the first and second spacial harmonics was to assign positive power to waves rotating in the direction of the rotor. One exception to this convention was made in plotting the 2^{nd} harmonics on figure (4.6), in which the positive traveling wave was assigned negative

power. This was done to show the negative traveling waves, which were dominant in this case, more clearly.

The inlet PSDs show activity at 100-120 Hz, as well 25-30 Hz. The 30 Hz oscillation is mainly 1-D and starts to grow 500 revolutions prior to surge. The 100-120 Hz oscillation has a large zeroth harmonic and smaller 1st and 2nd harmonic components. The vaneless space PSDs show a large 1st harmonic with the same spectral content as the inlet. Surge inception may be linked to growth in the 30 Hz or 100-120 Hz oscillations.

4.3 Surge at the 85% Speed, Open Inducer Bleed Valve

Surge data during an acceleration transient near the 85% speed was investigated on the engine configured with the 5 bar inserts. The surge event occurred during transition from the 84% to 88% speed. Figure (4.7) shows these points on the compressor inlet flow map. This figure also shows the point prior to transition for the surge occurrence mentioned in section 4.4.

Figure (4.8) shows the scroll pressure during the transition. One surge cycle occurs at t=0 and the engine recovers to complete the transition to the 88% speed. The large amplitude low frequency (about 1 Hz) oscillations observed are the result of interaction between the engine fuel controller, engine dynamics and the water brake used to dissipate the power.

Time resolved data of the span prior to this surge are shown in figure (4.9). Oscillations at the inlet are seen to be axisymmetric while those at the vaneless space have the same circumferential structure as the 100-120 Hz mode observed prior to surge at the 95% speed. The oscillation frequency in this case was about 27 Hz and was probably due to the Helmholtz resonator mode. Chapter 3 had shown that this mode was essentially axisymmetric near the 85% speed. In this case no region of axisymmetric flow was observed at the vaneless space during the 150 ms of oscillation. Many researchers refer to low amplitude oscillations that occur due to the Helmholtz mode as mild surge.

Impeller and diffuser rotating disturbances were not observed in the time traces during the precursor period and surge inception may be due to growth in the oscillation observed at the vaneless space. Surge inception behavior seems to support this hypothesis. Figure (4.10) shows the inlet and vaneless space time traces during surge. The bottom three traces (0, 60, 120 degrees) are observed to decrease immediately prior to surge, while the other two traces increase. The flow then breaks down and surge occurs. The inlet time traces clearly show the N_1 shaft frequency of 700 Hz prior to surge.

Figure (4.11) shows power spectra of the spacial fourier coefficients. Growth is clearly seen at 25-30 Hz in all the plots. The first and second harmonics for the inlet pressure perturbations also show a sustained rotating disturbance at about 90-100 Hz. The source of this disturbance is not known.

4.4 Surge at the 85% Speed, Closed Inducer Bleed Valve

Surge during an acceleration transient near the 85% speed was also investigated with the inducer bleed bypass valve closed. Figure (4.6) shows the stable operating point prior to the transition. The engine was returned to idle to recover after the surge event and therefore no stable post-surge operating point is shown.

Figure (4.10) presents the inlet and vaneless space traces prior to surge. 27 Hz oscillations are observed at the inlet, with a 340 Hz oscillation occurring immediately prior to surge. An expanded view of the region prior to surge is shown in figure (4.11). The 340 Hz oscillation may be a rotating disturbance, but two transducer traces (transducer located 75 and 255 degree) cast doubt as to whether this is the case. The 2^{nd} from bottom (75 degrees) is a 15 psi full scale pressure transducer and appears not to have sufficient sensitivity to observe the oscillation. All other transducers are 5 psi full scale and clearly show the oscillation. The 4^{th} trace from bottom (255 degrees) does not align well and is shifted by about 70 degrees.

The oscillation observed here would have a speed of 50% the rotor speed if it were a rotating disturbance. This was calculated based on the stable operating point prior to surge. The vaneless space traces also showed oscillations at 340 Hz, but no clear rotating pattern could be identified.

Figure (4.14) shows the power spectra of the spacial fourier coefficients. Broad spectral content is observed over the whole frequency range. The Inlet harmonics show a peak at 25-30 Hz prior to surge. No peak is seen at 340 Hz because it only occurs about 10 ms before surge, and the PSD window averages it out.

4.5 Conclusions

Surge at the 95% speed was preceded by bursts of high amplitude 100-105 Hz oscillations observed throughout the engine. Between these bursts lower amplitude 120 Hz oscillations occurred. Impeller and diffuser rotating stall were not seen and surge inception may be due to growth in the 27 Hz oscillation, or the asymmetric vaneless space

oscillation discussed in chapter 3. During this oscillation, flow in one half the annulus was found to be 90 degrees out of phase compared to the other half.

Surge at the 85% speed with the inducer bleed valve open was preceded by behavior similar to that observed at the 95% speed. An asymmetric pattern similar to that of the 100-105 Hz was observed at the vaneless space. The oscillation frequency was 27 Hz, in this case, and was probably due to the Helmholtz mode. Although this mode was observed to be essentially axisymmetric during steady operation near the 85% speed, no region of axisymmetric flow was observed during the 150 ms prior to surge.

Surge at the 85% speed with the inducer bleed valve closed was preceded by an oscillation at 27 Hz oscillation, as well as a 340 Hz oscillation immediately prior to surge. The 340 Hz oscillation may be a rotating disturbance with a speed of 50% the rotor frequency.

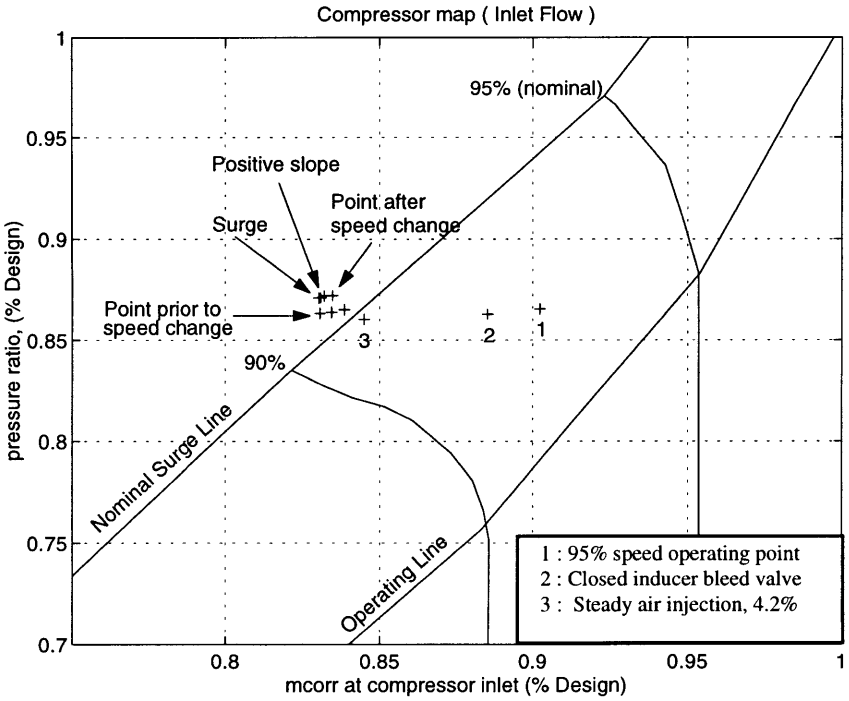

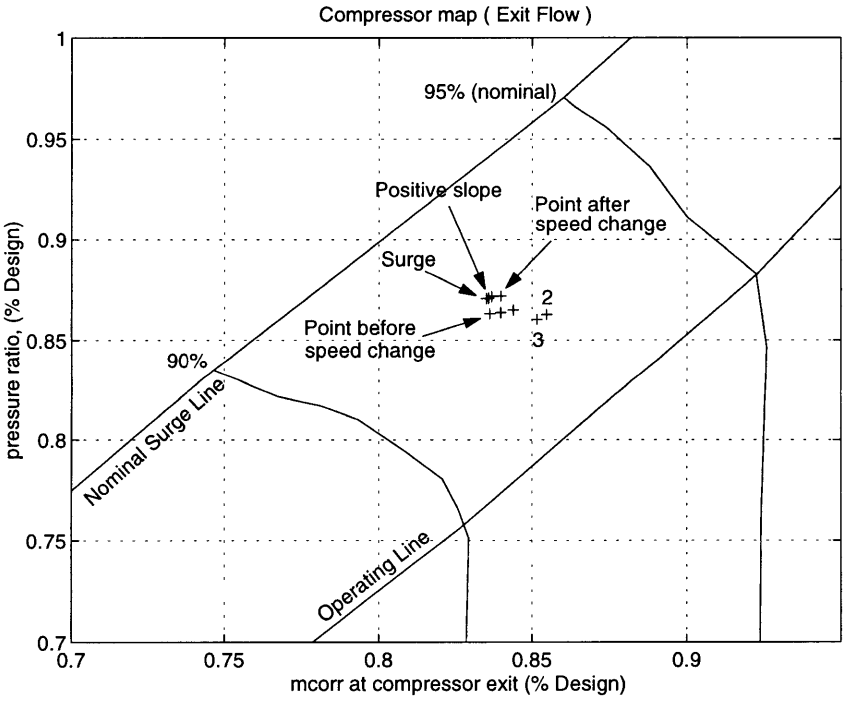

Figure (4.1) Compressor inlet and exit maps.

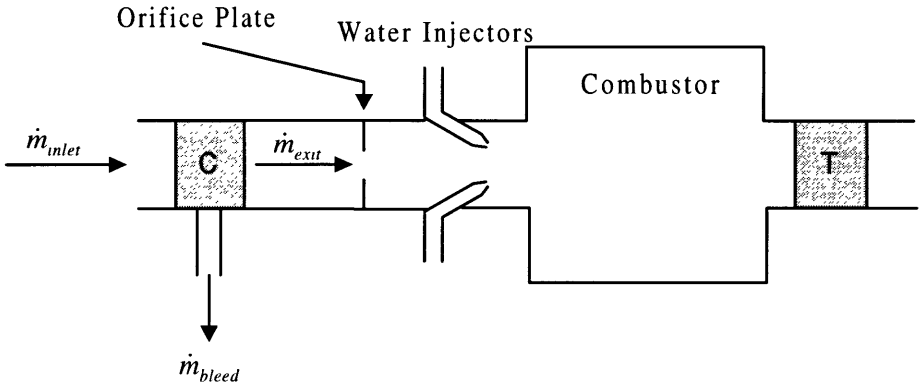

Figure (4.2) Relationship between compressor inlet and exit flow rate.

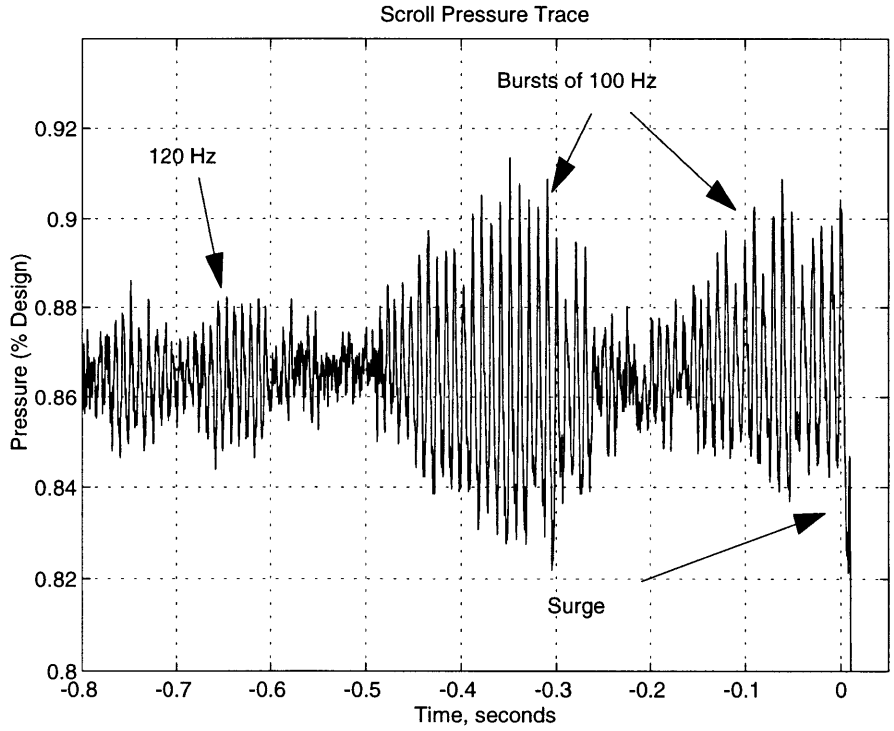

Figure (4.3) Scroll pressure prior to surge at the 95% speed line.

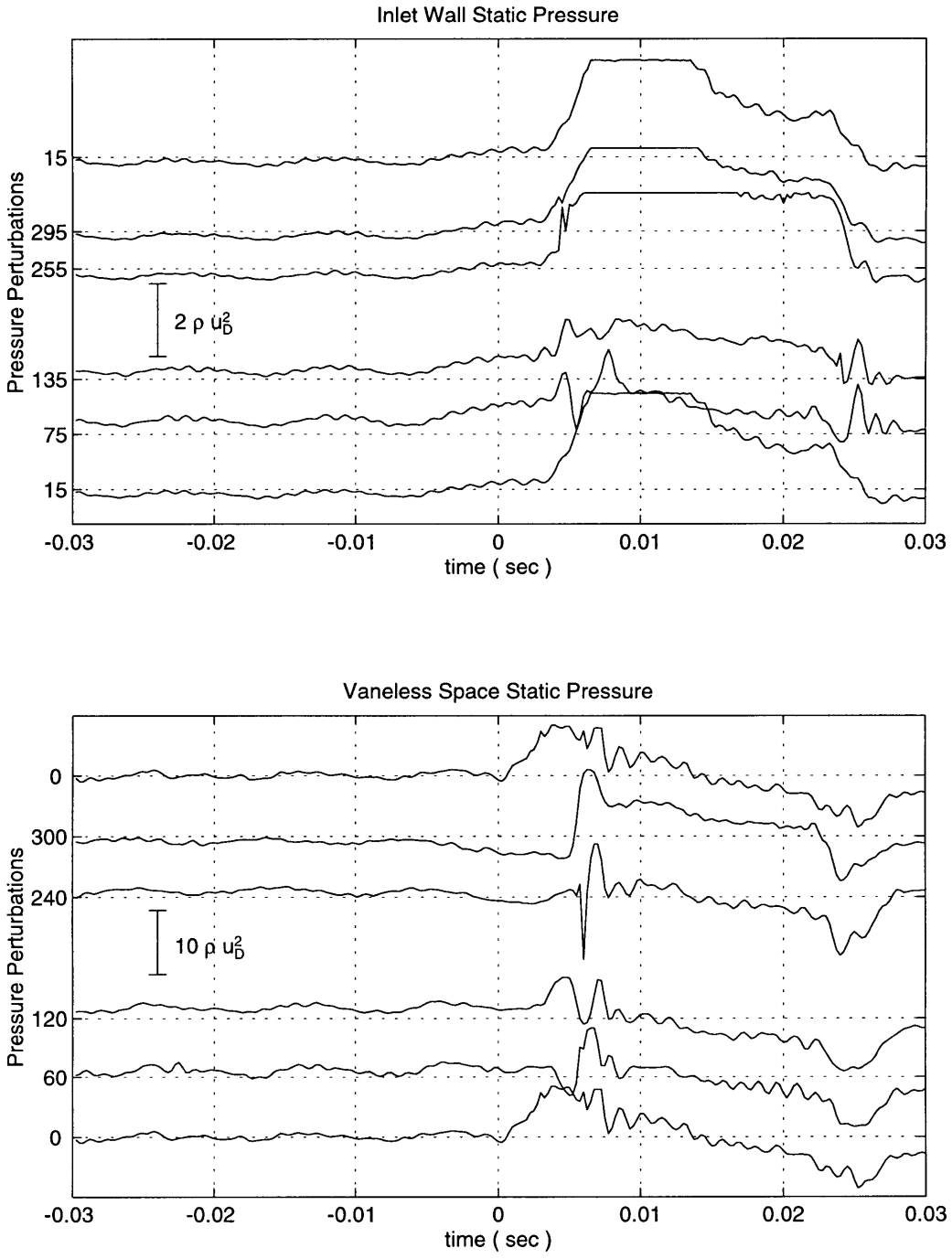

Figure (4.4) Surge inception behavior at the 95% speed line. Pressure perturbations non-dimensionalized by compressor inlet dynamic head at design point. Pressure tap circumferential location shown on y-axis

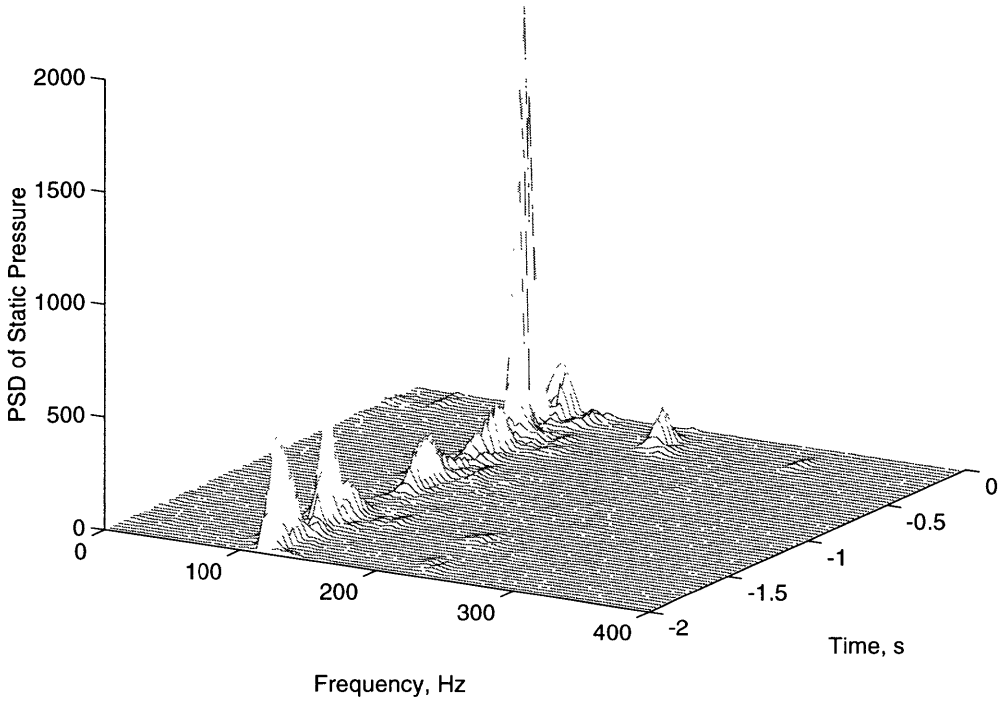

Figure (4.5) Waterfall plot of scroll pressure PSD. Same data as that shown in figure (4.3).

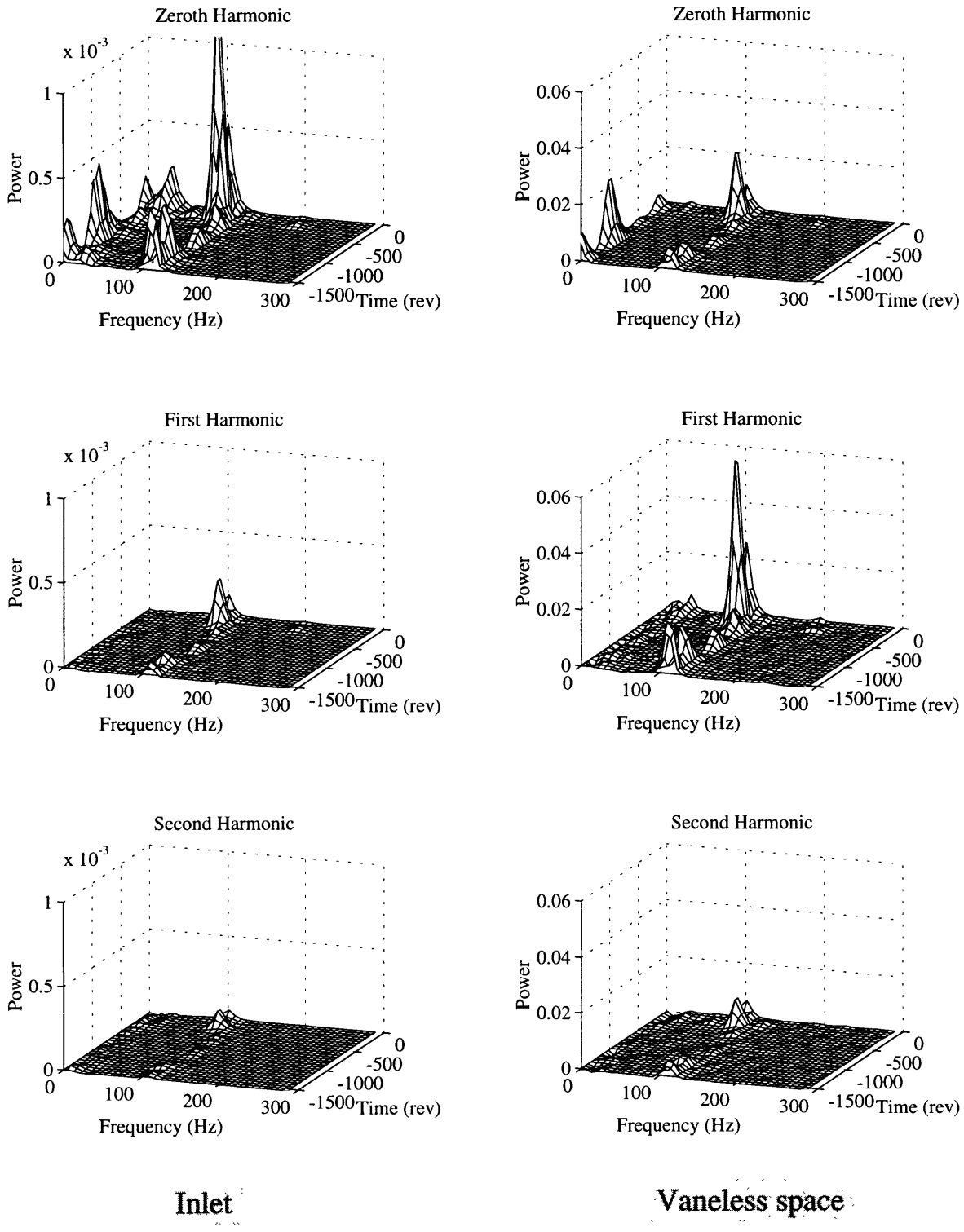

Figure (4.6) Power spectra of spacial fourier coefficients for the inlet and vaneless space static pressures. Time axis in units of revolutions prior to surge at the 95% speed.

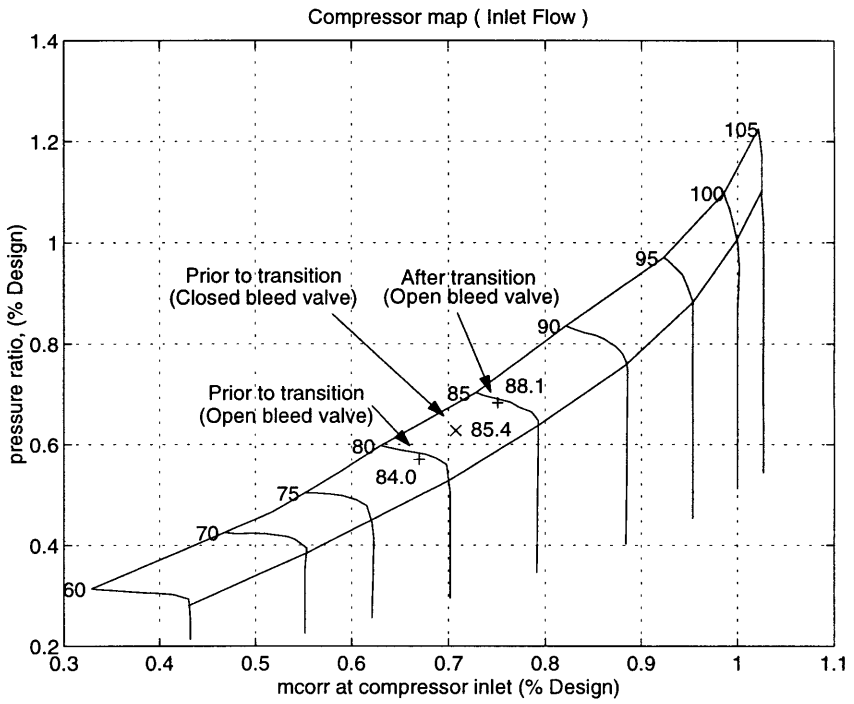

Figure (4.7) Compressor map showing points prior to transition from the 84/85% speed to higher speeds.

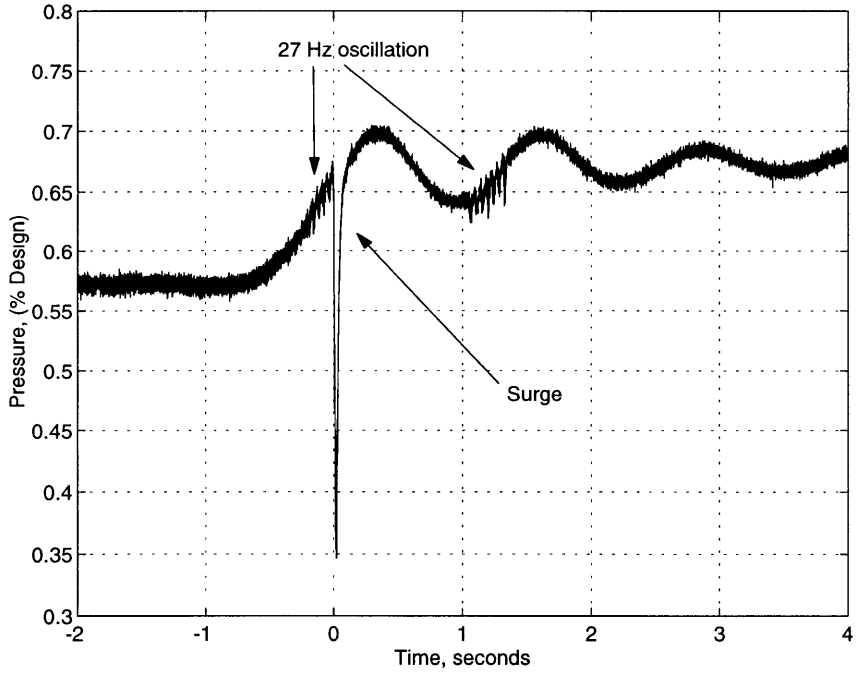

Figure (4.8) Scroll pressure during transition from the 84% speed to the 88% speed.

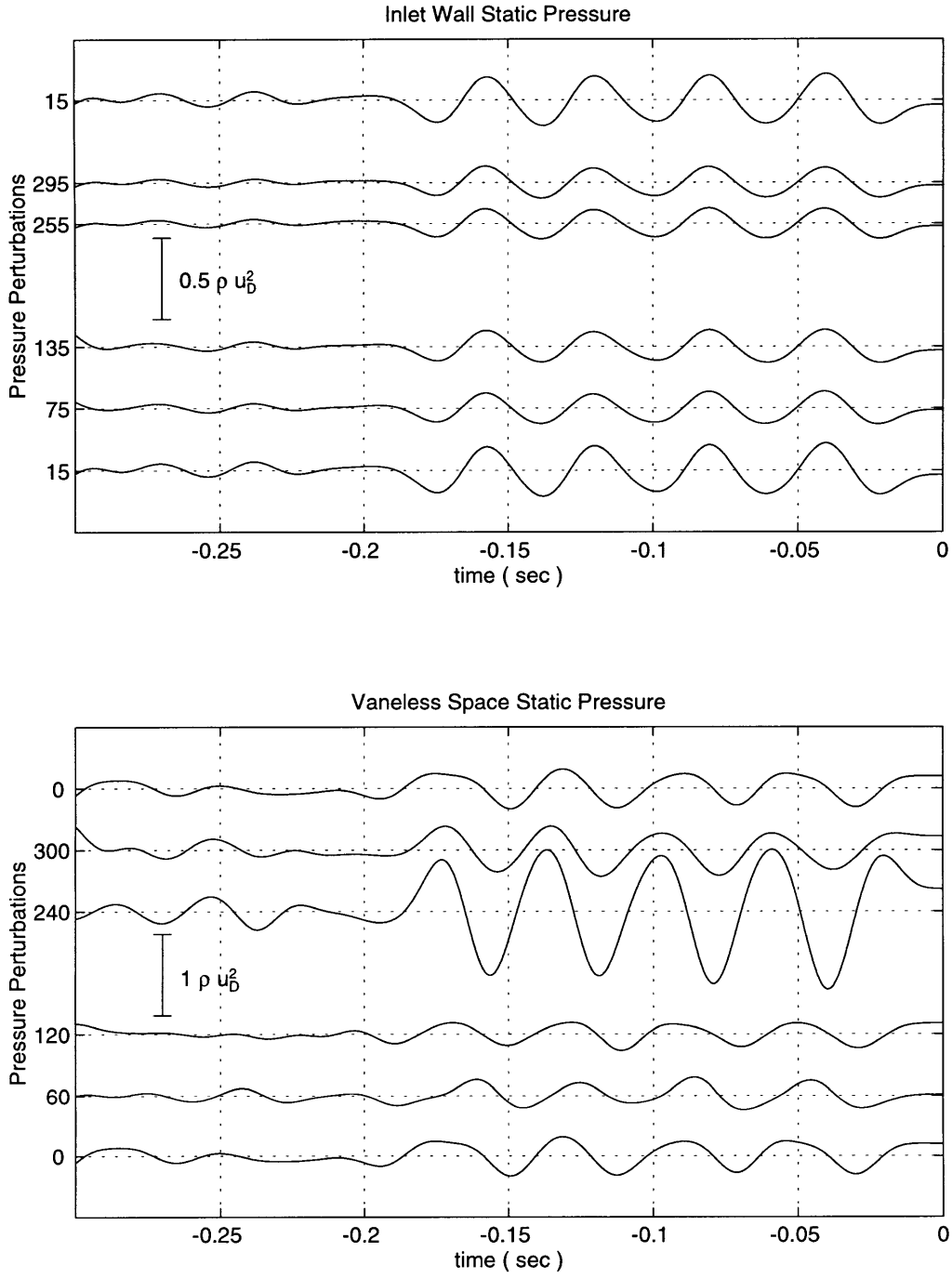

Figure (4.9) Inlet and vaneless space pressure perturbations immediately prior to surge near the 85% speed with an open inducer bleed valve. Perturbations are non dimensionalized by compressor inlet dynamic head at the design point. Circumferential location of pressure tap given along y-axis. 50 Hz low pass filtering

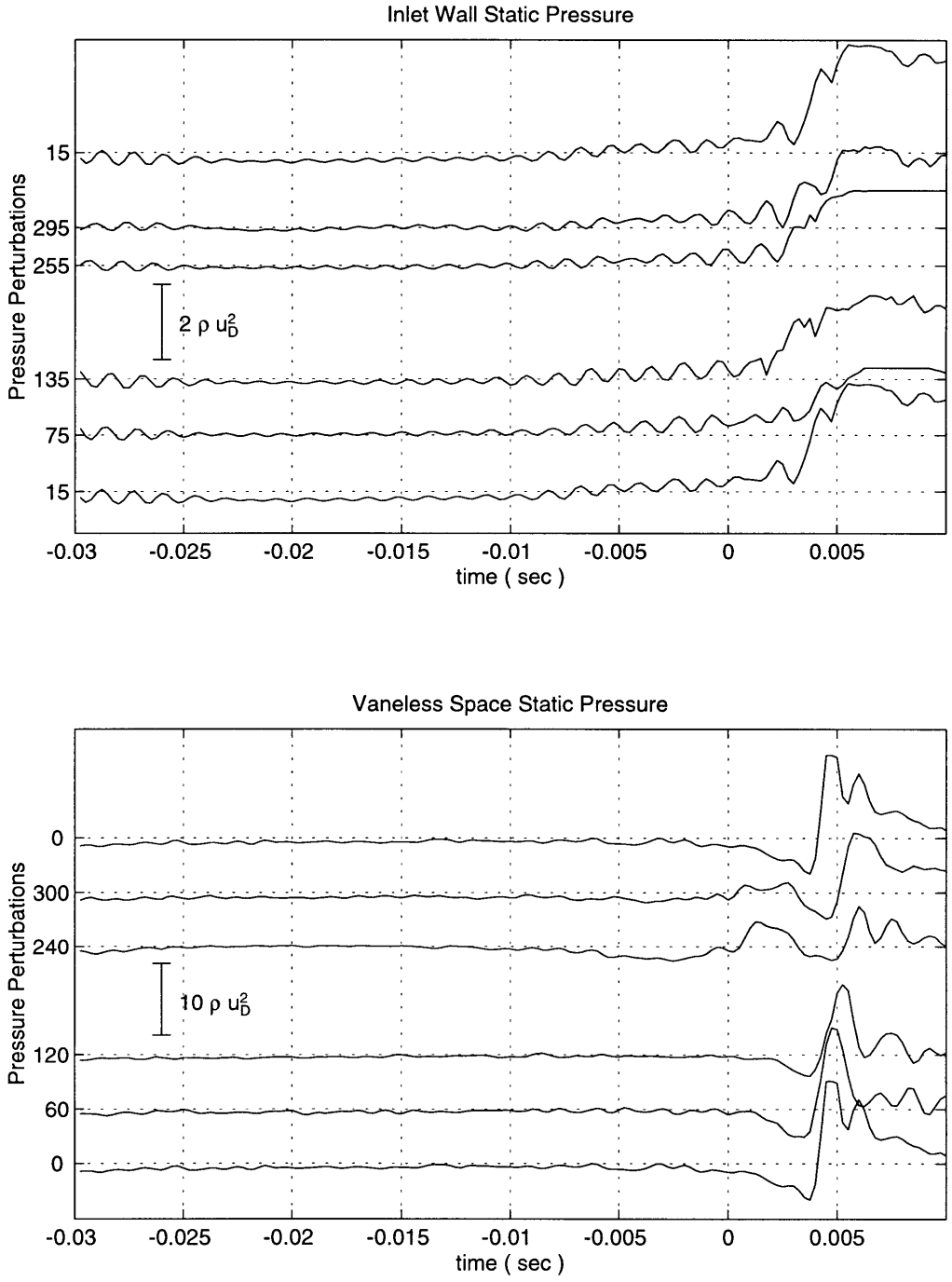

Figure (4.10) Surge inception behavior near the 85% speed with an open inducer bleed valve. Pressure Perturbations are non dimensionalized by compressor inlet dynamic head at the design point. Circumferential location of pressure tap given along y-axis.

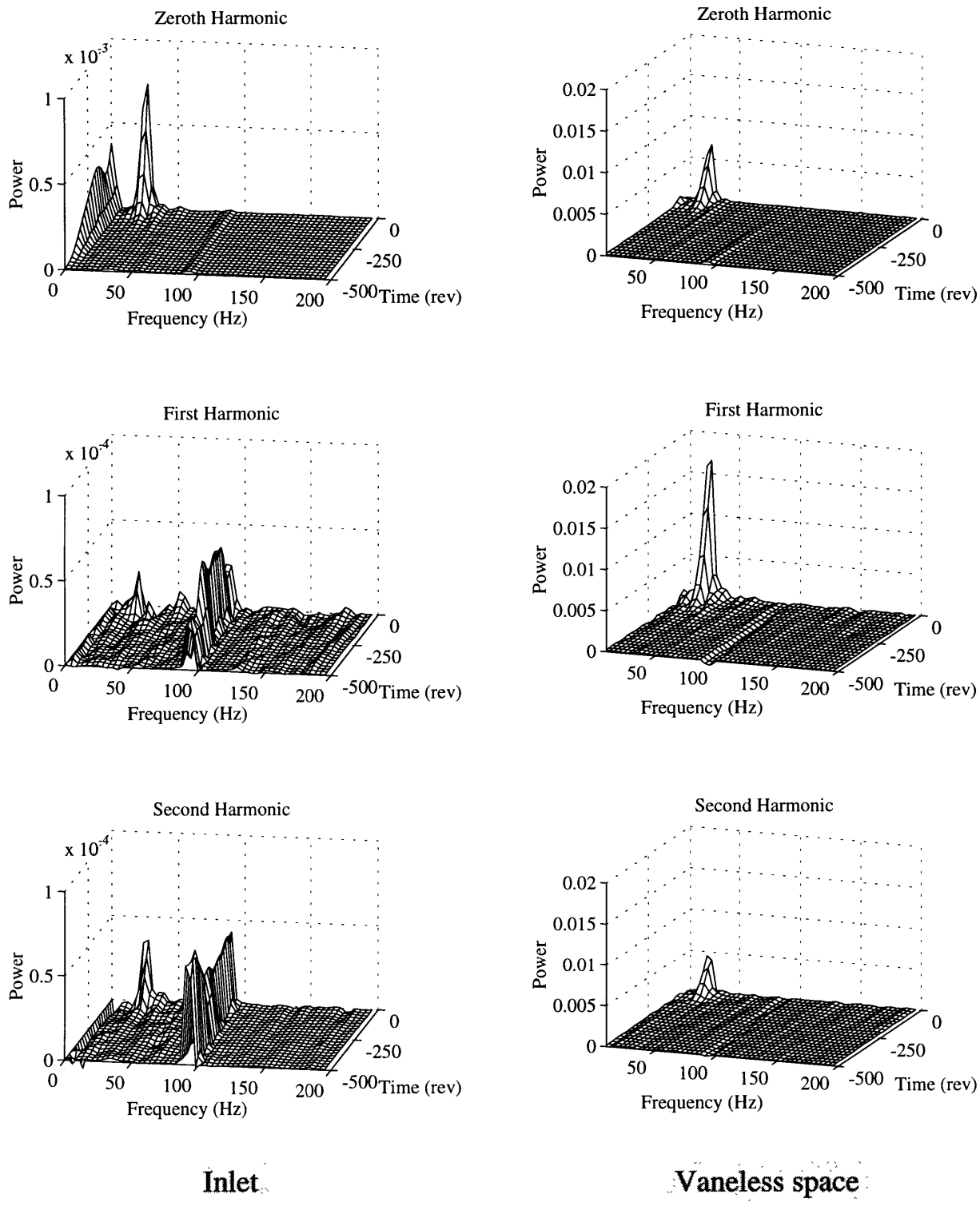

Figure (4.11) Power spectra of spacial fourier coefficients for the inlet and vaneless space static pressures. Time axis in units of revolutions prior to surge at the 85% speed.

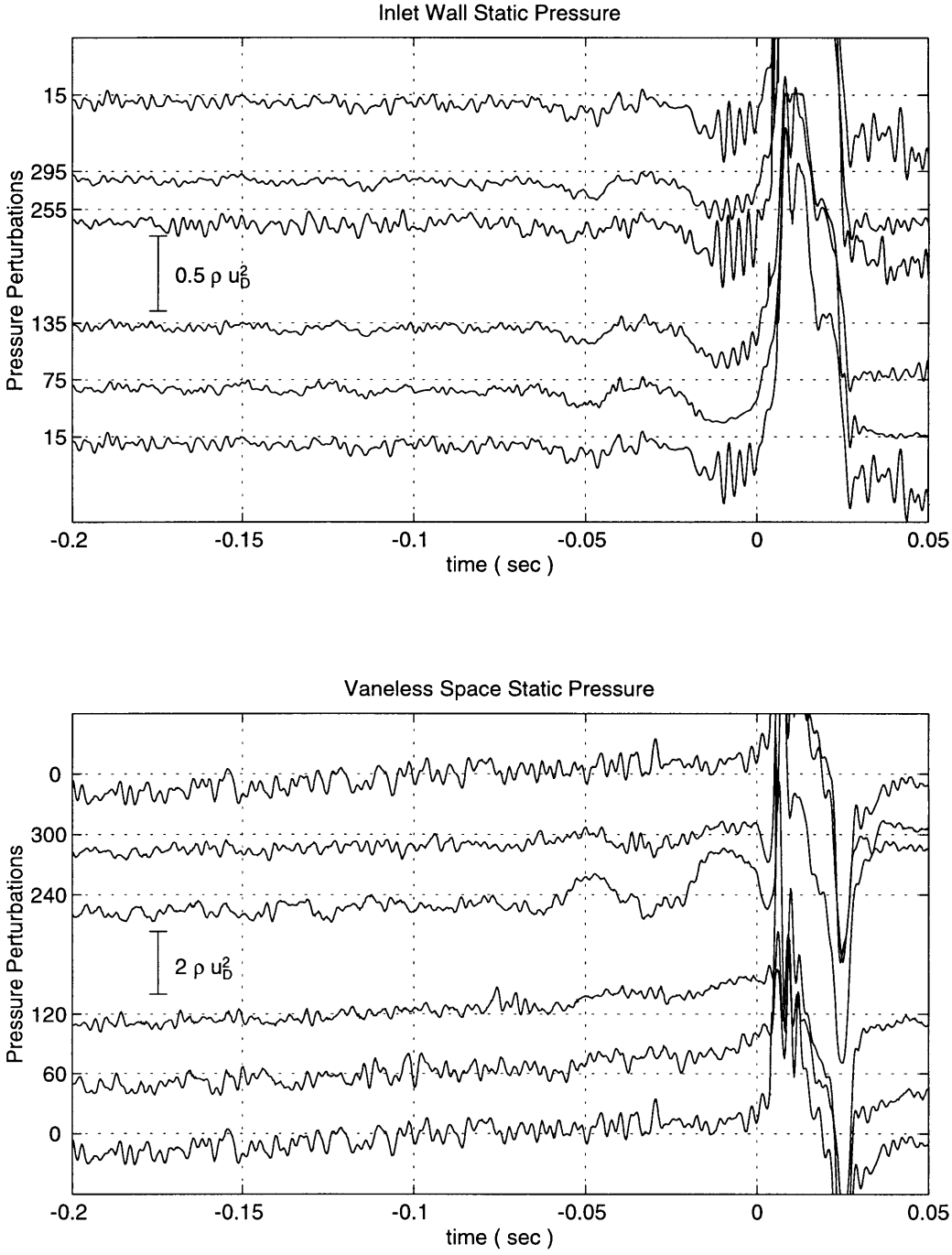

Figure (4.12) Presurge pressure traces during a transition from the 85% speed to higher power with the inducer bleed valve closed. Perturbations non dimensionalized by compressor inlet dynamic head at the design point. Circumferential location of pressure tap given along y-axis. 400 Hz analog filtering.

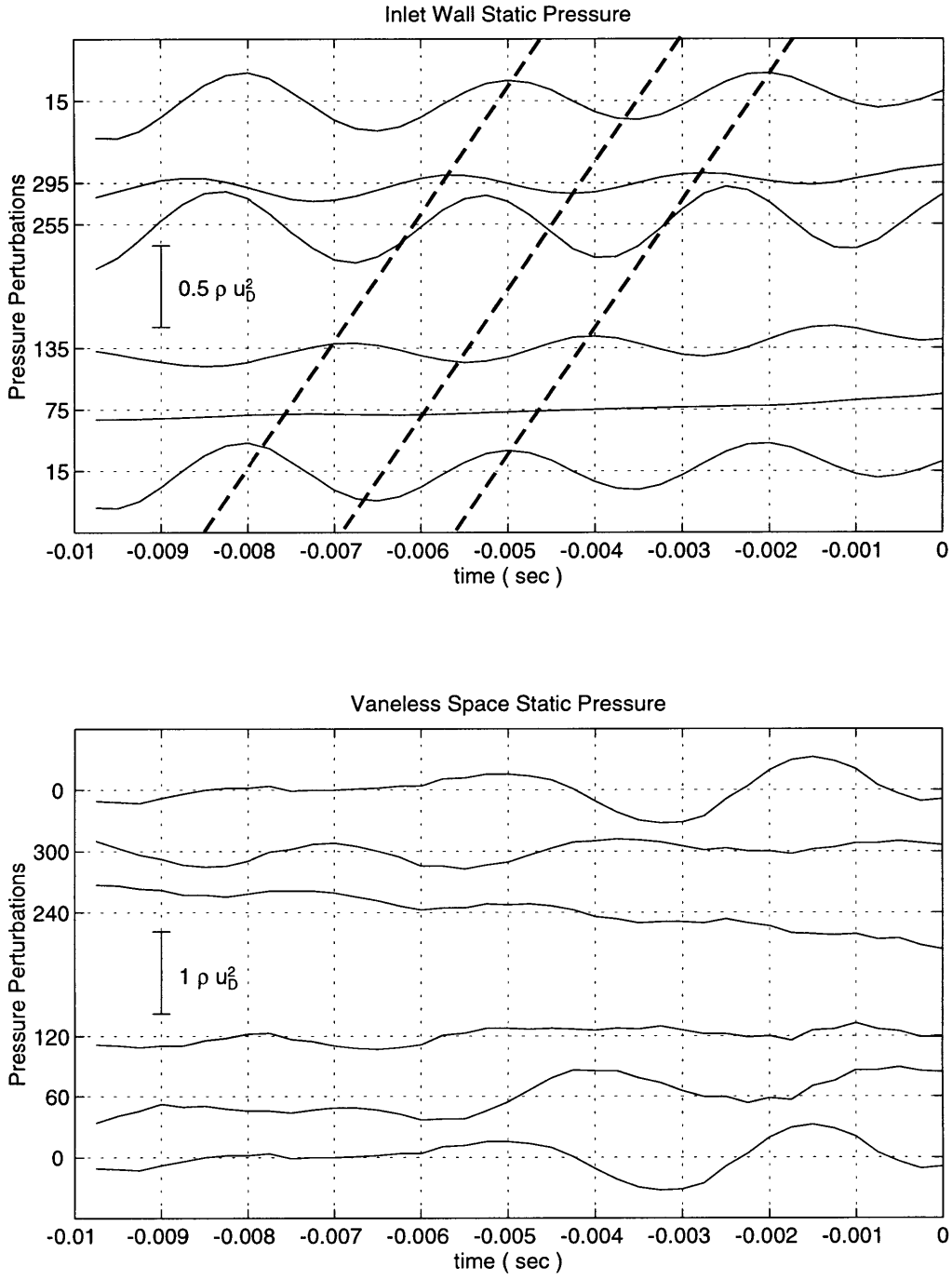

Figure (4.13) Expanded view of 340 Hz oscillation immediately prior to surge. Perturbations are non dimensionalized by compressor inlet dynamic head at the design point. Circumferential location of pressure tap given along y-axis. 400 Hz analog filtering.

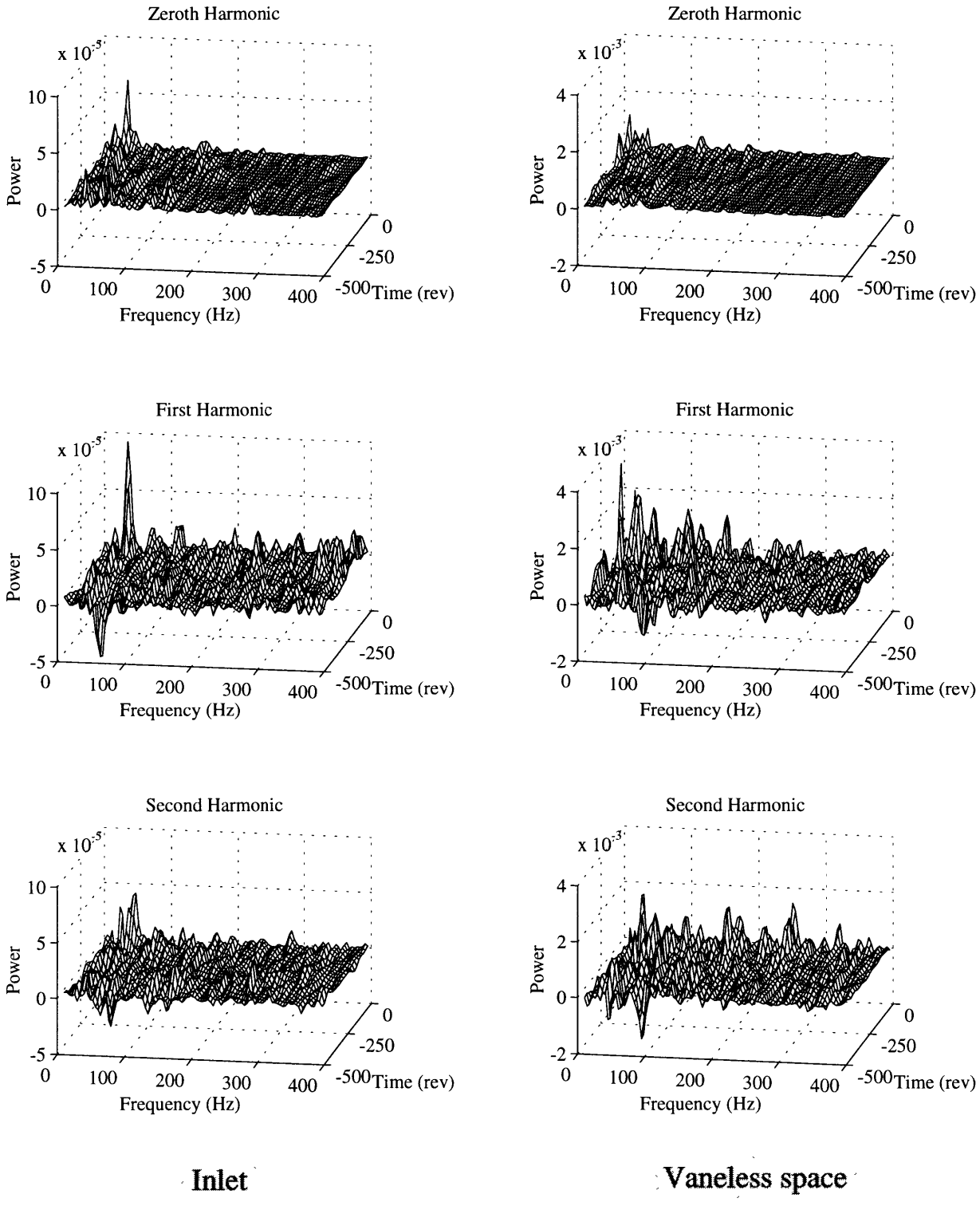

Figure (4.14) Power spectra of spacial fourier coefficients for the inlet and vaneless space static pressures. Time axis in units of revolutions prior to surge at the 85% speed with the inducer bleed valve closed.

Chapter 5

Forced Response Testing

5.1 Introduction

Chapter 5 describes the forced response measurements made as the compressor was throttled towards the surge line. Actuation was achieved by modulating the flow rate injected into the inducer bleed port about a mean injection level using the high speed valve (see chapter 2).

The sequence of events to reach the operating point at which forced response measurements were made, was to close the inducer bleed valve, increase air injection to the mean level, and then increase water injection to the level required for sufficient throttling towards the surge line.

Sections 5.2 and 5.3 discuss the effect of steady air injection and water injection on the operating point. Section 5.4 presents the results of forced response testing.

5.2 Steady Air Injection

The effect of steady air injection was investigated for the engine at 3 operating points along the 95% speed line. These operating points were :

1) The 95% speed with no inserts.
2) The 95% speed with the 5 bar inserts.
3) The 95% speed with the 5 bar inserts after the operating line had shifted.

Figure (5.1) shows the effect of closing the inducer bleed valve and steady air injection on the compressor inlet flow, and exit flow maps. The symbols used in this figure refer to the three cases listed above. The 3 sets of lines connect operating points at the 95% speed with the bleed valve open, the bleed valve closed, and with 3% steady air injection. The lines show the shape of the speed lines on the compressor inlet map.

As explained in chapter 4, inlet flow is the flow rate measured upstream of the compressor, while exit flow is the mass flow rate that goes through the combustor and

turbines when no water is injected into the discharge tubes. Because the nozzle guide vanes are choked, any reduction in the flow leaving through the inducer bleed valve is expected to cause a similar reduction in compressor inlet flow. Air injection into the inducer bleed port should further reduce the inlet flow rate.

Closing the inducer bleed valve and steady air injection reduce the inlet corrected flow and have a small effect on compressor exit corrected flow. For the first case listed above, where the compressor is operating near the choke point, flow injected through the inducer bleed port displaces inlet flow with no further effect on the pressure ratio.

As the compressor approaches the surge line (second and third case) closing the bleed valve and mean air injection result in a reduction in compressor pressure ratio and exit corrected flow. Table (5.1) and (5.2) summarize the effects of closing the inducer bleed valve and steady injection on the compressor corrected flow and pressure ratio. Table (5.1) references all pressure ratio and mass flow changes to the operating point prior to closing the bleed valve. Table (5.2) uses the largest injection flow rate to determine the effect on pressure ratio and mass flow rate. The reference point for this calculation is the operating point with the closed inducer bleed valve. Steady air injection is observed to have the largest effect on pressure ratio and compressor exit flow for points near the surge line.

Table (5.1) Effect of closing the inducer bleed valve on engine performance.

Operating point	$\Delta\dot{m}_{corr,inlet}(\%)$	$\Delta\pi$ (%)
(1)	-1.5%	0
(2)	-1.8%	-0.3%
(3)	-1.9%	-0.2%

Table (5.2) Effect of closing the inducer bleed valve on engine performance.

Operating point	$\dot{m}_{corr,air}/\dot{m}_{corr,inlet(95\%)}$	$\Delta\dot{m}_{corr,inlet}(\%)$	$\Delta\dot{m}_{corr,exit}(\%)$	$\Delta\pi$ (%)
(1)	4.7%	-4.2%	-0.2%	0
(2)	5.0%	-5.3%	-0.3%	-0.3%
(3)	4.9%	-5.4%	-0.5%	-0.4%

5.3 Water Injection

Water injection was used to throttle the engine towards surge so that transfer functions could be estimated at several point along the 95% speed line. Figure (5.2) shows the effect of water injection on the compressor inlet and exit maps. The numbers on the map refer to the following points:

1) 95% speed on the shifted 5 bar operating line.
2) Closed inducer bleed valve.
3) Mean air injection (4% of engine flow rate at the 95% speed with orifice inserts).
4) Water injection, 2.7% of engine flow rate (mean air injection always on during water injection).
5) Water injection, 6.1% of engine flow rate.
6) Water injection, 6.7% of engine flow rate.

Throttling the compressor from point (3) to point (4) resulted in a reduction in the compressor flow rate and an increase in pressure ratio. Successively increasing water injection after this level shows that the speed lines are essentially flat up to water injection levels of 6.7% of the engine flow rate. Note that an additional point has been included between points (4) and (5) to show the shape of the speed lines. The water injection level was not increased to the surge point in this case, but chapter 4 showed that the speed lines had a positive slope prior to surge.

Table (5.3) summarizes the effects of water injection on compressor inlet flow, exit flow, and pressure ratio. Water injection is observed to reduce the compressor inlet flow by 3-4% per 10% of injected water. The percentage varies depending on the level of water injection. The pressure ratio is observed to increase initially by about 0.4%, but it then remains almost constant up to a water injection level of 6% of design flow.

Table (5.3) Effect of water injection on the engine operating point.

$\dot{m}_{water}(\%Design)$	$\Delta\dot{m}_{corr,inlet}(\%Design)$	$\Delta\dot{m}_{corr,inlet}/\Delta\dot{m}_{water}$ (%/%)	$\Delta\pi$ (%)
2.4%	-0.7%	-0.29	0.43%
3.6%	-1.2%	-0.42	0.37%
5.4%	-1.9%	-0.39	0.28%
6.0%	-2.1%	-0.33	0.32%

5.4 Forced Response Testing

Forced response testing on engines is often complicated by low signal to noise ratios. The source of this problem is often a combination of high noise levels due to combustion, and low actuator power compared the engine power (power for compression or power output, 500 HP).

Researchers have investigated actuation schemes to determine the most effective means of forcing compression systems [11,16]. The Allison actuation scheme, described in chapter 2, was effective in forcing the engine up to frequencies as high as 500 Hz. This response has shown that proper selection of an actuation scheme allows use of low input power to effectively force systems with much higher power levels.

The procedure used to measure transfer functions on the Allison engine was discrete sinusoidal forcing at 30 frequencies between 6-500 Hz. Sinusoidal forcing was limited to 30 frequencies to reduce the testing time required to obtain the transfer functions. Data was analyzed using two different procedures with very similar results being obtained for frequencies up to 300 Hz. The first procedure estimated the transfer function, using the cross spectrum and power spectrum of the input and output signals (Matlab's "spectrum.m" function), for each discrete frequency and then extracted a single point out of the complete frequency range. Coherence was greatly improved with this method when forcing was done at the exact frequencies where the estimates were calculated. The second procedure used the correlational analysis method described by Ljung [20].

Forced response measurements were done at 3 points along the 95% speed as the compressor was throttled towards the surge line, Figure (5.2). The first point was the shifted 5 bar operating point with mean air injection and no water injection, while the other two points were with water injection. Table (5.4) summarizes the compressor corrected mass flow rates and pressure ratios at the three points.

Table (5.4) Operating points at which the transfer functions were estimated.

Operating Point	$\dot{m}_{corr,inlet}(\%Design)$	$\dot{m}_{corr,exit}(\%Design)$	$\pi\ (\%Design)$
(3)	84.8%	85.2%	86.5%
(5)	82.8%	83.3%	86.8%
(6)	82.7%	83.2%	86.8%

The transfer function from valve command to scroll pressure is shown in figure (5.3). Four sets of poles appear to be located at 20, 30, 130, and 400 Hz. Growth is seen below 50 Hz, but no peak occurs at the Helmholtz resonator frequency (24-27 Hz). Despite the fact that no peak is seen 27 Hz, high amplitude (the actual amplitude depends on the operating point) forcing at this frequency was found to destabilize the compressor and surge the engine.

Growth is clearly seen at 130 Hz as the engine is throttled towards the surge line. This mode was observed to increase in amplitude, prior to surge, to a level that destabilized the compressor. The coherence observed around this peak shows that actuation is capable of effecting this mode.

The 400 Hz peak was determined to be an acoustic resonance in the circumferential plenum that feeds the inducer bleed slots (see figure (2.14)). Chapter 2 showed that the resonance occurred at 330 Hz for the cold plenum, and elevated temperatures should shift this resonance to higher frequencies. Figure (5.4) shows the transfer function from valve command to the inducer bleed plenum pressure. The amplitude is observed to roll off after about 140 Hz with zeros located at 250 Hz and the inducer bleed plenum resonance is clearly seen at 400 Hz.

Table (5.5) compares the peaks observed in the transfer functions to acoustic resonances and peaks seen during engine operation. The 30 Hz and 130 Hz transfer function peaks correspond well to acoustic resonances. The 20 Hz peak may correspond to the hot acoustic resonance predicted to occur at 15-16 Hz. Higher frequency acoustic resonances (327-356 Hz) are not seen in the transfer functions, but this may be difficult to confirm because of the high amplitude associated with the inducer bleed plenum resonance occurring at 400 Hz.

Figure (5.5) shows the transfer function from the plenum pressure to the scroll pressure. This figure shows the same trends as the valve command to scroll pressure transfer function with a few exceptions. The large peak at 400 Hz is no longer seen, and a small peak is observed at about 300 Hz. No oscillation was observed at this frequency during engine operation, and it has not been of importance for compressor stability.

Figure (5.6) Shows the transfer function from valve command to the 5 inlet pressure taps. Actuation is clearly observed to be axisymmetric well up to the 200 Hz range with variations in amplitude of about 4 dB, and variations in phase of less that 25 degrees.

Transfer functions were also estimated using the correlation analysis method. Figure (5.5) compares the result of this estimate to those calculated using Matlab's "spectrum.m" function. Both estimation methods showed very similar results up to 300 Hz and differences occurred above this frequency. The cause of these differences is not known,

and because engine instability appears to be related to frequencies below 200 Hz, this difference was not of concern.

Table (5.5) Comparison of acoustic resonances to peaks observed in PSD's during engine operation, and peaks seen in transfer functions.

Frequency measured (cold)	Frequency predicted (hot)	Peaks observed in the PSDs during engine operation (Hz)	Peaks observed in transfer functions (Hz)
11	14.7-16	10-16	20
20	26.8-29.2	24-26	30
75-78	102-111	110-140	-
100	134-146		120-130
244	327-356	320	-
400	536-584	500	-

5.5 Conclusions

Forced response measurements at several points along the 95% speed were made. Actuation was achieved by modulating air injected into the inducer bleed slots about a mean injection level. Water injection was used to throttle the engine toward the surge line.

Steady air injection was observed to displace flow coming through the compressor inlet with no effect on pressure ratio near the choke portion of the compressor characteristic. As the surge line was approached, however, steady injection caused a reduction in pressure ratio and compressor exit corrected flow due to increased losses and blockage.

Water injection was observed to effectively throttle the compressor towards the surge line. The throttling effect was estimated to be 3-4% of the compressor inlet corrected flow per 10% of water injection. The speed lines were observed to be fairly flat except for an increase in pressure ratio that occurred at low injection rates, and a positive sloped region prior to the surge point (see chapter 4).

Forced response measurements showed clear growth of the mode responsible for surge near the 95% speed, as the compressor was throttled towards the surge line.

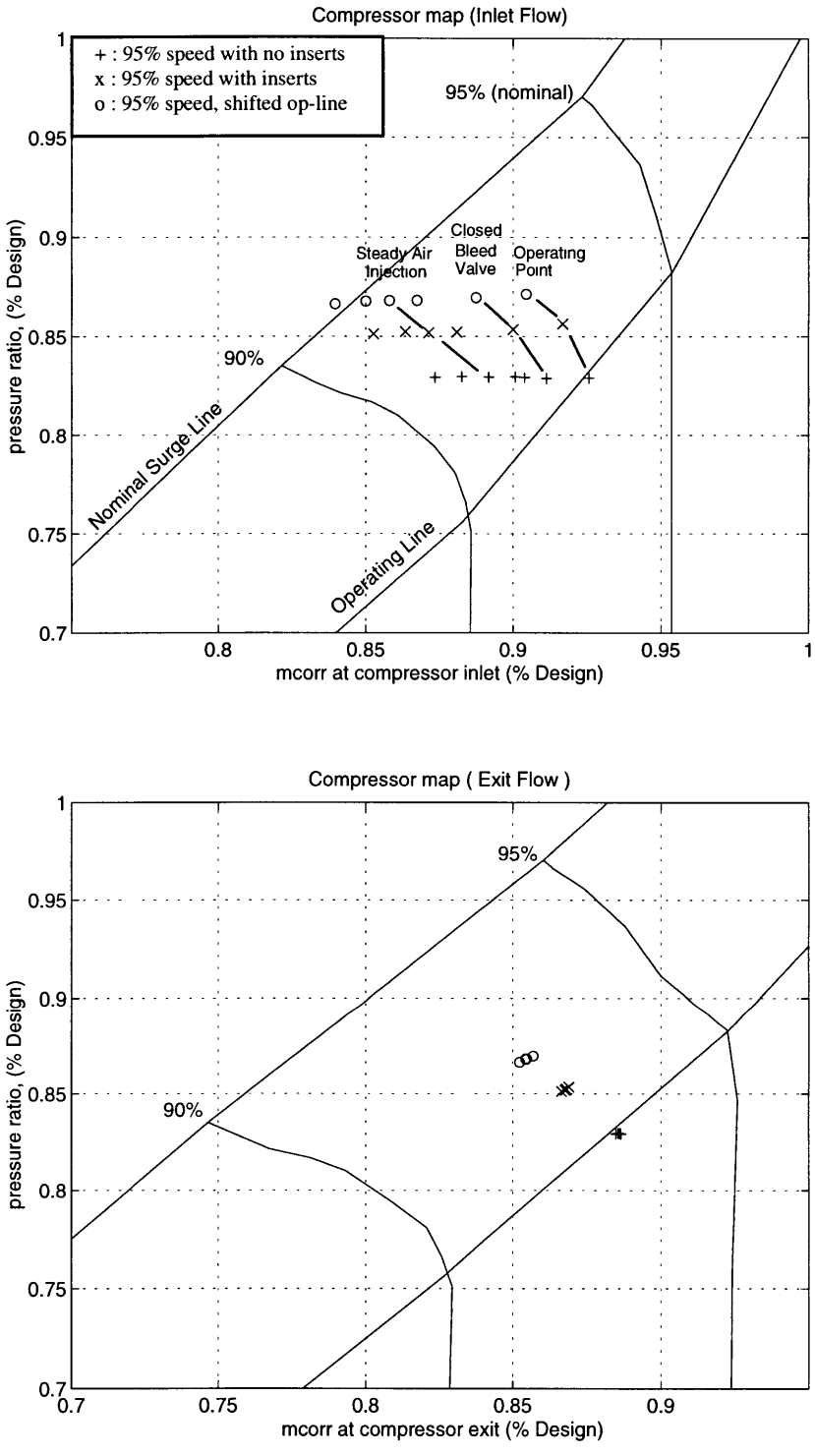

Figure (5.1) Effects of closing the inducer bleed valve and mean air injection on the compressor inlet and compressor exit operating points.

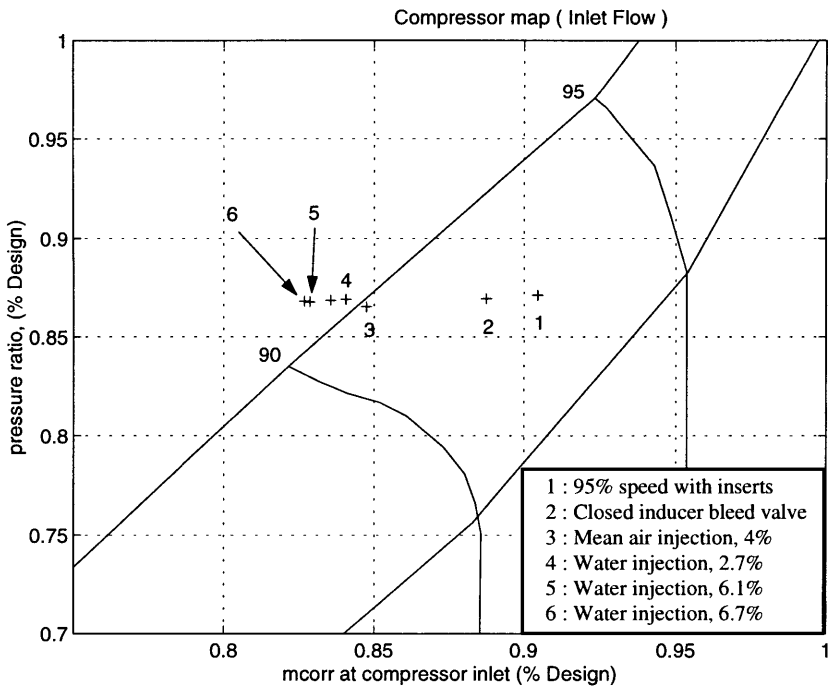

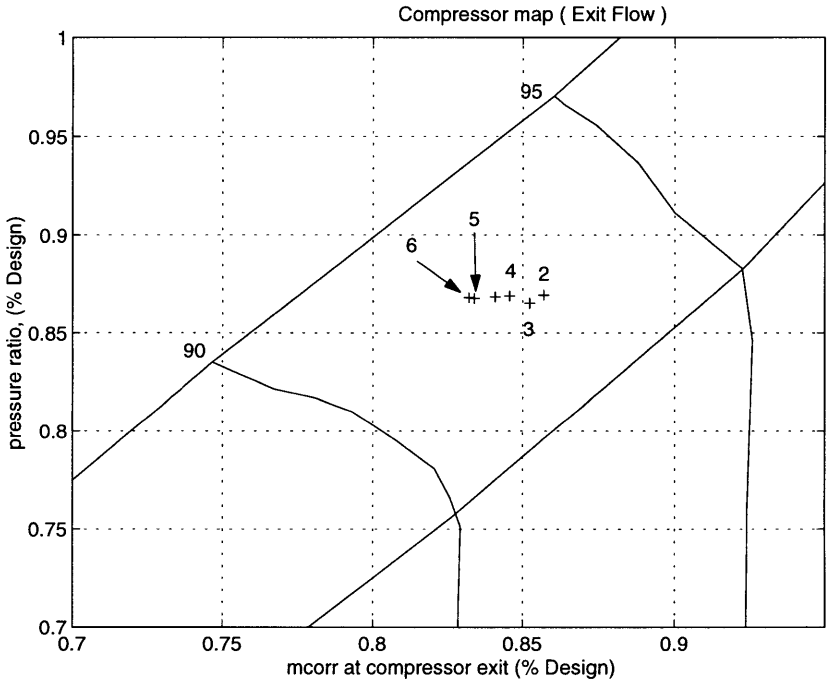

Figure (5.2) Effects of water injection on the operating point and forced response points.

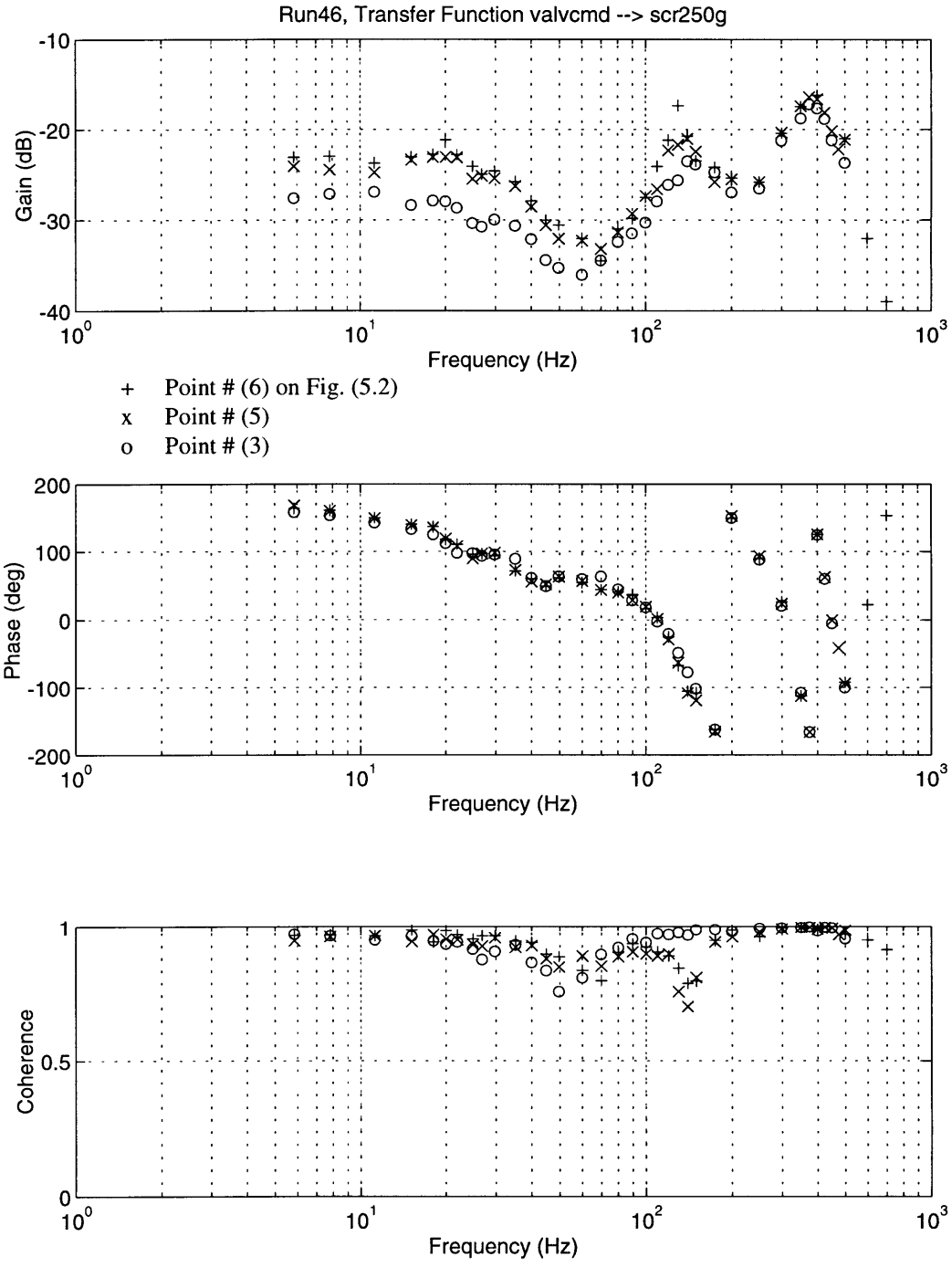

Figure (5.3) Valve command to scroll pressure transfer functions.

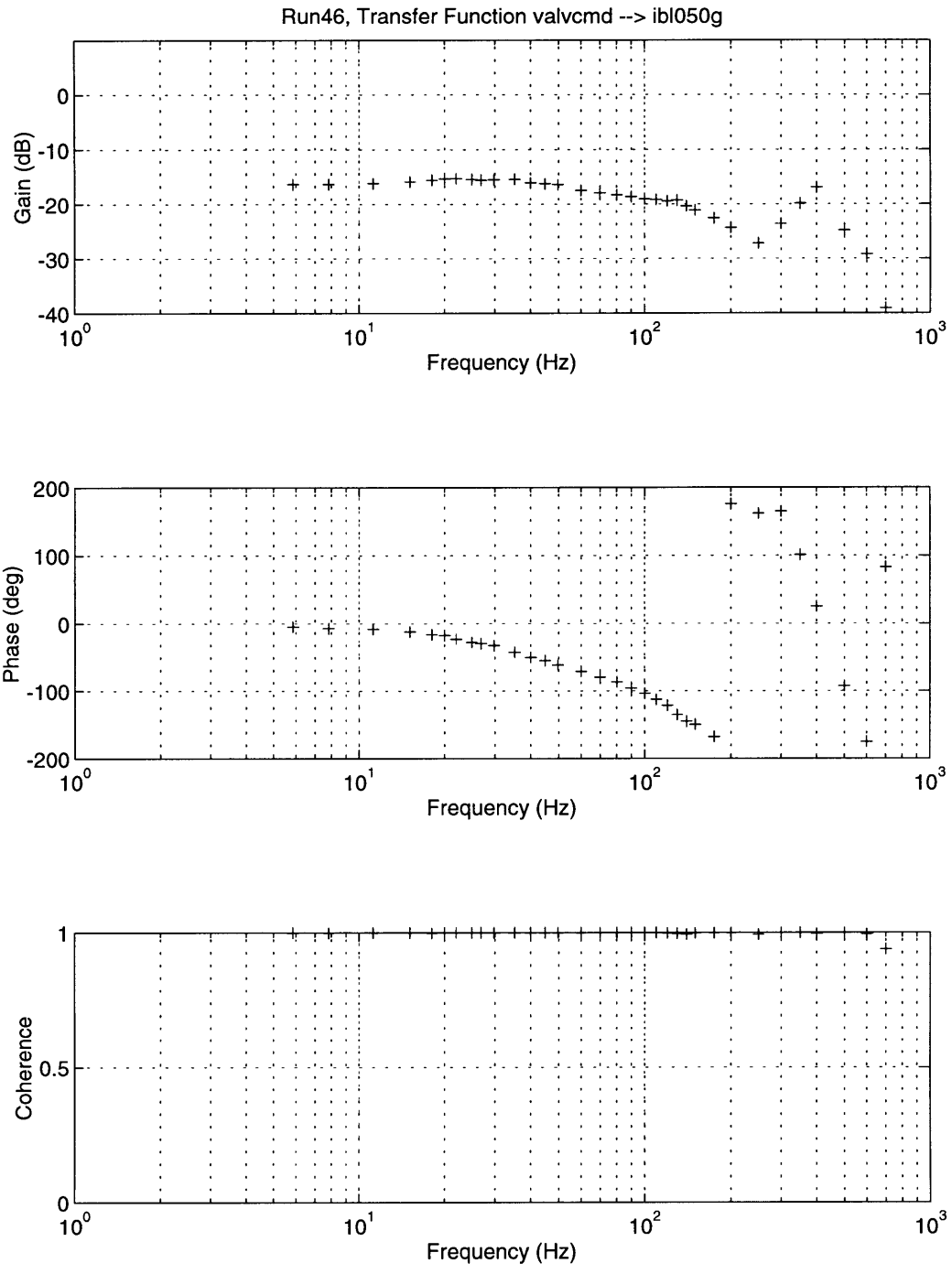

Figure (5.4) Valve command to inducer bleed pressure transfer function.

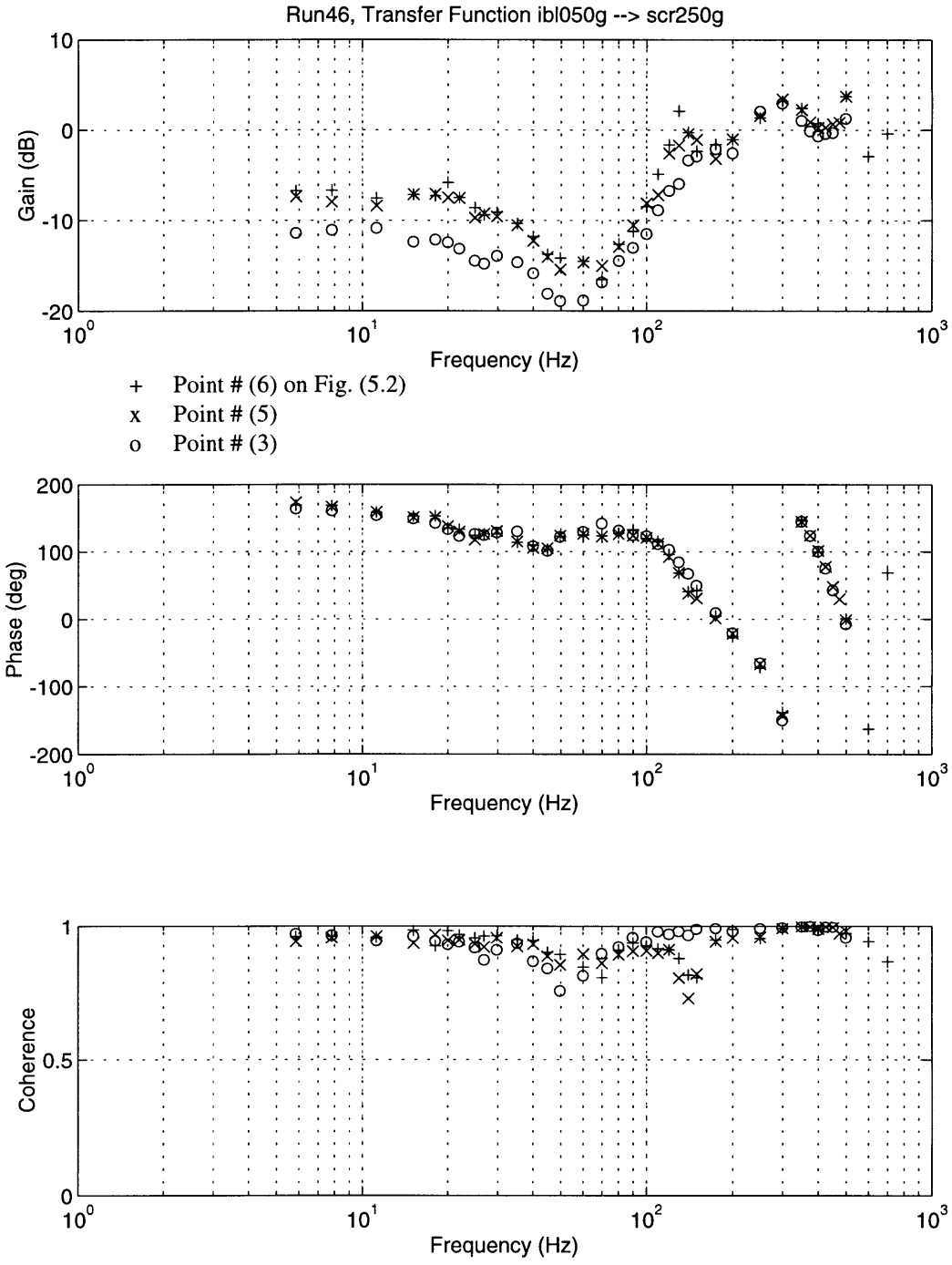

Figure (5.5) Inducer bleed pressure to scroll pressure transfer functions.

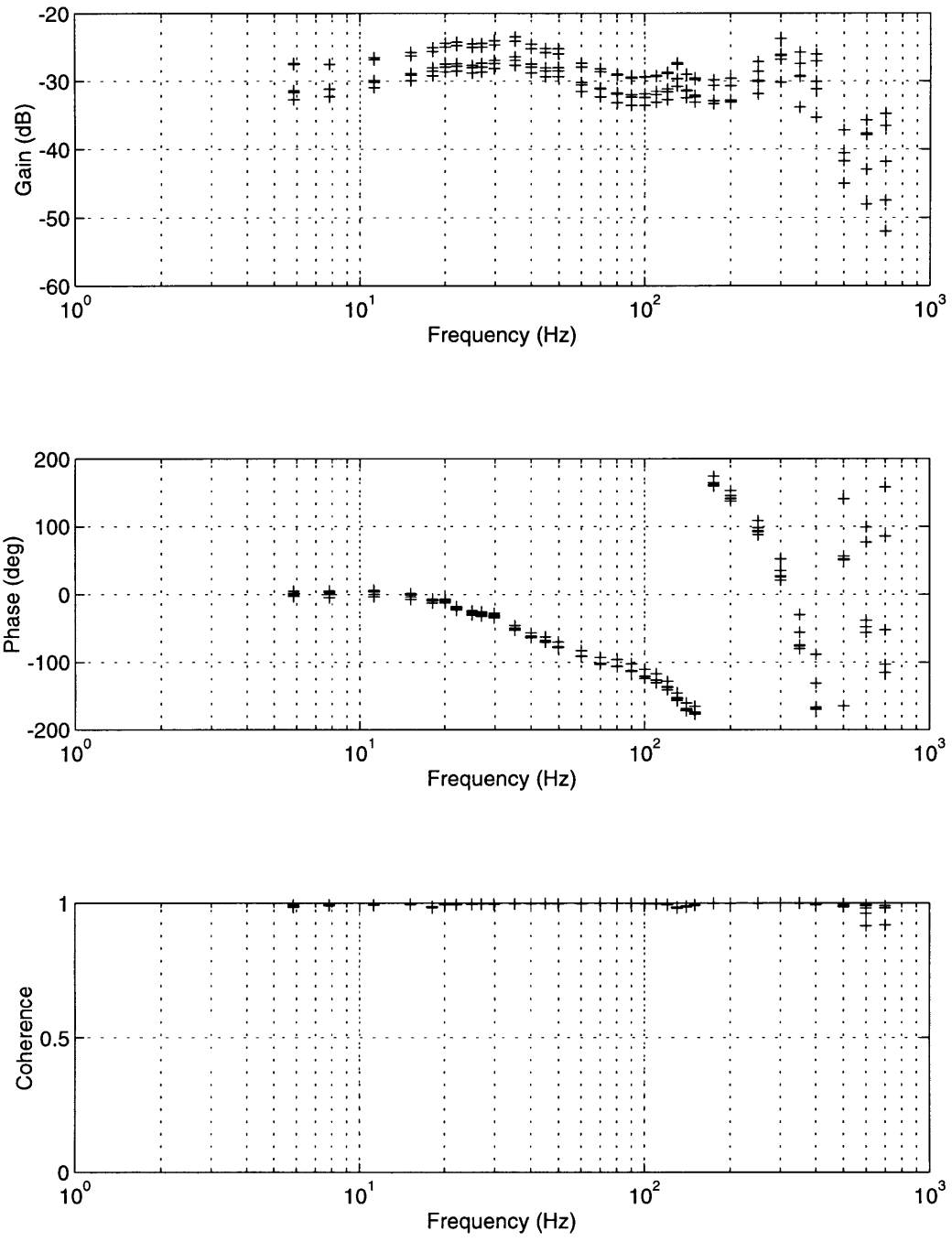

Figure (5.6) Valve command to inlet pressure transfer functions.

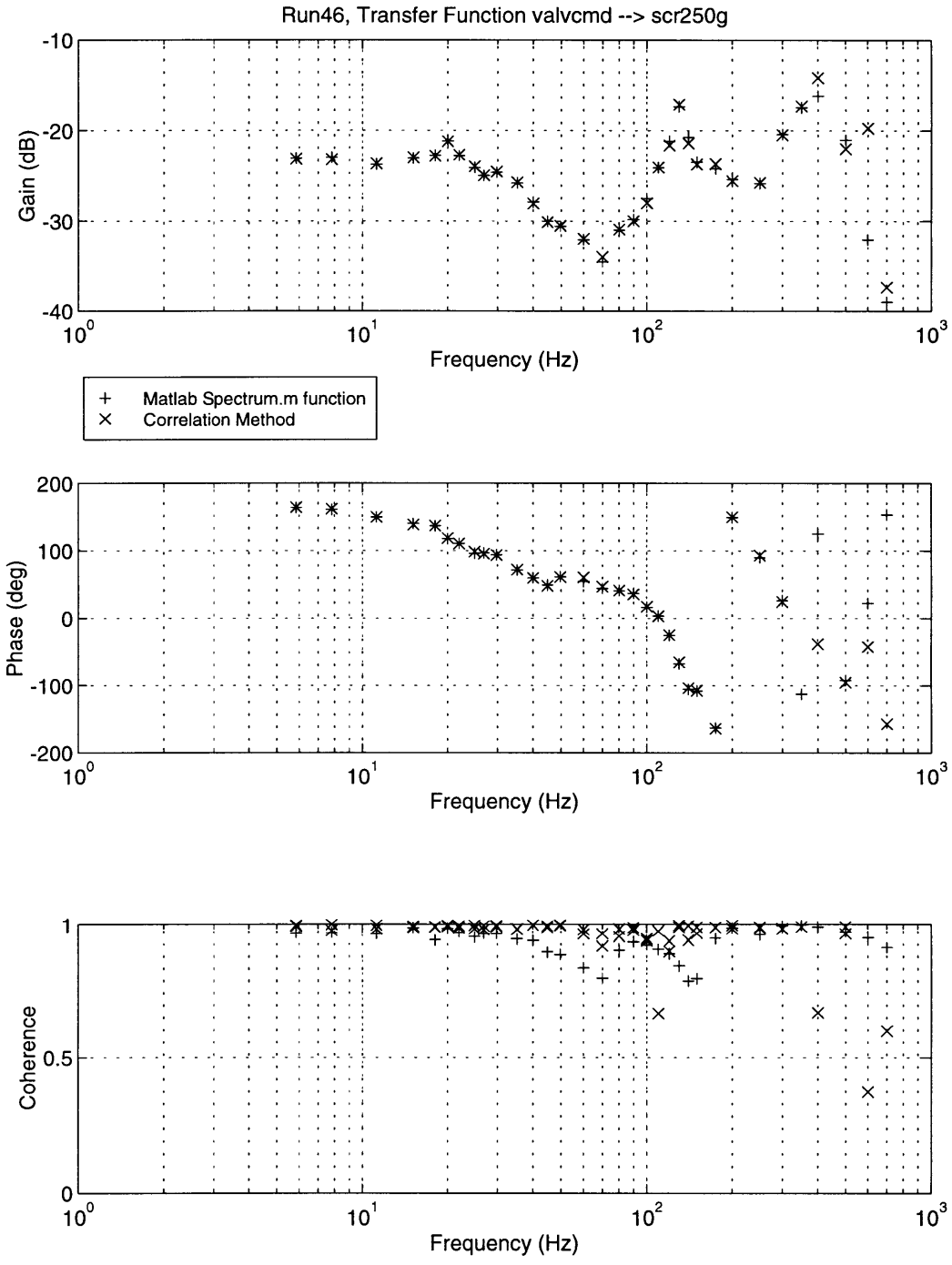

Figure (5.7) Comparison between Matlab's "spectrum.m" function and the correlation analysis method.

Chapter 6

Summary, Conclusions & Recommendations

6.1 Summary and Conclusions

Presurge behavior was investigated on an aircraft gas turbine engine. The engine was throttled towards the surge line using inserts that produced losses between the compressor and combustor, and water injection downstream of the compressor.

Forced response measurements were taken at 3 points along the 95% speed line. Actuation was achieved by modulating flow injected into the engine through the inducer bleed slots about a mean injection level.

The following conclusions are made concerning the work presented in this thesis:

1) The "5 bar inserts" shifted the operating point up the speed line to a new point where the pressure ratio had increased by 2.5% design and the corrected mass flow decreased by 3%. The inserts also had an effect on the engines spectral content; the power spectral density of an oscillation at 135 Hz decreased. This decrease may be due to increased damping caused by the orifice inserts (unsteady effect), or due to the change in the steady operating point that occurs when they are included; the new operating point may be more damped to oscillations at certain frequencies.

2) Water injection was used to throttle the engine towards surge. It resulted in a 2.1% design reduction in compressor inlet corrected flow for a water injection level of 6% design. Water injection also had an effect on the combustor's spectral content. For water injection levels above 4.8-5.4% design (5.4-6% engine flow), a large peak at 80 Hz and damping of frequencies above 130 Hz occurred. The 80 Hz peak may be due to the water pumps piston cycle.

3) Experimentally determined acoustic resonances, below 100 Hz, occurred at 11, 20, 52, 78, and 100 Hz. These resonances were estimated to shift by 35-45% due to temperatures observed in the engine at the 95% speed. Modeling showed that assuming

all volume with significant compliance to be at the combustion temperature over estimates the frequency shift by 30%. This assumption is made when one uses the ratio of the speed of sound for the hot and cold temperatures to estimate the frequency shift.

4) Spectral content growth was observed in the unforced engine at 24-26, 110-140, and 330 Hz as the engine speed was varied over the operating range. The 24-26 Hz mode was found to increase rapidly near the 85% speed line. This was the Helmholtz mode and oscillations were observed to be axisymmetric. The110-140 Hz mode was observed to increase as the engine was throttled towards the surge line at the 95% speed. The 330 Hz oscillation was found to be a rotating disturbance and was largest at the 71% speed.

5) Surge at the 95% speed was investigated with steady air injection into the inducer bleed, and water injection into the discharge tubes. Surge at this speed was preceded by bursts of high amplitude 100-105 Hz oscillations seen throughout the engine. Between these bursts lower amplitude 120 Hz oscillations occurred. Waterfall plots of the inlet and vaneless space pressure perturbations PSDs showed growth at 30 Hz and 100-120 Hz prior to surge. Impeller and diffuser rotating stall were not observed and surge inception may be due to growth in the 30 Hz or 100-120 Hz oscillation. This oscillation split the annulus along a diagonal with flow in one half 90 degrees out of phase compared to the other. During this oscillation pressure perturbations in one half the annulus were 90 degrees out of phase compared to the other half.

6) Surge due to acceleration transients was investigated near the 85% speed with the inducer bleed valve open and closed. Surge with the inducer bleed valve open was preceded by behavior similar to that observed at the 95% speed. An asymmetric pattern similar to that of the 100-105 Hz was observed at the vaneless space. The oscillation frequency was 27 Hz, in this case, and was probably due to the Helmholtz mode. Although this mode was observed to be essentially axisymmetric during steady operation near the 85% speed, no region of axisymmetric flow was observed during the 150 ms of presurge oscillations.

Surge at the 85% speed with the inducer bleed valve closed was preceded by an oscillation at 27 Hz oscillation, as well as a 340 Hz oscillation immediately prior to surge. The 340 Hz oscillation may be a rotating disturbance with a speed of 50% the rotor frequency.

7) Actuation for forced response measurements was achieved by modulating flow injected into the engine through the inducer bleed slots about a mean injection level. Actuation was axisymmetric up to 200 Hz and was effective in forcing the engine up to frequencies as high as 500 Hz.

8) Steady injection into the engine through the inducer bleed slots was found to displace flow coming in through the compressor inlet with no effect on pressure ratio near the choke portion of the compressor characteristic. As the surge line was approached, however, steady injection caused a reduction in pressure ratio and compressor exit corrected flow.

9) Forced response measurements were made at several points as the engine was throttled towards the surge line at the 95% speed. Transfer functions from valve command to scroll pressure showed that modes at 20, 30 and 110-140 Hz became less damped near surge. Actuation was capable of affecting these modes and feedback control may be capable of stabilizing the compressor.

6.2 Recommendations

The surge behavior at the 85% speed, with the inducer bleed bypass valve open, and at the 95% speed showed that a non axisymmetric oscillation occurs at the vaneless space during the precursor period prior to surge. During these oscillations pressure perturbations in one half the annulus were 90 degrees out of phase compared to the other half.

It was not clear whether this behavior was due to non axisymmetric pressure oscillations in the scroll and discharge tubes, or whether it was merely the compressor's response to high amplitude axisymmetric oscillations.

The source of the asymmetry observed in the vaneless space may be determined by locating multiple pressure transducers in the scroll or discharge tubes. This information may be used to design an adequate actuation scheme that can stabilize the compressor.

References

[1] Charles LeJambe, "Development and Application of a Multi-stage Navier-Stokes Solver: Application to a High Pressure Compressor Stage," Presentation at the Gas Turbine Laboratory, October 1996.

[2] Epstein, A.H., Ffowcs Williams, J.E., Greitzer, E.M., "Active Stabilization of Aerodynamic Instabilities in Turbomachines," AIAA Journal of Propulsion and Power, Vol. 5, No. 2, March-April 1989, pp.203-211.

[3] Emmons, A.W., Pearson, C.E., Grant, H.P., "Compressor Surge and Stall Propagation," Trans. ASME, Vol. 79, April 1955, pp. 455-469.

[4] Amann, C.A., Nordenson, G.E., Skellenger, G.D., "Casing Modification for Increasing the Surge Margin of a Centrifugal Compressor in an Automotive Turbine Engine", ASME Journal of Engineering for Power, Vol. 97, July 1975, pp. 329-336.

[5] Grietzer, E.M., "Surge and Rotating Stall in Axial Flow Compressors, Parts I and II," ASME Journal of Engineering for Power, Vol. 98, April 1976, pp. 190-217.

[6] Toyama, K., Rundstadler, P.W., Jr., Dean, R.C., Jr., "An Experimental Study of Surge in Centrifugal Compressors," Journal of Fluids Engineering, Vol.99, March 1977, pp. 115-131.

[7] Fink, D.A., "Surge Dynamics and Unsteady Flow Phenomena in Centrifugal Compressors," MIT Gas Turbine Laboratory Report No. 193, 1988.

[8] Ffowcs Williams, J.E., Huang, X.Y., "Active Stabilization of Compressor Surge," Journal of Fluid Mechanics, Vol. 204, pp. 245-262.

[9] Pinsley, J.E., "Active Control of Centrifugal compressors Surge," M.S. Thesis, Department of Aeronautics and Astronautics, Massachusetts Institute of Technology, October 1988.

[10] Gysling, D.L., "Dynamic Control of Centrifugal Compressor Surge Using Tailored Structures," M.S. Thesis, Department of Aeronautics and Astronautics, Massachusetts Institute of Technology, August 1989.

[11] Simon, J.S., "Feedback Stabilization of Compression Systems," MIT Gas Turbine Laboratory Report No. 216, March 1993.

[12] Ffowcs Williams, J.E., Graham, W.R., "An Engine Demonstration of Active Surge Control," ASME Paper 90-GT-224.

[13] Ffowcs Williams, J.E., Harper, M.F.L., Allwright, D.J., "Active Stabilization of Compressor Instability and Surge in a Working Engine," ASME Journal of Turbomachinery, Vol. 115, January 1993, pp. 68-75.

[14] Borror, S.L., "Natural and Forced Response Measurements of Hydrodynamic Stability in an Aircraft Gas Turbine Engine," M.S. Thesis, Department of Aeronautics and Astronautics, Massachusetts Institute of Technology, May 1994.

[15] Corn, B., "Surge Dynamics of a Helicopter Engine Gas Generator," M.S. Thesis, Department of Aeronautics and Astronautics, Massachusetts Institute of Technology, August 1997.

[16] McNulty, G.S., "A Study of Dynamic Compressor Surge Control Strategies for a Gas Turbine Engine," M.S. Thesis, Department of Aeronautics and Astronautics, Massachusetts Institute of Technology, September 1993.

[17] Berndt, R.G., "Actuation for Rotating Stall Control of High Speed Compressors," M.S. Thesis, Department of Aeronautics and Astronautics, Massachusetts Institute of Technology, January 1995.

[18] Chapman, D.C., "Model 250-C30/C28B Development," AGARD Conference Proceedings No. 282, "Centrifugal Compressors, Flow Phenomena and Performance", AGARD-CP-282, 7-9 May 1980, pp. 20-1 to 20-6.

[19] Tryfonidis, M., Etchevers, O., Paduano, J.D., Epstein, A.H., Hendricks, G.J., "Prestall Behavior of Several High-Speed Compressors," Journal of Turbomachinery, Vol. 117, January 1995, pp. 62-80.

.20] Ljung, L., "System Identification: Theory for the User," Prentice Hall, New Jersey, 1987.

Appendix A

Acoustic Duct Model for Engine

A.1 Derivation

The acoustic duct model is shown in figure (A.1). The duct is modeled using the 1-D wave equation, which may be written as a transmission matrix linking perturbations at one end of the duct to those at the other end, namely;

$$\begin{bmatrix} \tilde{p} \\ \rho_d \tilde{u} a_d \end{bmatrix}_{x=0} = \begin{bmatrix} \cos(\omega L/a_d) & j\sin(\omega L/a_d) \\ j\sin(\omega L/a_d) & \cos(\omega L/a_d) \end{bmatrix} \begin{bmatrix} \tilde{p} \\ \rho_d \tilde{u} a_d \end{bmatrix}_{x=L} \tag{A.1}$$

$\tilde{p}$ and $\tilde{u}$ are the pressure and velocity perturbations, respectively.

The plenum sets up a boundary condition that may be derived from the conservation of mass equation. Assuming isentropic compression and uniform pressure throughout the plenum gives:

$$\tilde{p} = \frac{\rho\, a_p^2 A}{Vs} \tilde{u} \tag{A.2}$$

Therefore an impedance may be defined at x=L as:

$$Z_L = \frac{\tilde{p}}{\tilde{u}} = \frac{\rho\, a_p^2 A}{Vs} \tag{A.3}$$

The boundary condition at the other end of the duct may be assumed to have an impedance Z_L. Substituting both expressions into equation (A.1) and solving for the characteristic equation gives:

$$\begin{aligned} &Z_L \cos(\omega L/a_d) + j\rho_d a_d \sin(\omega L/a_d) - \\ &\frac{Z_0}{\rho_d a_d}\left[Z_L j\sin(\omega L/a_d) + \rho_d a_d \cos(\omega L/a_d)\right] = 0 \end{aligned} \tag{A.4}$$

In order to see the effect of boundary condition changes one may assume that a plenum is placed at the inlet duct and vary its volume. In this case the boundary condition has a negative sign because of the direction in which velocity is assumed to have a positive perturbation. The impedance may be defined as:

$$Z_0 = \frac{\tilde{p}}{\tilde{u}} = -\frac{\rho a_p^2 A}{V_{inlet} s} \tag{A.5}$$

One would expect the inlet volume to be large when the Helmholtz resonator is small compared to the room in which it is located. Therefore, this assumption will be used initially to plot the acoustic resonant modes of the resonator. Later the effect of reducing the inlet volume will be investigated.

The system eigenvalues cause the left hand side of the characteristic equation to equal zero. Therefore the eigenvalues may be determined by plotting one over the left hand side of the characteristic equation (1/(left hand side)). Peaks in this figure would represent system resonances.

A.2 Results

Resonances predicted for the estimated engine dimensions are shown in figure (A.2). The model is seen to overestimate the measured acoustic resonances. The effect of increasing the plenum volume and duct length by 35% is also shown in this figure. Changing the plenum volume is seen to increase the first resonant frequency but not affect higher modes. Increasing the volume by 35% is equivalent to reducing the duct area. Changing the duct length by 35% affects all the resonant modes. The model with a duct length 35% longer than dimensions estimated for the engine (see chapter 2) predicts 3 of the measured acoustic resonances.

Figure (A.3) shows the effect of varying the inlet plenum volume. As the volume is reduced the resonant modes shift to higher frequencies. Volumes below 0.001 cubic meters and above 1 cubic meter result in no further shift in frequency.

Figure(A.4) shows the effect of temperatures that occur in the engine near the 95% speed on the resonances predicted by the model. The frequency shift ratio for the first 6 modes ranges from 1.36-1.43.

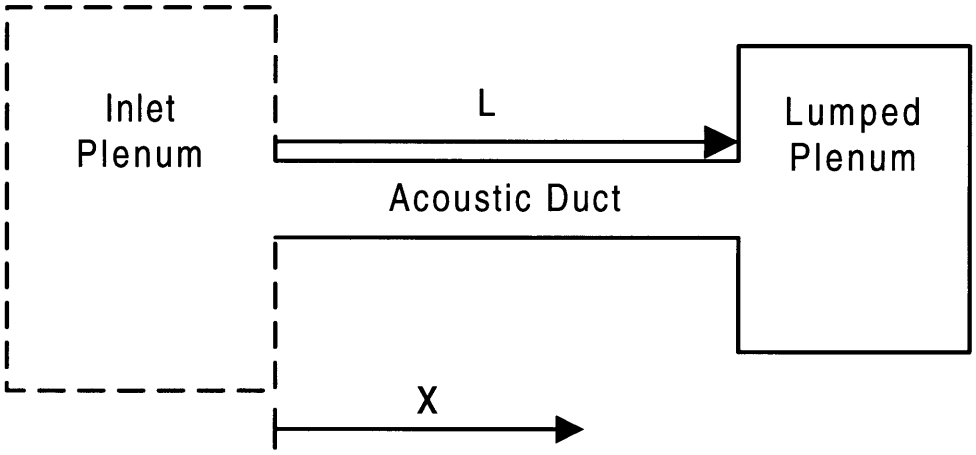

Figure (A.1) Acoustic Duct Model

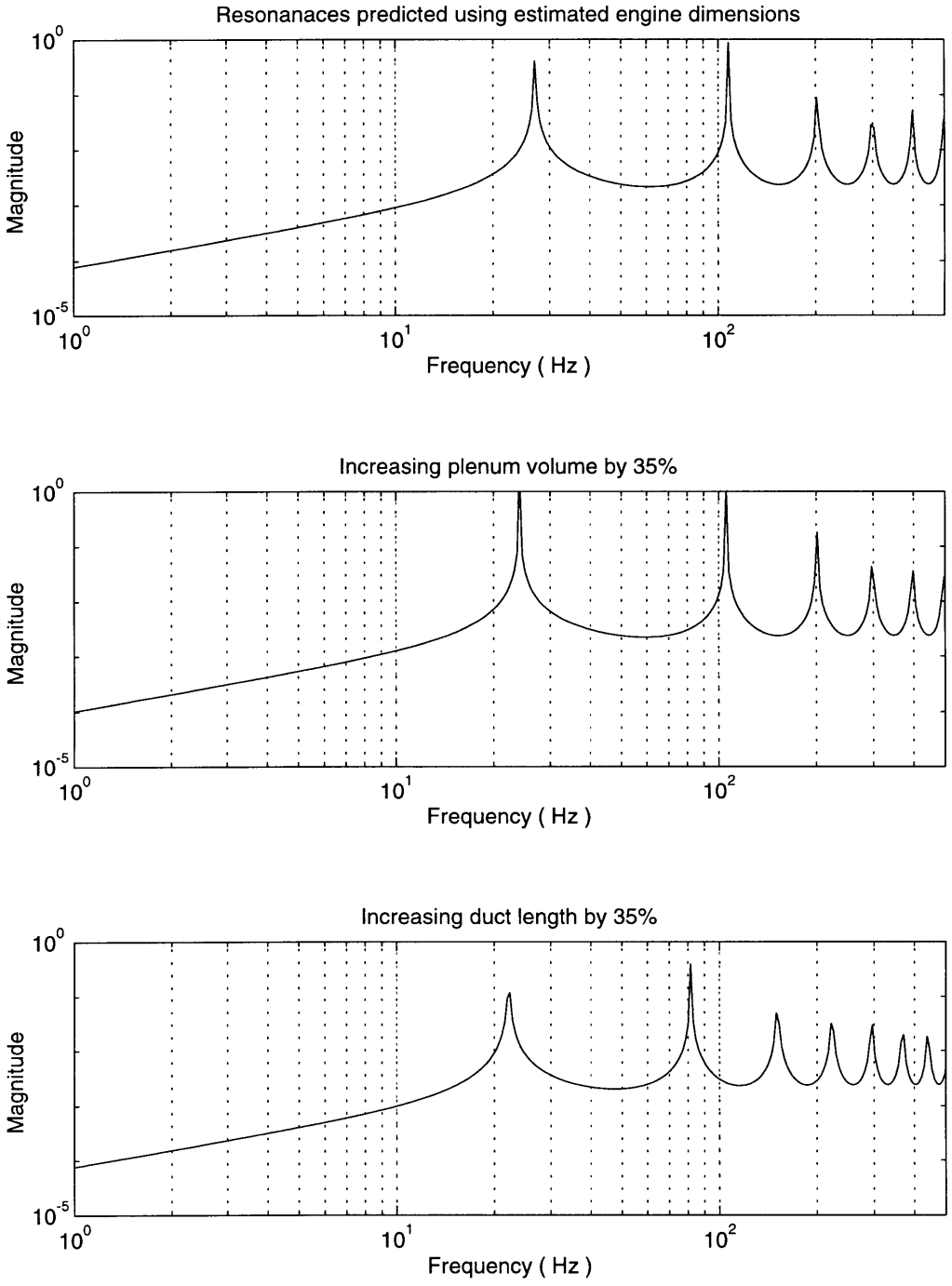

Figure (A.2) Predicted resonances for estimated engine dimensions, 35% increase in plenum volume and 35% increase in duct length.

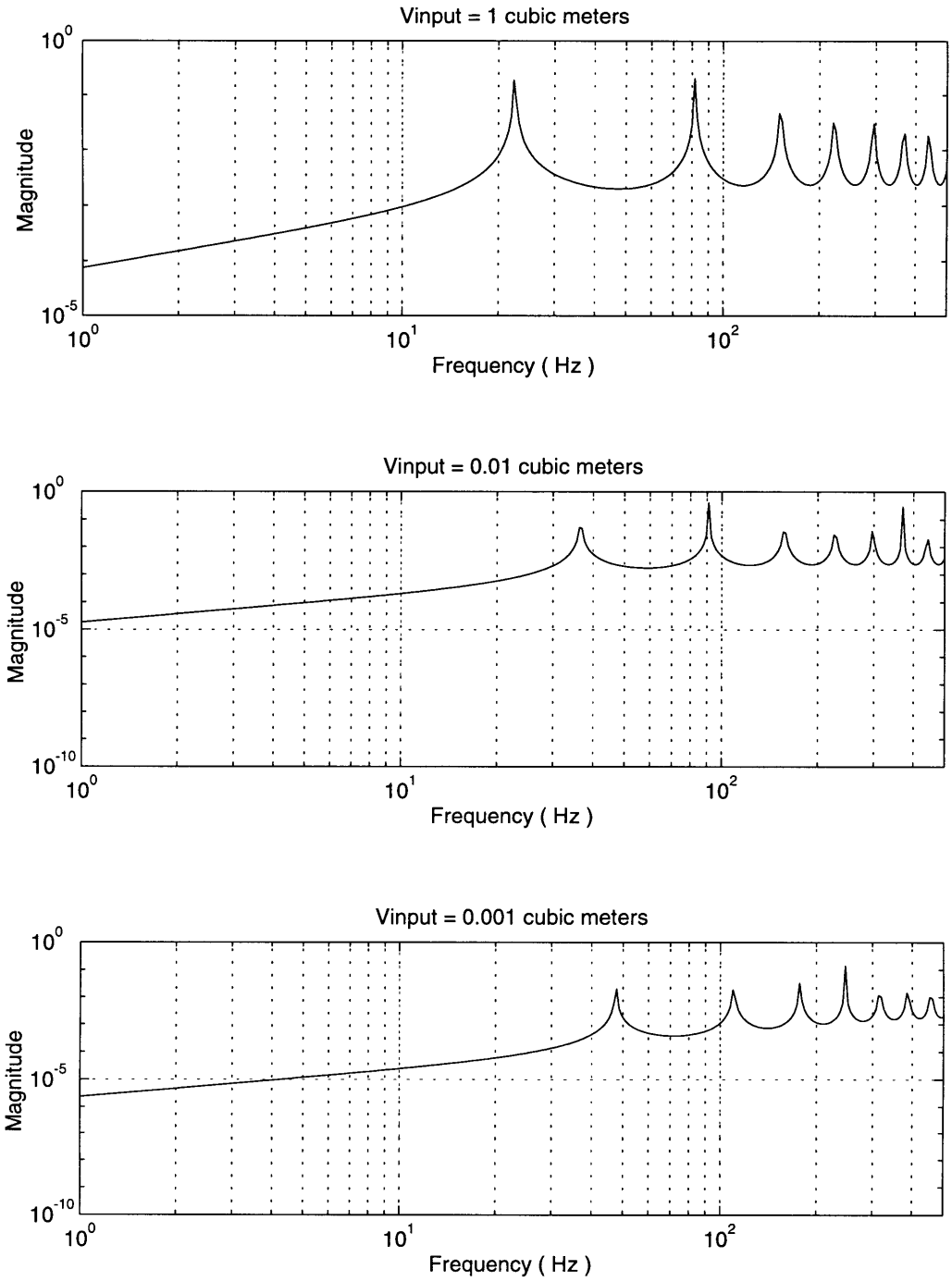

Figure (A.3) Effect of changing the inlet impedance by varying the size of the effective inlet volume.

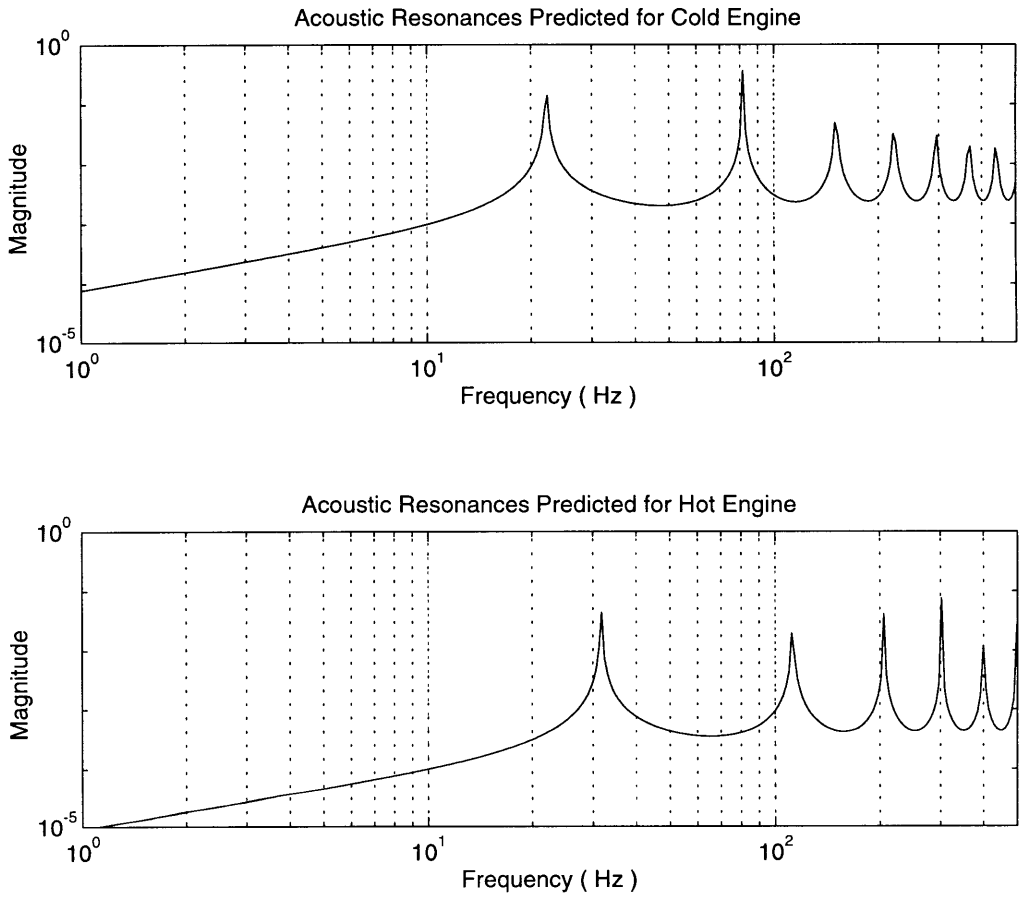

Figure (A.4) Frequency shift predicted by acoustic duct model due to temperatures that occur in the engine near the 95% speed